

POLITECNICO DI TORINO

Corso di Laurea Magistrale in Ingegneria Biomedica (Bionanotecnologie)

Tesi di Laurea Magistrale

**Mesoporous Silica Nanoparticle as advanced drug
delivery system: the effect of biomimetic lipid shielding**



Relatore: prof. Valentina Cauda

Candidato: Simona Villata

Anno Accademico 2019/2020

Ringraziamenti

Vorrei prima di tutto ringraziare Valentina Cauda, che ha avuto così tanta fiducia in me da darmi la possibilità di lavorare in un laboratorio dove non solo sono potuta crescere didatticamente e professionalmente, ma dove ho scoperto quella che ora è la mia passione e dove mi sono sentita guidata e incoraggiata come mai prima.

Naturalmente ringrazio la mia famiglia: il cuore grande dei miei genitori che non mi hanno mai negato nulla e nonostante io volessi essere adulta ed indipendente mi hanno sempre teso una mano quando mi trovo in difficoltà: vorrei che sapessero che se sono qui oggi il merito è soprattutto loro, che nemmeno per un secondo hanno smesso di credere in me e che mi hanno lasciata crescere senza mai abbandonarmi. Grazie a Mamma per i suoi preziosi consigli e per il suo affetto e grazie a Papà per la sua calma e per il suo umorismo.

Ringrazio mia sorella, in cui soprattutto nell'ultimo anno ho trovato un'amica, confidente e compagna di balli e risate: è vero che le sorelle non si scelgono ma sono felice che a me sia capitata lei.

Un pensiero va a tutti i miei fantastici nonni, che fanno parte di me: nonno Elio con la sua passione per la ricerca e la sua indomita curiosità, nonno Franco con la sua dedizione al lavoro, nonna Angela col suo sorriso, i suoi consigli e il suo ottimismo e nonna Emilia con la sua tenacia e dolcezza: spero di avervi resi tutti fieri.

Grazie anche a zio Marco, zia Anna e a mio cugino Matteo, che non si sono mai rifiutati di darmi un buon consiglio o anche solo una pacca sulla spalla. Ringrazio anche zio Sergio che, nonostante i suoi costanti "Mac ad bale!", so essere sempre stato dalla mia parte e che sarebbe venuto a prendermi a Madrid in macchina.

Se è vero che gli amici sono la famiglia che ci scegliamo non posso che ringraziare chi in questi anni ha fatto parte della mia vita: cominciando dai miei amici di sempre ringrazio Gio, che è stato ed è come un fratello per me, la persona che forse mi conosce meglio a questo mondo e di cui so che mi potrò sempre fidare. Ringrazio Isa, che mi ha sempre strappato un sorriso o teso una mano quando ne avevo bisogno e con cui è impossibile annoiarsi. Ringrazio Madda, con cui ho condiviso tantissimo in passato e di cui so di potermi sempre fidare. Ringrazio Megghi, su cui so che potrò sempre contare, anche se le nostre strade non sono più intrecciate come un tempo. A tutti loro vorrei dire che crescere con loro è stato bellissimo e che hanno riempito la mia vita di ricordi che non mi abbandoneranno mai e dei quali probabilmente tra trent'anni ancora rideremo insieme.

Un ringraziamento speciale va a tutte le coinquiline e a tutti i coinquilini che mi hanno accompagnata in questi anni, che sono stati, nel bene o nel male, i miei compagni di viaggio e di cui nonostante tutto porto un ricordo importante nel cuore. In particolare vorrei ringraziare Vale e Giuli: Vale, che mi ha fatto da mamma fin dal mio primo giorno a Torino e che a volte mi fa ancora da mamma dopo cinque anni, che nonostante veda due volte l'anno mi conosce come una sorella e che so sarà sempre pronta se avrò bisogno di lei e Giuli, la mia sorella adottiva che mi ha fatto capire che non c'è un limite al volersi bene e che ci si può sentire in famiglia anche senza avere legami di sangue: le voglio dire grazie per avermi sopportata anche quando nemmeno io mi sopportavo più.

Infine vorrei ringraziare i miei amici di Torino: quelli con cui semplicemente ho fatto passare qualche pomeriggio o qualche serata, quelli che nel tempo ho perduto di vista ma che mi hanno regalato ricordi meravigliosi, ma soprattutto Ale, la migliore confidente e compagna di avventure che potessi desiderare e con cui ho riso tanto da farmi venire il mal di testa e Anto, sempre pronto ad aiutare e che ha reso questi anni belli con i suoi sorrisi, la sua cucina e le sue battute (a volte) divertenti: vi auguro tutta la felicità insieme che vi meritate.

Non vorrei essere ripetitiva, ma ancora una volta grazie a tutti.

Simo

Abstract

In the last years, nanomedicine has gained a growing attention by the research community, thanks to the small size of the used devices, which allows an easy interaction with cells and biomolecules. For this purpose, in this Master Thesis Mesoporous Silica has a starring role, thanks to its well-known properties like biocompatibility, resistance to biodegradation, and drug uploading capacity. It has been used to produce Mesoporous Silica Nanoparticles (MSNs) of 40-50 nm in diameter and showing mesopores with uniform size (2-3 nm) through a template-assisted sol-gel self-assembly process. As MSNs do not have intrinsic imaging properties, their surface has been functionalized with amino-groups (-NH₂) in order to be labelled with fluorescent dyes, while the highly porous structure was used to upload the nanoparticles with a therapeutic cargo. Two different drugs against Multiple Myeloma were used: an inhibitor of the Ubiquitin Proteasome Pathway (Carfilzomib, CFZ), FDA approved, and the drug AGI-6780, which is an inhibitor of the enzyme isocitrate dehydrogenase 2 (IDH2). The choice of these two drugs is not accidental: previous studies revealed that the combination of these two drugs can induce a synergistic cell death even in those cells that developed drug resistance if treated only with CFZ. However, the drug AGI-6780 has at present failed the translation to clinical studies due to its strong hydrophobicity, which makes impossible to administer it through an oral or intravenous way. This obstacle can be overcome by the strategy reported in this Master Thesis, i.e. by encapsulating AGI-6780 in MSNs that can be uploaded with a consistent amount of drug thanks to their huge surface area (~1000 m²/g). Also CFZ was encapsulated in MSNs, as the two drugs have to be used in concomitance. Both drugs were uploaded by mixing MSNs and the drug in a dynamic condition. However, pristine MSNs are not colloidally stable in an aqueous environment like the human body. Therefore, another aim of this thesis was to try different lipid bilayer shielding formulations in order to optimize the colloidal stability, dispersibility, biocompatibility of the final lipid-coated MSNs. Firstly, synthetic lipid formulations were tested. One was composed by DOPC (1,2-dioleoyl-sn-glycero-3-phosphocholine). The second one was formulated by mixing DOPC and DOTAP (N-[1-(2,3-Dioleoyloxy)propyl]-N,N,N-trimethylammonium methyl-sulfate) at a molar ratio of 2:1. The third one was DOPC-CHOL-DSPE-PEG₂₀₀₀, prepared mixing DOPC, DSPE-PEG₂₀₀₀ (1,2-distearoyl-sn-glycero-3-phosphoethanolamine-N-[polyethylene glycol-2000]-amine) and cholesterol at a molar ratio of 55:44:2.

A further and more advanced biomimetic approach explored in this Master Thesis was to make the coating of MSNs with exosomes, that are extracellular vesicles of 30-200 nm in size, naturally produced by living cells. Here in particular, two different biological sources were tested: a human carcinogenic one (KB cancer cell) and healthy human cell line from blood white cells (B lymphocytes). Exosomes have been revealed to play an important role in cells communication with other cells from the same tissue or different tissues, and if of autologous origin they are not subjected to immune adverse response. To better understand extracellular vesicles and their application, a deep literature research has been done on extracellular vesicles and the possibility to engineer them and to synthesize artificial ones. In this Master Thesis it was proposed to include MSNs into exosomes in order to carry the inorganic nanoparticles straight to the target cancer cells in a highly biomimetic way. The experimental focus was devoted here on the coupling between MSNs and exosomes, to obtain an efficient enclosure of the MSNs inside the lipid biovesicles. *In vitro* tests were also carried out, using Human Multiple Myeloma cell line KMS-28, to evaluate the cell-uptake of covered MSNs and the IDH2 inhibition thanks to MSNs@SLB loaded with AGI-6780 and the viability of the cells treated with MSN@SLB loaded with Carfilzomib.

To conclude, the present Master Thesis can be considered the starting point of a really innovative, multifunctional and biomimetic drug delivery platform.

Index

	Pages
EVs and their evolution: from cellular products to engineering machines	5
1. Introduction	5
2. Natural EVs	5
2.1. Passive loading methods	9
2.1.1. Co-incubation	9
2.2. Active loading methods	9
2.2.1. Electroporation	9
2.2.2. Sonication	9
2.2.3. Extrusion	9
2.2.4. Freeze thaw	9
2.2.5. Chemical-based transfection	9
3. Engineered EVs	12
3.1. Indirect methods	12
3.2. Direct methods	16
3.2.1. Covalent methods	16
3.2.2. Non-covalent methods	16
3.2.3. Glycosylation	16
3.2.4. Hybridization	17
4. Synthetic and Chimeric EVs	20
4.1. Top-down approach	21
4.2. Bottom-up approach	22
Mesoporous Silica coated with different lipidic formulations as drug delivery system	25
1. Materials and Methods	28
1.1. MSNs Synthesis	28
1.2. Lipid Bilayer Formation	28
1.3. Exosomes isolation and coupling with MSNs	29
1.3.1. SV1 and SV2	29
1.3.2. SV3 and SV4	30
1.3.3. SV5	30
1.4. Characterization of the Nanoparticles	30
1.4.1. Fourier-transform Infrared Spectroscopy (FTIR)	30
1.4.2. TEM-Transmission Electron Microscope analysis	31
1.4.3. DLS- Dynamic Light Scattering and Z-Potential	31
1.4.4. Fluorescence Microscopy Imaging	31
1.5. Analysis on AGI-6780 and Carfilzomib	32
1.5.1. UV-VIS Spectroscopy	32
1.5.2. Drug Uptake and release of AGI-6780 and CFZ	33
1.5.2.1. Drug uptake of AGI-6780 and CFZ	33
1.5.2.2. Drug release of AGI-6780 in water	34
1.5.2.3. Drug release of AGI-6780 and CFZ in acellular environment	35
1.6. Cell Treatment	36
1.6.1. Cell culture conditions and reagents	36
1.6.2. Fluorescence microscopy imaging	36
1.6.2.1. Evaluation of the coupling between lipids and MSNs	36
1.6.2.2. Confocal and Time lapse fluorescent microscopy images of KMS-28	36
1.6.3. Flow cytometry analysis	37
1.6.4. IDH enzymatic activity	37
1.6.5. Treatment with Nanoparticles	37

1.6.5.1. Treatment with MSNs (MM4 and MM3) encapsulating CFZ coated with lipids	38
1.6.6. Cell viability	38
1.6.7. 1.6.7. FACS-Fluorescence-Activated Cell Sorting	38
1.7. Statistical Analysis	39
2. Results and Discussion	40
2.1. Lipid-coated MSNs design and characterization	40
2.1.1. DLS-Dynamic Light Scattering and Z-Potential	41
2.1.1.1. Dynamic Light Scattering	41
2.1.1.2. Z-Potential	43
2.1.2. Fluorescence microscopy imaging: Evaluation of the coupling between lipids or exosomes and MSNs	44
2.2. MSNs@SLB internalization into multiple myeloma cells	45
2.3. MSN@SLB for AGI-6780 uptake and stability over time	47
2.4. IDH2 enzymatic inhibition tests with AGI-6780 loaded MSNs	49
2.5. MSNs@SLB for Carfilzomib uptake and stability over time	50
2.6. Cellular viability tests with Carfilzomib loaded MSN@SLB	51
Conclusions	53
References	54

EVs and their evolution: from cellular products to engineered nanomachines

1. Introduction

Extracellular vesicles (EVs) are nowadays well known as small vesicles ($\leq 2\mu\text{m}$) [1] produced by almost all cell types, ensuring efficient communication among cells throughout the body, by transporting lipids, proteins, and nucleic acids [2] [3]. The presence of cell-type specific molecular signatures in these EVs has highlighted their potential role as biomarkers in a variety of diseases [2] [3]. Moreover, there is huge interest in applying EVs or synthetic EV-mimics in nanomedicine as drug delivery [4]. Their surface can be modified with the various macromolecules, including peptides, dyes or stealth polymers, for diagnostic purposes, cell tracking or even targeting other cells or tissues [5]. They have shown to have a role in the immune system modulation or as promoters of carcinogenicity [4] [5]. They have been recently shown to coat both organic and inorganic nanoparticles thus producing novel biomimetic hybrids [6]. Therefore, they are becoming the invisible warriors of the today nanomedicine, the camouflage suit for many devices and drugs [7].

The aim of this review is to give a deep overview of the EV-based solution in nanomedicine. Firstly, we will comment about the natural EVs, their biogenesis, their interactions with the cells thanks to their unique features, the methods used to encapsulate a cargo into them and their general application. We will then discuss some strategies used to engineer these extracellular vesicles, in order to make them more specific and advanced. In particular, we will focus on the functionalization of EVs surface with different molecules for various biomedical purposes, both with direct and indirect methods, and on the possibility to encapsulate a cargo through the engineering of the parental cells. At the end, we will have a look on the new frontier of EVs: the synthetic ones, that are under study in order to have well characterized, reproducible and scalable chimeric vesicles, containing only the necessary key elements for their specific purpose. In particular, we will analyze both bottom-up and top-down techniques.

Finally, we propose a clear and complete picture on the most interesting scientific efforts on EVs usages and modifications, their potential and the possibility to customize them for a specific nanomedicine application.

2. Natural EVs

EVs are secreted by all the cells and they have been found in everybody fluid, such as blood, urine, breast milk, saliva and cerebrospinal fluid [4]. They are vesicles with a bilayered lipid membrane, and they can be divided in apoptotic bodies, microvesicles and ectosomes, and exosomes [1] [2] [3]. EVs range in size from 50 nm to 2 μm [1]. EVs are produced both under physiological and pathological conditions and their main function is to carry messages from a cell to another one [4]. For example, tumour EVs have an important role in influencing processes as oncogenic transfer, immune modulation and pre-metastatic niche development [4]. This active role in tumour intracellular communication and signal transduction leads to focus the attention on these extracellular vesicles as innovative tools in the fighting against cancer [5].

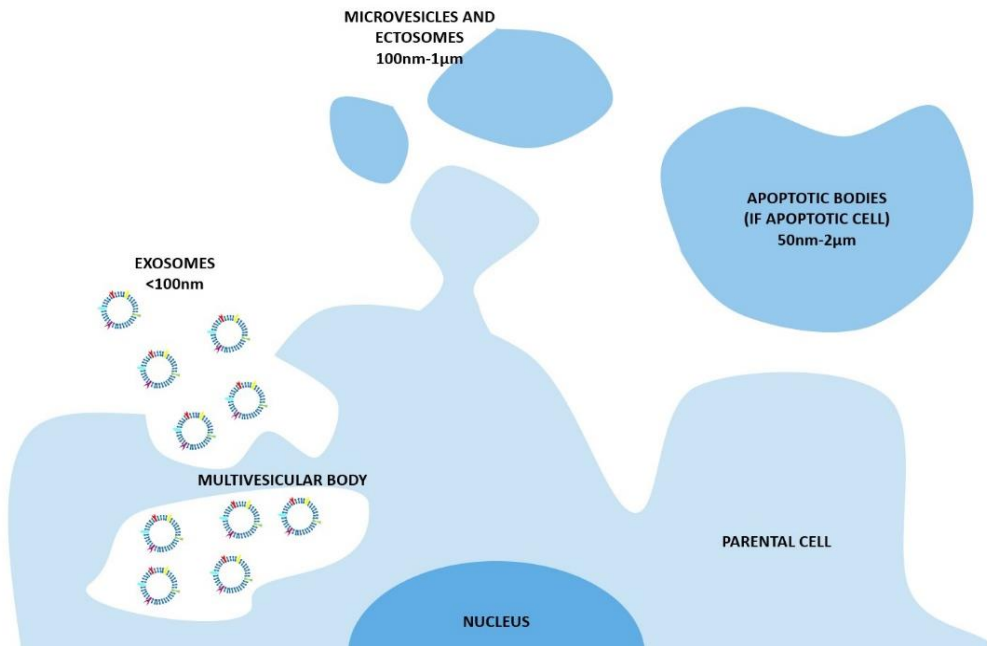


Figure 1: Biogenesis of EVs

To better understand how EVs can be used, we have to consider how they act in their natural environment. As shown in Figure 1, while microvesicles and ectosomes derive from the budding of the cellular membrane [1], exosomes originate in the cells from the intraluminal vesicles of the multivesicular body [1] [4], an endosome in which the intraluminal vesicles (membranous vesicles that are formed by inward budding of endosomal membranes) can be found [1] [4]. When the multivesicular body reaches the plasma membrane and fuse with it, the exosomes are released through exocytosis [6]. After their release in the extracellular space, EVs diffuse in intracellular fluids and, once they reach the target cell, they can be recognized and then be taken up by the target cell with four potential mechanisms, as shown in Figure 2 [1] [3] [4]:

- Through surface ligands: some proteins on the EV surface can bind to specific receptors on the target cell surface and the EV is engulfed by the cell membrane [3].
- Pinocytosis: the membrane of the target cell creates an inward protrusion which engulfs the EVs with its cargo, obtaining an endosome [4];
- Phagocytosis: may also play a role in EVs uptake, because cells with a phagocytic phenotype (some macrophages) internalize EVs that are subsequently identified in phagosomes [3];
- Fusion with plasma membrane: the membrane of EV is embodied in the plasma membrane of the cell and the cargo is released in the target cell [3];

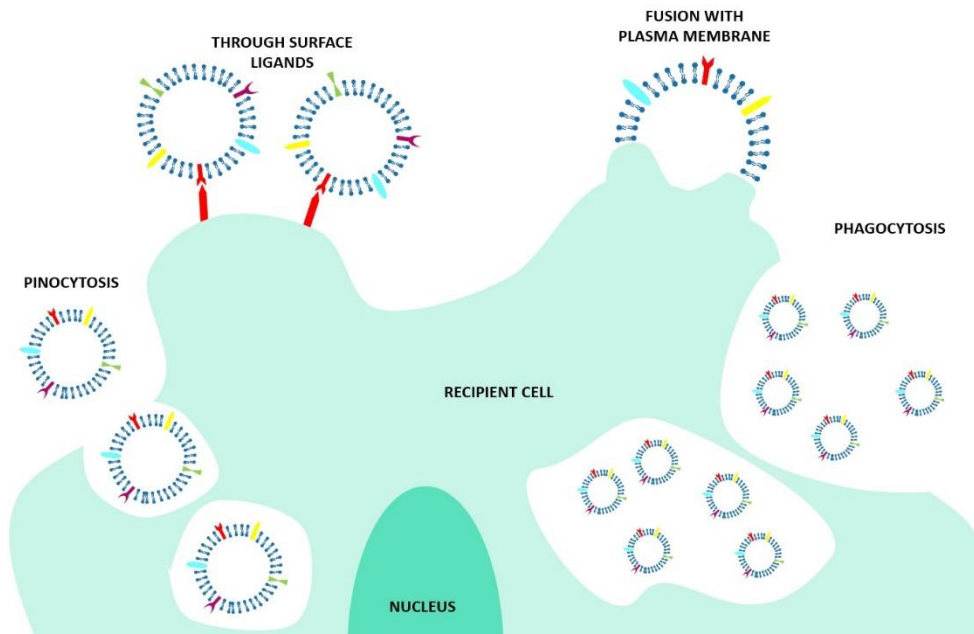


Figure 2. Mechanisms of cellular uptake of EVs

EVs seem to have different compositions and cargos depending on their parental cell origin [4]. However, it is experimentally hard to assess the specific EV composition because of the overlap in many components and the difficulty in obtaining a pure preparation of a certain EVs sub-population [4]. Anyway, the International Society for Extracellular Vesicles (ISEVS) in 2014 recommended defining EVs only the extracellular vesicles that present on their surface certain surface markers: TSG101, Alix, flotillin 1, tetraspanins like CD9, CD63 and CD81, integrins and cell adhesion molecules [8]. For what concerns the lipid content, it is known that EVs are composed, among other, by cholesterol, sphingomyelin and hexosylceramids [8]. In Figure 3 an illustration of an EV basic composition is reported.

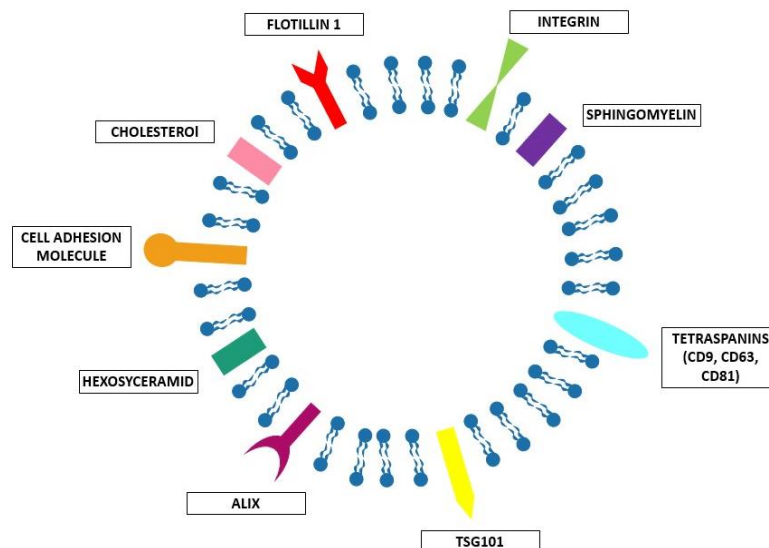


Figure 3. EV basic composition

It is not easy to obtain a pure EVs preparation: the most commonly used method to extract and isolate them is the differential centrifugation (ultracentrifugation) [9], as shown in Figure 4, top panel. In order to separate bigger objects to smaller ones (like the EVs), the EV-producing medium is subjected to a series of centrifugations, with different speeds) [9]. Larger particles sediment faster and are firstly removed, so the EVs are found in the final pellet) [9]. This is the best method nowadays, but it cannot assure the perfect separation of EVs that are often found in the last pellet with other biomaterials, like proteins and viruses) [9]. Furthermore, the different EV subpopulations can be separated only by certain immunorecognition or sucrose gradient, however at the expenses of the final yield. During the isolation EVs can aggregate and the high-speed centrifugation can damage them. There are various other isolation methods [10], as prominent and various literature reports have discussed, like the EV isolation kits [10] [11], size-based filtration [12], size-exclusion chromatography (SEC) [13], polymer precipitation [12], immuno-affinity purification [14] [15] and microfluidic-based isolation [16] [17]. As reported in Figure 4 in the lowest panel, in the isolation kits magnetic beads coupled with antibodies are used to recognize the EV surface antigens [10]. The advantage of this method is to avoid any ultracentrifugation step (and even centrifugation ones, as in the peculiar scheme reported in Figure 4) that could damage the EVs. Among the disadvantages it can possibly be an unsatisfactory release of the vesicles from the magnetic beads after separation and the low yield, that makes this method good for small volumes only [10].

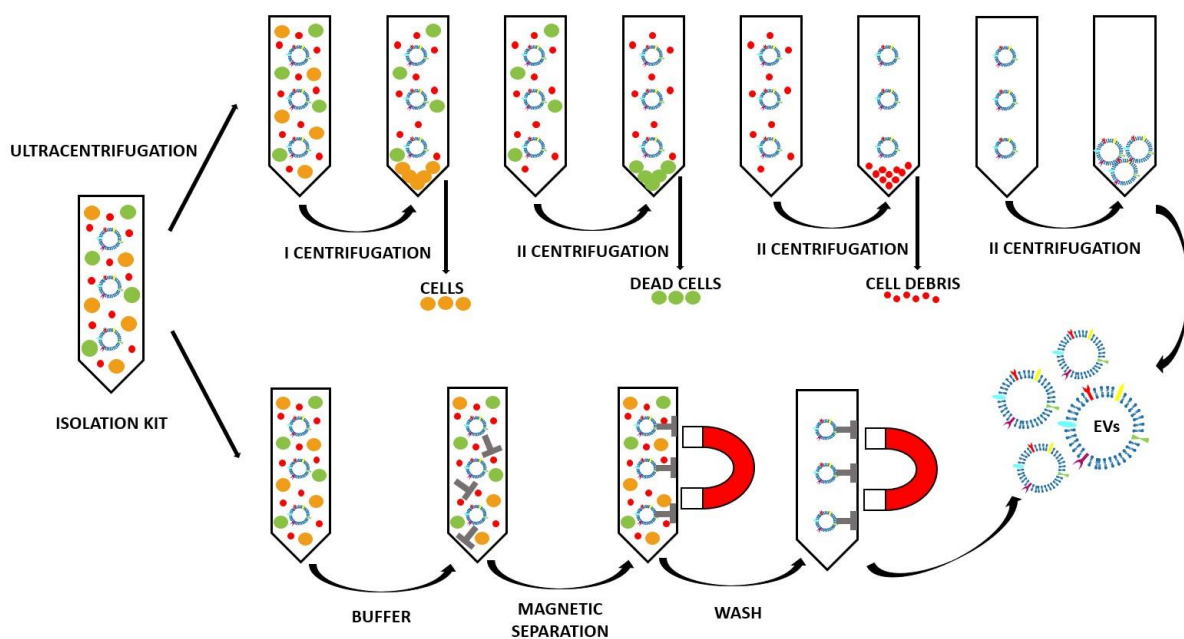


Figure 4. Example of EVs isolation: differential ultracentrifugation and isolation kit processes

Since EVs are natural carriers in cellular communication, they are investigated as drug delivery systems [4]. EVs present low immunogenicity, no cytotoxicity and high biostability, they can load different cargos and they are able to target the recipient cells [4]. They are also biodegradable by cells and their clearance rate is lower than synthetic objects [18]. In fact, it has been demonstrated that the surface of some types of EVs is decorated with CD47, a protein that works as a “don’t eat me” signal for the macrophages [19]. Another important skill is that EVs, as natural carriers, can cross barriers like the blood brain barrier, that are very difficult to overcome with bare drugs or other strategies [20]. EVs have been also reported to also act as carriers of various molecules:

- Hydrophilic components: like hydrophilic drugs, but also miRNA, siRNA, DNA and proteins. They can be encapsulated in the hydrophilic core of the EV [21].
- Hydrophobic drugs, that can be incorporated in the lipid bilayer [21].

- Macromolecules for imaging, tracking (as fluorophore-conjugate antibodies) and targeting purposes. They can be bound with surface modifications to the EV lipid bilayers or surface proteins [21].

There are different EV loading strategies, once they have been isolated, as reviewed in Table 1 and schematized in Figure 5. They will be discussed in detail in the following sections.

2.1. Passive loading methods

2.1.1. Co-incubation

The cargo and the EVs are just incubated for a period of time at room temperature [22] [23] [24] or at 37°C [25] [26] [27]. It is a very simple method, with the advantage to preserve the morphology of the EVs [5]. The cargo can diffuse into the EV following the concentration gradient and cross the membrane thanks to the small dimension and the lipophilic nature [25] [26], or (as curcumin [23]) causing a lipid rearrangement of the membrane that facilitates the entry of the molecule. Other molecules, such as glucose, can be internalized by energy-dependent mechanisms (glucose channels) [27]. For the loading of nanoparticles, it is possible that the EVs adhere and then adsorb on the surface of the nanoparticles [28]. This method has however two main drawbacks: the low loading efficacy and the difficulty to assess the purity of the final preparation [19].

2.2. Active loading methods

2.2.1. Electroporation

It consists in the application of an electrical field in a conductive (electrolyte) solution where the EV and cargo are dispersed. The electrical field creates temporary pores in the EV lipidic bilayer, that allow the penetration of the cargo in the EVs [19]. This is important when large and hydrophilic molecules (for example siRNA [29] and miRNA) have to be incorporated, as they can not diffuse through the membrane like the small hydrophobic ones [24]. The main drawback of the electroporation method is the aggregation of EVs that must be limited through the optimization of the protocol [19].

2.2.2. Sonication

After EVs and cargo are mixed together in a water-based medium, they are sonicated with a homogenizer ultrasonic probe [22] [25]. The cargo can penetrate because the shear forces from sonication induce the EV membrane deformation [19]. It seems that the integrity of the membrane can be restored, however irreversible damages to EVs and possible aggregation can take place [25].

2.2.3. Extrusion

After EVs and cargo are mixed together, they are loaded into a lipid extruder with a 100-400 nm porous membrane and then extruded [22] [24]. It is not yet clear how the membrane structure and properties are modified with this method [19].

2.2.4. Freeze thaw

This method provides repeated cycles of freezing at -196 °C in liquid nitrogen and thawing at room temperature of the solution of EVs and cargo [22]. The efficiency is higher than co-incubation method, but lower than the mechanical-based methods, like the sonication and extrusion [19]. Another drawback is that these freeze-thaw cycles can induce the aggregation of the EVs and modification of the membrane properties, i.e. protein orientation [5].

2.2.5. Chemical-based transfection

A surfactant is used to destabilize the membrane of the EVs to allow the penetration of the cargo [19]. Saponin is the mostly used surfactant [22] [24]: while guaranteeing a good cargo loading efficacy into EVs, it could be toxic for living cells.

Table 1. The various EV loading methods

Parental cells	Cargo	Loading conditions	Recipient cells	Treatment condition	Application	Ref.
Co-incubation						
H1299 and YRC9	Doxorubicin conjugated with gold NPs	Incubated at 37 °C with 250 rpm for 2 h	H1299, A549, MRC9 and Dox-sensitive HCASM	1 × 10 ⁵ cells/well and EVs with the equivalent of 5 µg Dox/well	Anticancer activity against Human Lung Cancer Cells	[26]
RAW 264.7	Paclitaxel	Incubated at 37°C for 1 hour with shaking	MDCK _{WT} , MDCKMDR1 and 3LL-M27 <i>IN VIVO</i> : C57BL/6 mice	5'000 cells/well and exosomes <i>IN VIVO</i> : i.n. 10 ⁷ particles/10µl × 2	Overcome multiple drug resistance in cancer cells	[25]
KB	ZnO nanocrystals	Various loading conditions	KB	3 × 10 ⁴ cells/well and EVs with the equivalent of 15 µg/mL of ZnO nanocrystals	Treatment of cancer cells	[30]
RAW 264.7	Enzyme catalase	Incubated at RT for 18 hours	PC12 <i>IN VIVO</i> : C57BL/6 female mice	50'000 cell/well and EVs 230 µg total protein/mL <i>IN VIVO</i> : i.n. or i.v. 2.4 × 10 ¹⁰ EVs	Parkinson's disease therapy	[22]
HeLa	MOF loaded with calcein	Incubated at 37°C for 1.5 h with shaking	HeLa	1'000 cells for each EVs concentration (10–140 µg/mL)	Efficient Drug Delivery Platform	[28]
MSCs	Glucose-coated gold NPs	Incubated for 3 h at 37 °C	<i>IN VIVO</i> : C57bl/6 male mice	<i>IN VIVO</i> : i.n. and i.v. 2.8 × 10 ⁹ EVs	<i>In vivo</i> neuroimaging	[27]
EL-4, MDA-MB231, 4T-1	Curcumin	Mixed at 22 °C, then sucrose gradient centrifugation	RAW 264.7 <i>IN VIVO</i> : 7- to 10-week female C57BL/6j mice	Exosomal curcumin 20 µmol/l, LPS 50 ng/mL <i>IN VIVO</i> : i.p. 4 mg/kg exosomal curcumin, 18.75 mg/kg LPS	Deliver anti-inflammatory agents to activated myeloid cells <i>in vivo</i>	[23]
MDAs, hUVECs, hMSCs and hESCs	Porphyryns of different hydrophobicities	Incubated at RT for 10 min	MDA-MB231	20'000 cells/well and EVs diluted 1:2 from the Stock solution (1.5 mg/mL of Por)	Improve the cellular uptake and photodynamic effect of porphyryns	[24]
Electroporation						
RAW 264.7	Paclitaxel	1'000 kV for 5 ms, then incubated at 37°C for 30 min	MDCK _{WT} , MDCKMDR1 and 3LL-M27	5'000 cells/well and exosomes <i>IN VIVO</i> : i.n. 10 ⁷ particles/10µl × 2	Overcome multiple drug resistance in cancer cells	[25]
MDAs, hUVECs, hMSCs and hESCs	Porphyryns of different hydrophobicities	200 Ω, 500 µF, 200 mV and pulse time of 20-30 ms	MDA-MB231	20'000 cells/well and EVs diluted 1:2 from the Stock solution (1.5 mg/mL of Por)	Improve the cellular uptake and photodynamic effect of porphyryns	[24]
B16-F10	5 nm SPIONs	High voltage setting	The formulation wasn't tested with cells or animals	The formulation wasn't tested with cells or animals	Maximizing exosome colloidal stability	[31]
HeLa, HTB-177, CD14 ⁺ monocytes and CD14 ⁻ lymphocytes	siRNA	0.150 kV/100 µF	HTB-177, CD14 ⁺ monocytes and CD14 ⁻ lymphocytes	0.5x10 ⁴ cells/well and 30 µl of exosomes with siRNA at 2 µmol/mL	Deliver exogenous siRNA to monocytes and lymphocytes	[29]

follows from previous page						
Parental cells	Cargo	Loading conditions	Recipient cells	Treatment condition	Application	Ref.
Sonication						
RAW 264.7	Paclitaxel	20% amplitude, 6 cycles of 30 s on/off, 2 minutes pause, then incubated at 37°C for 60 min	MDCK _{WT} , MDCKMDR1 and 3LL-M27	5'000 cells/well and exosomes <i>IN VIVO</i> : i.n. 10 ⁷ particles/10µl × 2	Overcome multiple drug resistance in cancer cells	[25]
RAW 264.7	Enzyme catalase	Sonicated twice at 500 v, 2 kHz, 20% power, 6 cycles by 4 sec pulse /2 sec pause	Neuronal PC12 <i>IN VIVO</i> : C57BL/6 female mice	50'000 cell/well and EVs 230 µg total protein/mL <i>IN VIVO</i> : i.n. or i.v. 2.4 ×10 ¹⁰ EVs	Parkinson's disease therapy	[22]
Extrusion						
RAW 264.7	Enzyme catalase	Extruded (x10 times) with 200 nm pores diameter	Neuronal PC12 <i>IN VIVO</i> : C57BL/6 female mice	50'000 cell/well and EVs 230 µg total protein/mL <i>IN VIVO</i> : i.n. or i.v. 2.4 ×10 ¹⁰ EVs	Parkinson's disease therapy	[22]
MDAs, hUVECs, hMSCs and hESCs	Porphyryns of different hydrophobicities	Extruded at 42°C (31 times) with 400 nm pore diameter	MDA-MB231	20'000 cells/well and EVs diluted 1:2 from the Stock solution (1.5 mg/mL of Por)	Improve the cellular uptake and photodynamic effect of porphyryns	[24]
Freeze thaw						
RAW 264.7	Enzyme catalase	Incubated for 30 min, then -80° C, then RT (three times)	Neuronal PC12 <i>IN VIVO</i> : C57BL/6 female mice	50'000 cell/well and EVs 230 µg total protein/mL <i>IN VIVO</i> : i.n. or i.v. 2.4 ×10 ¹⁰ EVs	Parkinson's disease therapy	[22]
Chemical-based transfection						
MDAs, hUVECs, hMSCs and hESCs	Porphyryns of different hydrophobicities	Addition of 0.1 mg/mL saponin at RT for 10 min	MDA-MB231	20'000 cells/well and EVs diluted 1:2 from the Stock solution (1.5 mg/mL of Por)	Improve the cellular uptake and photodynamic effect of porphyryns	[24]
HeLa, HTB-177, CD14 ⁺ monocytes and CD14 ⁻ lymphocytes	siRNA	Addition of HiPerFect , then incubated for 10 min at RT	HTB-177, CD14 ⁺ monocytes and CD14 ⁻ lymphocytes	0.5x10 ⁴ cells/well and 30 µl of exosomes with siRNA at 2 µmol/mL	Deliver exogenous siRNA to monocytes and lymphocytes	[29]
RAW 264.7	Enzyme catalase	Addition of 0.2% saponin, shaker for 20 min at RT, then incubated at RT for 18 hours	Neuronal PC12 <i>IN VIVO</i> : C57BL/6 female mice	50'000 cell/well and EVs 230 µg total protein/mL <i>IN VIVO</i> : i.n. or i.v. 2.4 ×10 ¹⁰ EVs	Parkinson's disease therapy	[22]
HeLa and HT1080	siRNA	Addition of lipofectamine and incubated for 30 min at RT	HeLa and HT1080	0.5 × 10 ⁶ cells/well and varying amounts of exosomes (0–460 µg)	Deliver siRNA to recipient cells <i>in vitro</i>	[32]

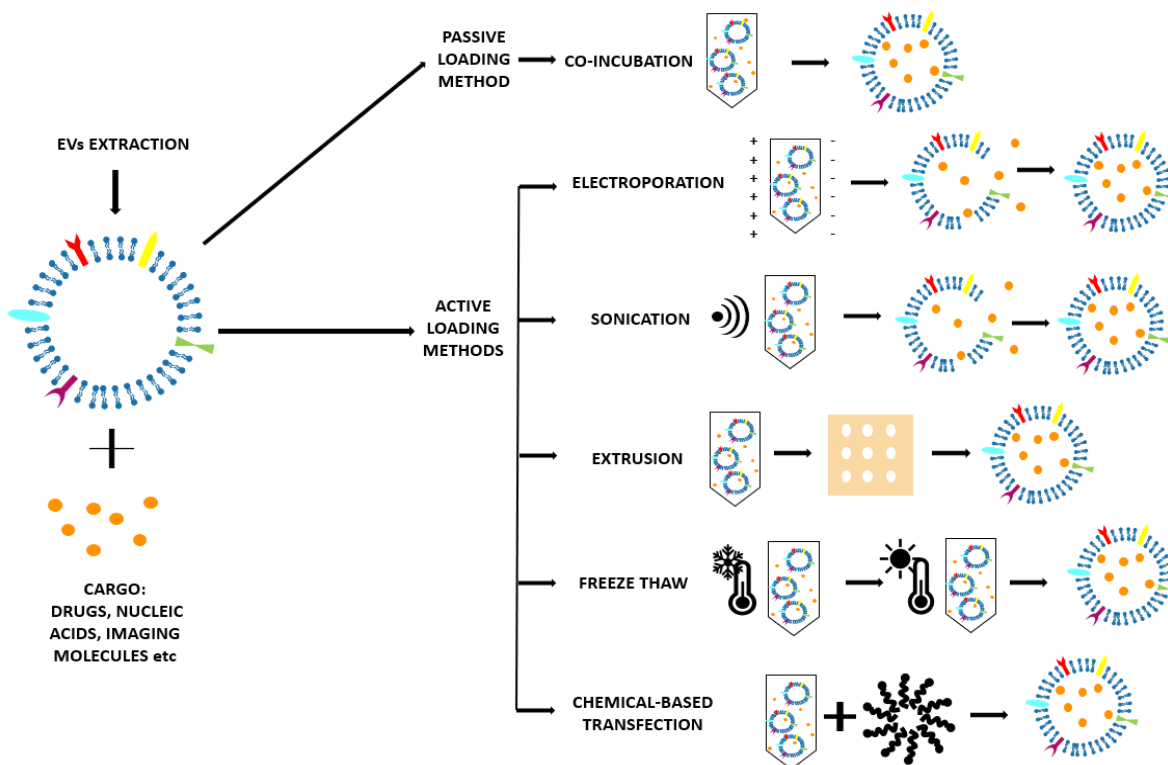


Figure 5. Scheme of the various loading methods with which it is possible to load EVs with the desired cargo

It is very interesting to notice that in some works different loading methods were tried, so that to compare them and to find the best solution for the EV final application. In [25], the authors performed co-incubation, electroporation and sonication and they found out that sonication gives the best results in terms of amount of loaded drug, followed by electroporation and co-incubation. They also demonstrated that the sonication process does not damage the protein and lipid structures of the EVs. Haney *et al.* [22] performed co-incubation, sonication, extrusion, freeze thaw and chemical-based transfection and they found out that sonication, extrusion and chemical-based transfection give the highest loading efficiency, a sustained release and they proved the capability of these formulations for targeted delivery *in vitro* and *in vivo*. In [24], Fuhrmann *et al.* performed co-incubation, electroporation, extrusion and chemical-based transfection and they found out that with chemical-based transfection the loading of the drugs was up to 11-fold higher compared with the other methods tested (co-incubation, electroporation and extrusion). The extruded EVs were demonstrated to cause cytotoxicity, whereas exosomes loaded with the same cargo, porphyrin, but by co-incubation or electroporation did not show significant cytotoxicity. Finally, Shtam *et al.* [29] performed both electroporation and chemical-based transfection. They found out that while chemical-based transfection was inapplicable for their purpose, electroporation, after the optimization of the parameters, was successful at introducing the heterologous siRNAs into the exosomes.

3. Engineered EVs

After their isolation, EVs can be modified in order to obtain enhanced targeting and biomimetic features [5]. This concept is called engineering of EVs because, starting from a naturally-derived EVs, the product is a vesicle with the desired behaviour [19]. It is important to highlight that an extracellular vesicle can be modified both acting on the parental cells (indirect method) and by directly modifying the vesicle, once it has been isolated (direct method) [5]. Another important branch of the EVs engineering is their hybridization after their isolation, where EV membranes are fused with synthetic liposomes [33].

3.1. Indirect methods

This method is based on the engineering of the parental cells, i.e. the cells that will produce the EVs [33]. First, parental cells can be genetically or metabolically modified to alter the surface expression of the produced EVs and thus enhance their targeting ability and biocompatibility [5]. This can be carried out by inserting the coding sequence of the ligand of interest inframe to the coding sequences between the signal peptide and N-terminus of the mature peptide of a transmembrane protein [19]. Using a retrovirus or a lentivirus as gene transfer vector, this package is transmitted and expressed in parental cells [33]. At this point these transfected parental cells will produce EVs with the desired peptide expressed on their surface. In Table 2 and Figure 6 are reported some applications of this indirect method [5] [33].

Secondly, parental cells can be incubated with drugs or drug-loaded (or even gene-loaded) nanoparticles (NPs) in a sublethal concentration [5]: after a certain time, the therapeutic molecules or NPs will be internalized into the cells and then these cells will produce EVs containing a certain fraction of drug or drug-loaded NPs [5]. In this case, the loading of the cargo is obtained through the engineering of the parental cells [19]. For example, mesenchymal stromal cells (MSCs) can acquire strong anti-tumor activity after priming with Paclitaxel (PTX) because MSCs secrete a high amount of membrane microvesicles that will contain the drug [34]. Another study reported how melanoma cells can be loaded with Survivin T34A and Gemcitabine to produce exosomes that carry the drug to treat the pancreatic adenocarcinoma [35]. Doxorubicin and Metotrexate have been loaded into tumoral cells and their apoptotic bodies containing the drug were used to kill tumor cells with reduced side effects [36]. Cells have been loaded with NPs too: SPIONs have been loaded in mesenchymal stem cells to produce charged EVs to treat leukemia [37], iron oxide NPs and a photosensitizer have been encapsulated in HUVECs and human macrophages to obtain EVs to treat respectively prostate and prostate and cervical cancer [38] [39]. Gene therapy can also be carried out with this approach: for example, mesenchymal stem cells have been loaded with different miRNA to obtain EVs with different aims: increase sensitivity of tumour cells to chemotherapeutic drugs (miRNA-122 [40] and anti-miRNA-9 [41]), inhibit the migration of osteosarcoma cells with miRNA-143 [42] and inhibit glioma growth with miRNA-146b [43].

Table 2. Applications of the membrane functionalization through the indirect methods

Parental cells	Functionalization	Cells engineering conditions	Recipient cells	Treatment conditions	Application	Ref.
HEK293	Tetraspanins (CD63, CD9, CD81)	Transfected at 40~60% confluency using plasmid DNA (1~2 µg/well) for 48h with PureFection Transfection Reagent or FuGENE6 t.r.	HEK293	Cells at confluency of 80% and 50 µg of exosomes	Tracking, imaging and targeting drug delivery	[44]
GM-CSF	Lamp-2b fused to the neuron-specific RVG peptide	Transfected 4d using 5 µg of pLamp2b and 5 µl of TransIT LT1 t.r.	C2C12 and Neuro2A <i>IN VIVO</i> : C57BL/6 mice	Exosomes (12 µg proteins) and 400 nanomoles of si-RNA <i>IN VIVO</i> : i.v. 150 µg of exosomes	Delivering of siRNA to the brain in mice with a reduced immunogenicity	[45]
Immature dendritic cells (imDCs)	Lamp2b fused to CRGDKGPDG	Transfected with the vector expressing iRGD-Lamp2b fusion proteins using Lipofectamine 2000 t.r.	MDA-MB-231 <i>IN VIVO</i> : BALB/c nude mice	2 mM Dox loaded exosomes <i>IN VIVO</i> : i.v. EVs 3mg/kg Dox loaded exosomes	Targeted tumour therapy	[46]
Neuro2A	GPI	Transfected with pLNCX-DAF-R2 or pLNCX-DAF-EGa1 using TransIT 2020 t.r.	Neuro2A, HeLa and A431	40'000 cells/well or cells at a confluency of 80–90% and EVs at 5 µg/mL,	Promoting tumour cell targeting	[47]
HEK293	GE11 or EGF	Transfected with pDisplay encoding GE11 or EGF using FuGENE HD t.r.	HCC70 HCC1954 MCF-7 <i>IN VIVO</i> : RAG2 ^{-/-} mice	1 × 10 ⁵ breast cancer cells and 1 µg of exosomes <i>IN VIVO</i> : i.v. 1 µg of exosomes, once per week for 4 weeks	Delivering of antitumor microRNA to EGFR-expressing breast cancer cells	[48]

follows from previous page

Parental cells	Functionalization	Cells engineering conditions	Recipient cells	Treatment conditions	Application	Ref.
BT474, SKBR3, HER2+, JAWSII DCs, 4T1-HER2 and bmDCs	CEA and HER2 coupled to the C1C2 domain of lactadherin	Transfected with p6mLC1C2 containing either human CEA (nt 1-2025) or human HER2/neu (nt 1-1953)	<i>IN VIVO</i> : C57BL/6J and BALB/c mice, hCEA or HER2 transgenic mice	<i>IN VIVO</i> : 2.6×10 ¹⁰ or 5.2×10 ⁹ or 1.05×10 ⁹ viral particles	Increasing vaccine potency	[49]
HEK293-F, E6 and CT26	PSA and PAP coupled to the C1C2 domain of lactadherin	Transfected with pPSA/Zeo, pPSA-C1C2/Zeo, pPAP/Hygro, or pPAP-C1C2/Hygro, using Lipofectamine LTX reagent and PLUS Reagent	<i>IN VIVO</i> : Male BALB/c or C57BL/6 mice	<i>IN VIVO</i> : 5E7 TCID50 of the MVA-BN-PRO viral vectors once every 2 weeks for a total of 3 treatments.	Targeting of tumour antigens to improve antigen immunogenicity and therapeutic efficacy	[50]
DCs	C1C2 domain of lactadherin	Transfected with modified p6mLC1C2 or pcDNA6-Myc/His using Fugene 6 t.r.	<i>IN VIVO</i> : Balb/C mice	<i>IN VIVO</i> : six inoculums of YAC exosomes with HLA-A2 or five inoculums of YAC/HLA-A2 exosomes with pMAGE-A3	Usage of antibodies against tumour biomarkers to attach the drug target candidates	[51]
THP-1	RGD- DSPE-PEG and/or DSPE-PEG-SH	Incubated with DSPE-PEG-SH and/or DSPE-PEG-RGD for 2 d	MCF-7 and HeLa <i>IN VIVO</i> : tumour-bearing mouse	4×10 ⁵ cells/mL and 100 µL per well of 50 µg/mL exosomes <i>IN VIVO</i> : i.v. 200 µL of exosomes at 5 mg/mL	Active targeted chemo-photothermal synergistic tumour therapy	[52]
THP-1	DSPE-PEG-Biotin and/or DSPE-PEG-FA	Incubated with DSPE-PEG-Biotin and/or DSPE-PEG-Folate for 2 days	HeLa <i>IN VIVO</i> : C57BL/6 mice	40 µg/mL of EVs <i>IN VIVO</i> : i.v. EVs with a total of 1.16 mg iron	Rapid isolation and enhanced tumour-targeting	[53]
Cal 27 cells	DSPE-PEG-Biotin and DSPE-PEG-Folate	Incubated with DSPE-PEG-Biotin and DSPE-PEG-Folate	MDA-MB-231 <i>IN VIVO</i> : BALB/C mice	Series of dose and concentration <i>IN VIVO</i> : 18–22 g of EVs via the tail vein	Enhanced target and synergistic therapy for breast cancer	[54]
HUVECs	DSPE-PEG-biotin (to then attach SA-QDs)	Cultured with DSPE-PEG-biotin for several days and then incubated with SA-QDs	EPCs <i>IN VIVO</i> : nude mice bearing A2058 xenografts	Short-term incubation <i>IN VIVO</i> : injection	Antitumor siRNA delivery	[55]
HUVECs	DSPE-PEG-biotin and SA-FITC	Incubated in modified medium containing 40 µg/mL DSPE-PEG-biotin for several days	HepG2 and 3T3 fibroblast <i>IN VIVO</i> : cervical cancer-bearing male BALB/c mice	5×10 ³ cells per well and 0, 10, 40, 80, 100 and 200 mg/mL of exosomes <i>IN VIVO</i> : exosomes at 5 mg/mL, 200µL per mice	Active targeted drug delivery to tumour cells	[56]
HEK 293T cells	GlucB with sshBirA to conjugate streptavidin-Alexa 680	Transduced with lentivirus vectors, CSCW-Gluc- (IRES-GFP or CSCW-GlucB-IRES-GFP, then infection with CSCW-sshBirA-IRES-mCherry lentiviruses	<i>IN VIVO</i> : athymic nude mice spiked with EV-GlucB	<i>IN VIVO</i> : injected with a bolus of 100 µg EV-GlucB via retro-orbital vein or via tail vein	Multimodal imaging <i>in vivo</i> , as well as monitoring of EV levels in the organs and biofluids	[57]
B16BL6	Streptavidin-lactadherin and biotinylated GALA	4×10 ⁶ cells/dish transfected with the plasmid vector pCMVSAV-LA	MHC class I molecules of DCs	5×10 ⁴ cells/well and exosomes (1 µg of protein) diluted in 0.1 mL of Opti-MEM	Efficient cytosolic delivery of exosomal tumour antigens	[58]

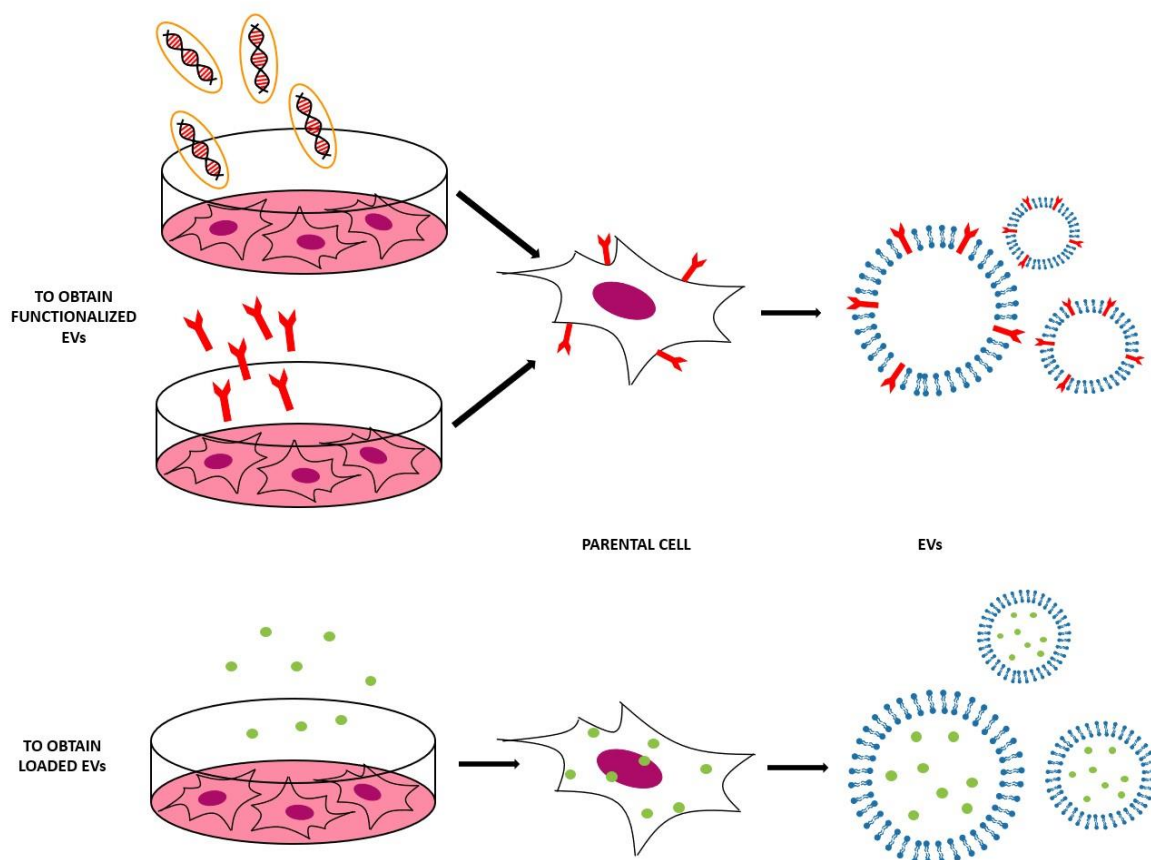


Figure 6. Scheme of the indirect methods used to engineer the EVs, both to functionalize EVs with the molecules of interest (to obtain EVs that expose this molecule on their surface) and to obtain EVs loaded with the desired cargo.

As it is possible to notice, it is important to focus not only on the technical challenges of producing engineered EVs with the indirect methods, but also on the various biological issues that are concerned before, during, and after the EV engineering. As a preliminary step before the engineering process, it is important to design the engineered EVs and to make the right choice in terms of parental cells. Many authors decided to use common cell lines, like endothelial ones (HUVECs) [55] [56] or dendritic cells (DCs) [46] [49] [51], while the others worked with more specific cell lines. From the literature, it is evident that the main challenge in the choice of the parental cells is to become able to work with patient's derived cells in a controllable way and introducing scalable protocols. For example, one of the critical issues is to obtain EVs with compatible characteristics as those of the cells with which they will interact. During the engineering it is important to choose the proper surface modification to achieve the purpose and also to pay attention to the possible unwanted effects. Another challenge is to identify the most efficient way to obtain the functionalization. One of the most popular choices is to transfect the parental cells with the right plasmid vectors and their building is nowadays an important investigation subject in the biological field [44] [45] [46] [47] [48] [49] [50] [51] [58]. The other popular approach is to incubate the cells with DSPE-PEG to both link and further space the membrane from the targeting molecules. Such functional lipids can be actually bound to targeting ligands like biotin, folate, thiol groups or RGD. Biotin can selectively bind to streptavidin, used for further functionalization [54] [55] [56]. Folate is able to target specific cancer cells [53] [54], while thiol groups are useful in many binding reactions [52]. RGD is one of the most common sequence of cellular attachment at the extracellular matrix [52].

After the functionalization, the main biological challenge is to choose the most appropriate cell line or animal model to test the engineered EVs: one of the most popular choices is to use immortalized cell lines, as for example HeLa [47] [52] [53], 3T3 [56] and Neuro2A [45] [47].

Obviously, the main biological challenge of EV testing is to test the formulations on the cells of interest without the drawbacks in terms of time-consuming protocols and scalability obstacles in order to move from *in vitro* to *in vivo* testing easily. Most of the authors that tested their formulation *in vivo* chose transgenic [48] [49] or non-transgenic mice that bear [52] [55] [56] or not [45] [46] [50] [51] [53] [54] autologous tumor or xenografts and that could be athymic [57] or not. Unfortunately, these animal models are not complex enough to simulate the human system and more investigation efforts must be pursued to develop more appropriate testing platforms.

3.2. Direct methods

Several methods are used to modify the surface of EVs after their isolation. These modifications can be carried out to achieve more specific targeting or mimetic features [33]. Most frequently, the aim is to obtain fluorescent and magnetic labelling to track EVs, their biodistribution and pharmacokinetics to investigate their possible diagnostic and therapeutic applications [5]. As EVs are very delicate, it is necessary to pay attention to the reaction conditions to avoid their disruption and aggregation due to inappropriate temperature, pressure and osmotic stresses [19]. Working in mild conditions can help to obtain the most controlled results [5]. After their isolation, EVs surface can be modified in different ways as reported in Table 3 and Figure 7.

3.2.1. Covalent methods

As the classical crosslinking is not enough specific and efficient, the most used covalent method nowadays is the Click Chemistry approach, also known as azide alkyne cycloaddition [59]. With this reaction, an alkyne moiety is reacted with an azide group to form a stable triazole linkage [59]. Some studies also used a copper catalyst to accelerate the reaction [60], but several authors demonstrated that a successful binding can be obtained also without the copper catalyst [61]. One of the strengths of this method is that the experimental conditions are mild and that it can take place in both organic and aqueous media (water, alcohols, dimethyl sulfoxide - DMSO) [62]. The yield is high, the method simple, and it does not impact on EVs size nor on the target cell uptake [62]. This method has however some drawbacks: the alkyne modification of the EV surface most likely occurs on the amine groups of the proteins instead of those of the phospholipids, introducing the possibility that the EV protein function may be inhibited [59]. By controlling the number of alkyne groups, it is possible to avoid the over modification of EV membrane proteins: with a standard calibration curve it has been estimated that approximately 1.5 alkyne modifications are made for every 150 kDa of EV protein [63]. A very common approach is the PEGylation, the modification of EVs surface with polyethylene glycol to extend the circulation half time of the EVs. The drawback of PEGylation is that the PEG corona reduces also the EV-cell interaction and the cellular uptake of the EVs [64]. This disadvantage can be overcome by functionalizing the distal end of the PEG chain with a targeting ligand [5].

3.2.2. Non-covalent methods

These methods are based on mild reactions, such as electrostatic interactions, receptor-ligand bindings, and lipid-conjugated compounds post-insertion into the EV's lipid bilayer [5]. Electrostatic approaches usually involve highly cationic species adhering on negatively charged functional groups present on the biological membranes [5]. A possible drawback of these methods is that certain cationic nanomaterials can cause cytotoxicity and that they are typically taken up into the cells via endocytosis, leading to lysosomal degradation [19].

3.2.3. Glycosylation

Glycosylation is at the base of many biological functions of EVs, like cargo proteins recruitment and cellular recognition and uptake [65] [66]. Alterations in glycosylation pattern has been associated with different pathologies, for example cancer, and these changes are closely correlated with the specific malignant transformation and progression. This evidence has led to make glycan structure a useful target for anti-tumor applications in theranostics [67] [68]. The manipulation of glycosylation can be done using either enzymes or not.

3.2.4. Hybridization

This method implies the fusion of natural EVs with their artificial counterpart, liposomes, to optimize the properties of native EVs [19]. This can be obtained thanks to the lipid composition of EVs membrane. In this way, the colloidal stability of EVs is improved, increasing their half-life in blood and modifying their immunogenicity profile, possibly decreasing it [59]. The lipid composition has been evidenced to impact on the cellular uptake: EVs hybridized with neutral or anionic lipids have a higher possibility to be taken up by cells than the ones hybridized with cationic lipids [59]. Moreover, hybridization of EVs increases the vesicles size (in a technique-dependent way): this is a drawback because it decreases the *in vivo* retention of the vesicles, but also an advantage as it can improve the drug encapsulation efficiency [59]. Native EVs are actually very small in size and thus limited in their ability to encapsulate large molecules, while larger hybridized EVs can carry larger cargos [59].

Table 3. Applications of the direct methods and graphical abstracts from the references.

Parental cells	Functionalization	Functionalization step	Recipient cells	Treatment conditions	Application	Ref.
Covalent						
PC12 cells	TAMRA-NHS	200 μ L of Exos added to 1 mL 0.1 M sodium bicarbonate with 100mg TAMRA-NHS	PC12 cells	1×10^8 cells and 100 μ L of exosome solutions	Visualizing of cellular uptake and intracellular trafficking of exosomes	[69]
4T1 cells	Alkyne groups conjugated with azide-fluor 545	80 μ g of exosomes in PBS, Cu (II) sulfate pentahydrate, 1.44 M l-ascorbic acid and bathophenanthroline disulfonic acid disodium salt trihydrate	4T1 cells	Cells at a confluency of 75% and 5 μ g of exosomes in 100 μ L RPMI	Surface functionalization of exosomes	[63]
Neuro2A and platelets	EGFR conjugated to DMPE-PEG derivatives	Conjugation in a 8.6 : 1000 molar ratio of nanobody : DMPE-PEG-maleimide micelles and then mixed with EVs	A431 and Neuro2A <i>IN VIVO</i> : CrI:NU-Foxn1nu mice with human tumour xenografts	3×10^4 cells/well and 8 μ g/mL of EVs <i>IN VIVO</i> : i.v. of 2.5 μ g of EVs in 100 μ L PBS	Enhancing cell specificity and circulation time of EVs	[64]
Bovine serum	DSPE and chemical conjugation by NHS-PEG	Physical: DSPE-PEG-biotin mixed with the EXOs (500 μ g in PBS) Chemical: NHS-PEG-biotin reacted with the primary amines (500 nmol) on the EXOs.	RAW264.7, DC2.4 and NIH3T3 <i>IN VIVO</i> : mice	6×10^5 or 4×10^5 cells/well and EXOs at an ICG concentration of 5.8 μ g per well <i>IN VIVO</i> : s.i. at a Dil dose of 1.52 μ g/kg	Efficient delivery of immune stimulators and antigens to the lymph nodes <i>in vivo</i>	[70]
RAW 264.7 cells and BMM from C57BL/6 mice	DSPE-PEG or DSPE-PEG-AA	Addition of DSPE-PEG or DSPE-PEG-AA at 50 μ g/mL	<i>IN VIVO</i> : C57BL/6 with induced pulmonary metastases	<i>IN VIVO</i> : i.v. injected with the exos at 10^8 particles/100 μ L, n = 4 per group	Targeted Paclitaxel delivery to pulmonary metastases	[71]

follows from previous page

Parental cells	Functionalization	Functionalization step	Recipient cells	Treatment conditions	Application	Ref.
Covalent						
HEK293T cells	FA, PSMA RNA aptamer and EGFR RNA aptamer conjugated to 3WJ	Cholesterol-triethylene glycol was conjugated into the arrow-tail of the pRNA-3WJ to promote the anchorage of the 3WJ onto the EV membrane	MDA-MB-231, KB, LNCaP (PSMA+), PC3 (PSMA-) <i>IN VIVO</i> : KB xenograft mice model	Incubation with cells <i>IN VIVO</i> : 1 dose of equivalent 0.5 mg siRNA/kg every 3 days total 6 doses	Control RNA loading and ligand display on EVs for cancer regression	[72]
RAW 264.7	NRP-1-targeted peptide RGE	Surface modification with sulfo-NHS that can react with azide-modified RGE peptide, using salts and copper as catalyst	U251, and Bel-7404 <i>IN VIVO</i> : orthotopic glioma-bearing BALB/c nude mice	Cells and Exos at the equivalent of 15 µg/mL of Cur/SPIONS <i>IN VIVO</i> : i.v. of Cur/SPIONS at 800 µg/200 µg Exos/200 µL PBS	Facilitate simultaneous imaging and therapy of glioma <i>in vitro</i> and <i>in vivo</i>	[73]
Non-Covalent						
HeLa	Cationic lipid formulation, LTX and GALA	20 µL LTX added to a solution of exosomes and 20 µL GALA and incubated for 20 min at room temperature	HeLa and (CHO)-K1	2 mL with 2×10^5 cells and 20 µg/mL of exosomes	Enhancing cytosolic delivery of exosomes	[74]
RTCs	Superparamagnetic magnetite colloidal nanocrystal clusters	1 mL of serum incubated with 200 µL of M-Tfs solution for 4 h at 4°C	H22 cells <i>IN VIVO</i> : Kunming mice bearing a subcutaneous H22 cancer	0.1 mg/mL of EXOs in a simulated blood circulation at 32.85 cm/s (artery), 14.60 cm/s (vein), and 0.05 cm/s (capillary)	Targeted drug delivery vehicle for cancer therapy with magnetic properties	[75]
Human serum and C2C12	Rhodamine-labelled M12-CP05 FITC-labelled NP41-CP05	CP05 (200 µg/mL) incubated with nickel beads, added into the precentrifuged serum (200 µL) and incubated for 30 min at 4°C under rotation	<i>IN VIVO</i> : dystrophin-deficient and immunodeficient nude mice and C57BL/6 mice	<i>IN VIVO</i> : i.m. 1 or 2 µg of EXOs, i.v. EXOs in 100 µL of saline solution	Enabling targeting, cargo loading and capture of exosomes from diverse origins.	[76]
4T1, MCF-7, and PC3	DiR labelling	5 µL of DiR, at a concentration of 220 µg/mL in ethanol, were mixed with 220 µg exosomes or liposomes in 100 µL PBS for one hour	<i>IN VIVO</i> : Balb/c, nude, and NOD.CB17-Prkdcscid/J mice with either 4T1 cells or PC3 cells	<i>IN VIVO</i> : i.v. 60 µg of DIR-labeled exosomes in 200 µL PBS or i.t. 60 µg of DIR-labeled exosomes in 50 µL PBS	Biodistribution and delivery efficiency of unmodified tumour-derived exosomes	[77]
Glycosylation						
MLP29	Neuraminidase	Surface glycosylation of the EVs was manipulated by treatment with neuraminidase to remove the terminal residues of sialic acid	<i>IN VIVO</i> : wild-type mice	<i>IN VIVO</i> : i.v. of the EVs	Modification of the glycosylation of EVs to alter their biodistribution <i>in vivo</i>	[78]

follows from previous page

Parental cells	Functionalization	Functionalization step	Recipient cells	Treatment conditions	Application	Ref.
Glycosylation						
U87 and GBM8	Glycosylation and insertion of targeting ligand to DC-SIGN	Treated with a pan-sialic acid hydrolase Neuraminidase for 30 min at 37°C and/or incubated with palmitoyl-LewisY while vortexing for 10 min.	MoDCs	500'000 cells incubated with EVs for 45 min on ice to allow receptor binding	Enhancing receptor-mediated targeting of dendritic cells	[79]
HEK293FT	Glycosylation of targeting-peptide-Lamp2b fusion proteins	1.5 mL of 0.971 M sucrose was slowly pipetted underneath the 8.5 ml of exosome solution	HEK293FT and Neuro2A	Cells at 50% confluency and EVs for 2 h at 37 °C	Stabilization of exosome-targeting peptides	[80]
Hybridization						
HEK293FT	CRISPR/CRISPR-associated protein 9 (Cas9) system	Addition of the plasmid-liposome complex to exosomes and incubated at 37 °C for 12 h in a volume ratio of 1:2	MSCs	Incubation with cells at 90% of confluency	Efficiently encapsulate large plasmids and be endocytosed in MSCs	[81]
RAW 264.7, CMS7-wt and CMS7-HE	DOPC, DOPS, DOTAP, DOPS/PEG-DSPE	Exosomes (300 µg/mL, protein) mixed with 100 µM liposomes in a volume ratio of 1:1 and then several freeze-thaw cycles	HeLa cells	4.5 µg protein in exosome incubated with 1×10 ⁵ HeLa cells for 4 h at 37 °C	Control and modify the performance of exosomal nanocarriers	[82]
HUVECs and MSCs	Phosphatidylcholine, Phosphatidylethanolamine and PEG	Liposomes and EVs were mixed at 40 °C in a total volume of 40–200 µL (2×10 ¹⁰ or 2×10 ¹¹ objects). liposome/EV ratio of 1:1, 1:9 or 9:1 in PBS. PEG was added at 5–30% (w/v)	THP1-derived macrophages and CT26	100,000 cells per well and hybrid EVs containing 1 mol % of DiR, cells and 400 µL of mTHPC-loaded hybrid EVs or (3D) 500 cells and mTHPC-loaded hybrid EVs	Design of personalized biogenic drug delivery systems	[83]
J774A.1	L-α-phosphatidylcholine and Cholesterol	EVs (200 µg protein) used to hydrate the dry 1000 µg of lipid film in a final volume of 1 mL, then the solution was extruded through 400 and 200 nm polycarbonate membrane filter	K7M2, 4T1 and NIH/3T3	10'000-20'000 cells and 4 mL of 50 µg/mL of hybrid EVs at 37°C for 3h or 48 h	Tumour targeted drug delivery	[84]

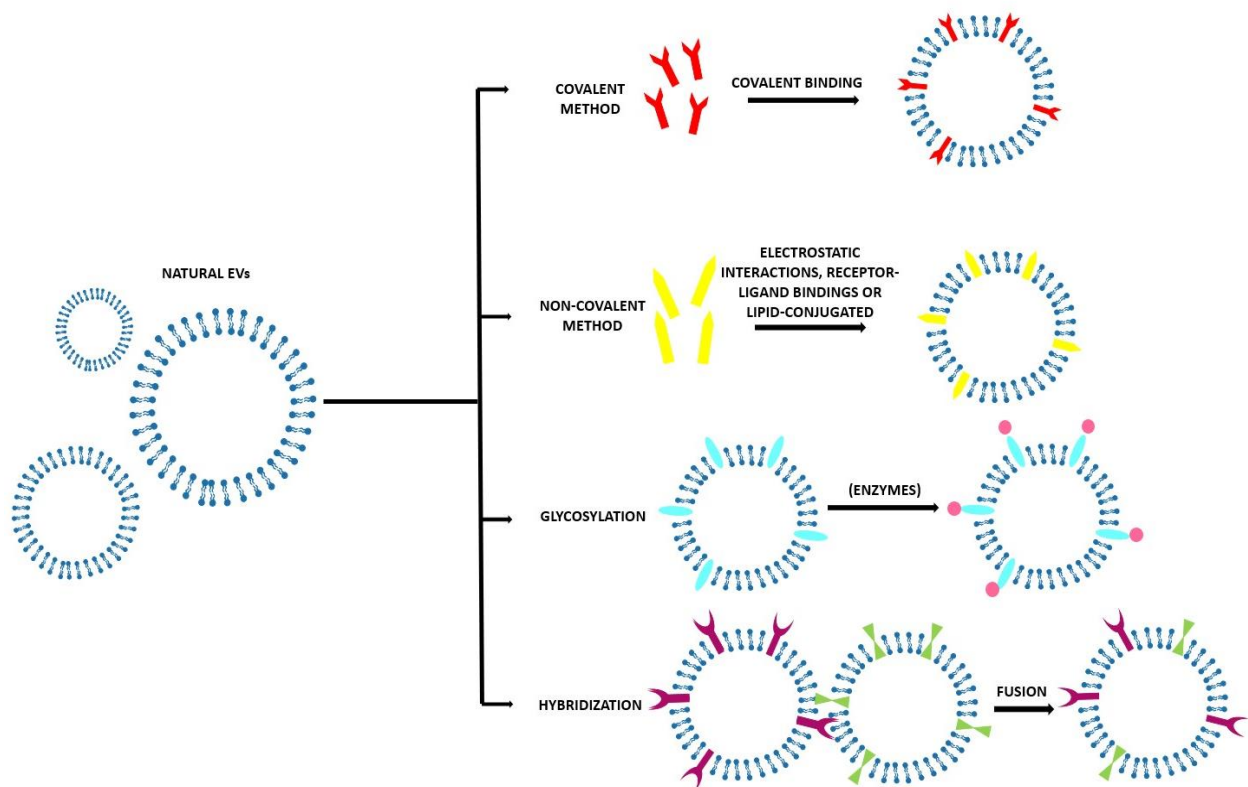


Figure 7. Scheme of the various direct methods to obtain engineered EVs with the desired characteristics and with the molecules of interest on the surface.

As for the indirect methods, it is important to remember that the technical challenges to engineer the EVs with the different direct methods are directly correlated with the biological challenges that are fundamental in every step of the EVs engineering, from the preliminary design to the real-environment testing. For what concerns the choice of the parental cells, in some works the authors chose the RAW 264.7 macrophages, an immortalized cancer cell line [71] [73] [82], other immortalized cell lines like HeLa [74] or Neuro 2A [64], or even extracted the desired cells directly from mice [71] or human serum [76]. As stated before, the main biological challenge is to find a scalable and controllable way to use the patient's cells as source, in order to obtain EVs that are possibly compatible to the patient environment. For what concerns the functionalization, it is important to find the proper molecule for the desired purpose and a variety of functionalization are reported in the literature, as mentioned above. As for the indirect methods, the use of DSPE-PEG [70] [71] [82] or DMPE-PEG [64], as spacer to expose the functionalization, is a commonly used strategy. Finally, for both *in vitro* and *in vivo* the testing steps, the biological challenges are the same listed above and analyzed for the indirect methods in terms of choice of the best cell line and/or animal model.

At this point, it is clear that the functionalization of EVs with ligands and other molecules can boost up their stability in blood circulation, capability of localize the target site and increase their intracellular delivery efficiency [85]. The main drawback of the EV engineering is the introduction of the risks of altering the orientation of membrane proteins, which may compromise their biological functionalities or even induce immunogenicity [33]. Further risks of the EV engineering are associated to the hiding of these proteins or to the damage or disruption the EV membrane [85]. For this reason, developing bioinspired, synthetic and chimeric EV-like alternatives is increasingly promising to broaden the therapeutic application of these natural biovesicles [85].

4. Synthetic and Chimeric EVs

As stated before, EV-based nanomedicine has many advantages as the specificity in targeting and the innate biomimicry. However this approach has severe drawbacks too, like the lack of purification protocols at a

large-scale clinical grade, the potential safety concerns, the parental cell dependent composition and the inefficient drug payload [85]. These reasons are keeping EVs far from becoming a therapeutic reality [85]. To overcome these drawbacks, some alternative strategies have been promoted to develop artificial EVs. To build these particular devices, two main methods have been developed: the top-down and the bottom-up ones.

4.1. Top-down approaches

The top-down method is based on the disruption of the cells of interest in little fragments that will then self-assemble in nanovesicles and microvesicles of various sizes with the same membrane features of the initial cell. The breaking of the cell membrane is physically obtained and for this reason these vesicles are also called physical-origin EVs. As they are obtained from cells, they are a good imitation of EVs and they incorporate the proteins and the biologically active molecules, but the yield of the production can increase by 100 times [86]. These artificial EVs can be obtained in two different ways: the simplest is extruding the cells through polycarbonate membranes with decreasing pores size (for example from 10 μm to 5 μm to 1 μm [86]). The choice of the pore size is important: in this way the cells, that are typically bigger than 10 μm , are disrupted by the first membrane while organelles bigger than 1 μm are retained by the last membrane. The obtained vesicles have thus a diameter in the range below 1 μm .

The other top-down method consists in using a microfluidic device that contains an array of hydrophilic microchannels. After injecting the cells in this device, they undergo to the shear-stress and they break in the membrane fragments that will then reassemble mainly in nanovesicles. One of the main advantages of top-down methods is that the techniques to modify cells before EVs isolation can be easily applied in this case too in order to obtain specific components on the artificial EVs membrane [87]. As the nanovesicles are directly derived from cells, they have a high biocompatibility, reduced clearance and enhanced delivery efficacy thanks to the increased cellular uptake. These nanovesicles can be used to carry cargos or as therapeutic agents (without cargos) for cancer immunotherapy [88], cell proliferation and tissue regeneration [89]. The top-down approach has disadvantages too: it is necessary (as for natural EVs) to have a purification protocol and it is very difficult to control the production and standardize the properties of these artificial EVs. The biological challenges that are directly linked with the top-down method in terms of parental cells choice and *in vitro* and *in vivo* testing are the same listed for the engineered EVs.

Some examples of top-down approaches are reported in Table 4 and Figure 8.

Table 4. Applications of the top-down methods.

Precursor Cells	Recipient Cells	Application	Ref.
Extrusion			
U937 and RAW 264.7	TNF- α treated HUVECs <i>IN VIVO</i> : colon adenocarcinoma induced CT26 mouse	Targeted delivery of chemotherapeutic drugs	[86]
RAW 264.7 and HB1.F3	<i>IN VIVO</i> : male BALB/c mice	Radiolabelling of EVs with $^{99\text{m}}\text{Tc}$ -HMPAO to understand <i>in vivo</i> distribution and behaviour of exosomes.	[90]
Murine mouse embryonic stem cell line D3	NH-3T3	Gene delivery of endogenous, precursor cell characteristic RNA (mOct 3/4 and mNanog)	[91]
Murine mouse embryonic stem cell line D3	Primary murine skin fibroblasts from BL6/C57 mice	Investigate the ability of these nanovesicles to improve proliferation by treating cells with the nanovesicles	[92]
Non-tumorigenic epithelial MCF-10A cells	MCF-7 <i>IN VIVO</i> : BALB/C nu/nu mice	Evaluation of the EVs biosafety and uptake efficiency for the delivery of CDK4 siRNA	[93]
MSCs	MDA-MB-231 <i>IN VIVO</i> : nude BALB/c mice	Targeted delivery of Paclitaxel for cancer treatment	[94]
H19-OE lentiviral vector transfected HEK293	HMEC-1 <i>IN VIVO</i> : diabetic rat model	Treatment of diabetic wounds through the delivery of lncRNA-H19	[95]

follows from previous page			
Precursor Cells	Recipient Cells	Application	Ref.
Extrusion			
MIN6 and NIH3T3	<i>IN VIVO</i> : BALB/c and NSG mice	Facilitate the differentiation of bone marrow cells to insulin-producing cells (β -cells)	[96]
Primary hepatocytes	Primary hepatocytes <i>IN VIVO</i> : two-thirds PH mouse model (C57Bl/6)	Promote hepatocyte proliferation and liver regeneration	[97]
ASCs	MLE-12 <i>IN VIVO</i> : C57BL/6 mice	Inhibition of emphysema through increasing the proliferation rate of lung epithelial cells	[98]
MSCs	RAW 264.7 <i>IN VIVO</i> : wild-type mice C57BL/6	Treatment of sepsis by down-regulate the cytokine storm induced by bacterial outer membrane vesicles (OMVs) in mice	[99]
M1 macrophages	CT26 and BMDMs <i>IN VIVO</i> : CT26-bearing mice	Repolarize M2 tumour-associated macrophages (TAMs) to M1 macrophages that release pro-inflammatory cytokines and induce antitumor immune responses	[100]
Natural killer (NK) cells NK92-M1	D54, MDA-MB-231, CAL-62 and HepG2 <i>IN VIVO</i> : female BALB/c nude mice	Immunotherapeutic agent for treatment of cancer	[88]
Microfluidics			
Murine embryonic stem cells (ES-D3)	NIH 3T3	Exogenous material delivery (polystyrene beads)	[101]
Murine embryonic stem cell line-D3	NIH-3T3 fibroblasts	Gene delivery of RNAs, Oct 3/4 and Nanog	[102]

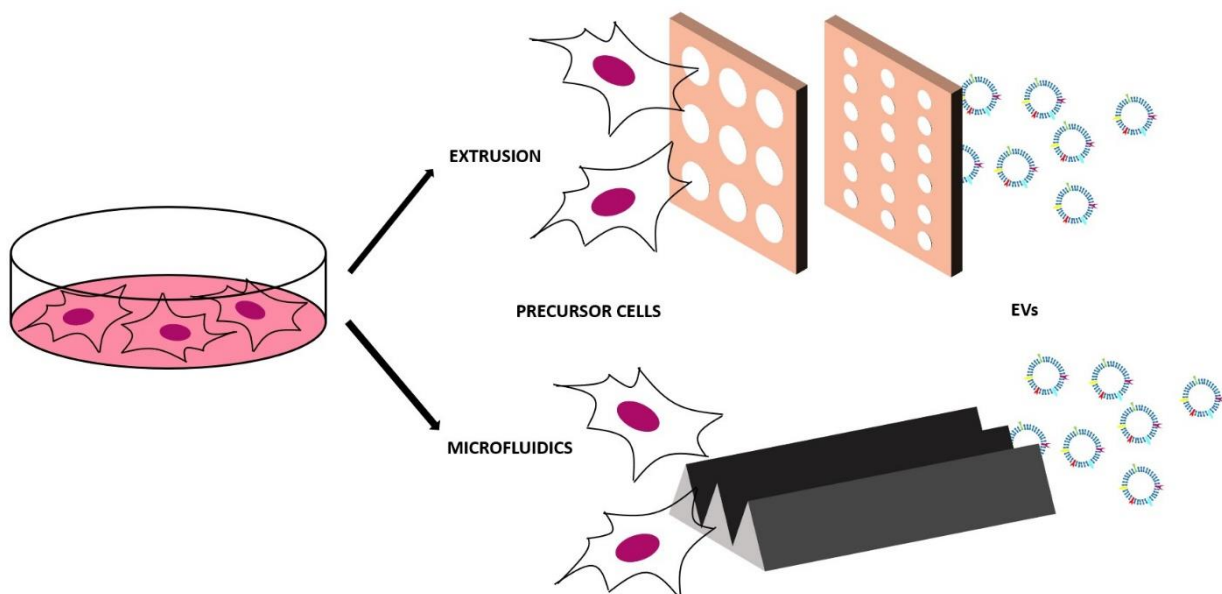


Figure 8. Scheme of the two main top-down approaches to produce synthetic EVs: extrusion and microfluidics

4.2. Bottom-up approach

The bottom-up method starts from small components, i.e. molecular building blocks to obtain complex structures, namely the synthetic EVs [85] [87]. The aim is to mimic the natural EVs using specific lipids composition and then functionalize this synthetic lipid bilayer (liposome) with the proteins that are necessary for the targeting/biomimetic purposes with the same techniques used to engineer the natural EVs [87]. This method has been developed starting from two important hypotheses:

1. Not all the components in natural EVs are essential for the specific therapeutic application [85].
2. Liposomes have a spherical lipid bilayer structure as the EVs and their properties, like diameter, lipid composition, functionalization, can be tuned [87].

To obtain the starting liposome, two main techniques apply [87]: the simplest is the thin film hydration in which a dried film of lipids is hydrated by an aqueous medium containing the desired cargo [87]. The other one is based on a microemulsion approach and micelle assembly in the medium containing the compound to be encapsulated [87]. Both methods present the advantage to produce fully artificial EVs, with the wanted clean composition, scalable production protocol and the use of pharmaceutical acceptable components, that makes bottom-up EVs a high pharmaceutical grade product [87]. However, bottom-up methods have also drawbacks: it is necessary to have a deep knowledge of every EVs component to understand how to build a synthetic one, the high-purity lipids are often very expensive and it is possible that during the process the proteins lose their function [85].

Examples of bottom-up approaches are reported in Table 5 and Figure 9.

Table 5. Applications of the bottom-up methods and graphical abstracts from the references.

Formulation	Recipient cells	Application	Ref.
PC:CHOL:DSPE-PEG:DSPE-PEG-MAL liposome coated with: MHC Class I/ peptide complexes, anti LFA1, anti CD28, anti CD27, anti 4-1BB, anti CD40L and T cell receptors in the form of Fab antibody regions	T-cells <i>IN VIVO</i> : BALB/c mice	Targeted immunotherapy, inducing antigen-specific T-cells responses	[103]
DOPC/SM/Chol/DOPS/DOPE at a molar ratio of 21/17.5/30/14/17.5 liposome with siRNA (siNC, FAM-siNC and siVEGF)	A549 and HUVEC	Delivery of VEGF siRNA in a more efficient way and with less cytotoxicity	[104]
DOPC/SM/Chol/DOPS/DOPE at a molar ratio of 21/17.5/30/14/17.5 liposome integrated with connexin 43 (Cx43)	A549 and U87 MG	Delivery of siRNA	[105]
CH/PC/SM/Cer at a weight ratio of 0.9/1/0.4/0.03 functionalized with recombinant human integrin $\alpha 6\beta 4$ protein, Bovine Serum Albumin and Lysozyme	A549 <i>IN VIVO</i> : mice bearing lung cancers	Targeted delivery of therapeutic oligonucleotides to lung adenocarcinoma cells (microRNA-145 mimics)	[106]
Phosphatidylcholine, SM, ovine wool cholesterol, and DOGS-NTA in a weight ratio of 55:30:10:5 liposome bonded with histidine-tagged APO2L/TRAIL	<i>IN VIVO</i> : adult female NZW rabbits	Treatment of antigen-induced arthritis (AIA)	[107]
Phosphatidylcholine, sphingomyelin (SM), cholesterol, DOGS-NTA-Ni liposome with rAPO2L/TRAIL	Jurkat clone E6.1, U937, U266 and MM.1S	Apoptosis-inducing ability haematological tumours	[108]
Cremophor EL, PC, DOPE and DC-Chol liposome conjugated with DEC205 monoclonal antibody	DCs	Development of antigen carriers for specific DCs targeting.	[109]
* Membrane proteins derived from RBCs (containing high CD47 levels to inhibit phagocytosis) and MCF-7 cancer cells (containing specific adhesion proteins) integrated into synthetic phospholipidic bilayers	MCF-7, HeLa and RAW264.7 <i>IN VIVO</i> : MCF-7 tumour-bearing nude mice	Higher tumour accumulation, lower interception and better antitumor therapeutic effect	[110]
* Proteins derived from the leukocytes' plasmalemma through extrusion integrated into a synthetic phospholipid bilayer (DPPC, DSPC and DOPC and cholesterol)	<i>IN VIVO</i> : BALB/C mice	Selective and effective delivery of dexamethasone to inflamed tissues, and reduced phlogosis in a localized model of inflammation	[111]
* Membrane proteins derived from leukocytes from human blood and immortalized J774 murine macrophages within the lipid bilayer of liposome-like nanovesicles (DPPC, DOPC and cholesterol in a molar ratio of 4/3/3)	HUVECs <i>IN VIVO</i> : Balb/c mice	Avoidance of macrophage uptake and promoting the adhesion to inflamed endothelium	[112]

*In these works, the EVs-like nanovesicles are obtained with a bottom-up technique, but they integrate cellular membrane fragments that are extracted from cells with a top-down approach.

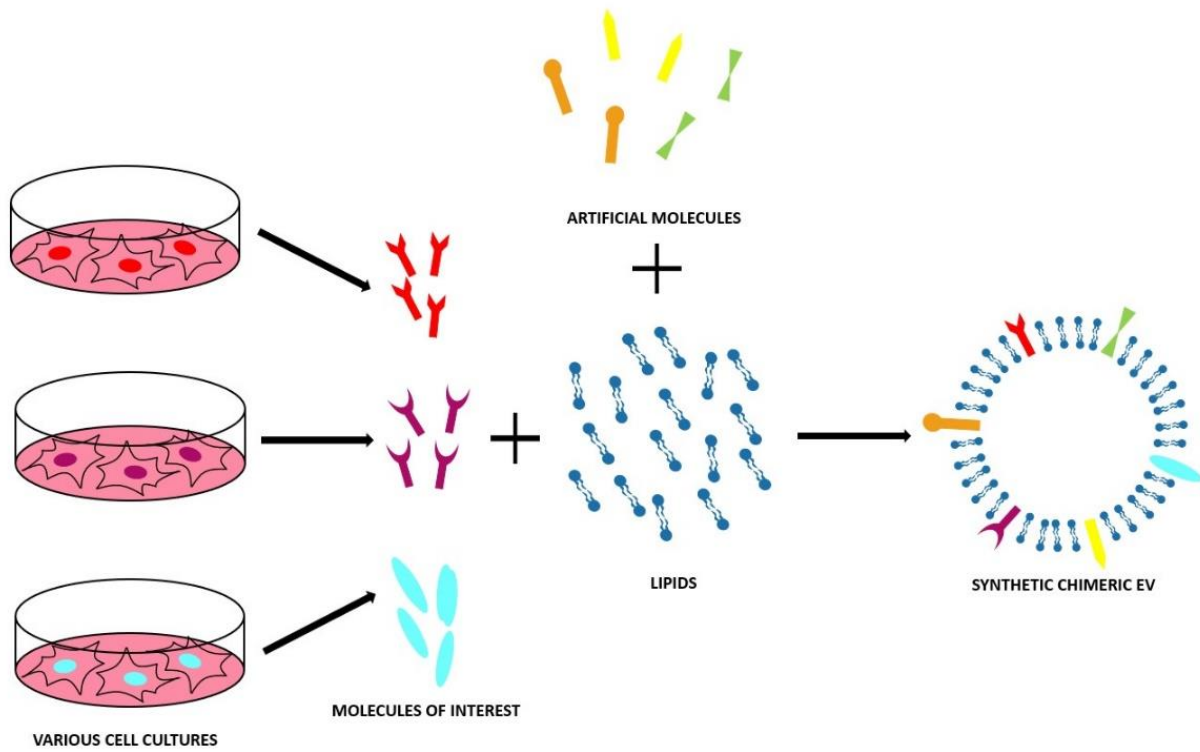


Figure 9. Scheme of the bottom-up approach to obtain synthetic chimeric EVs using artificial compounds or molecules from cells

Mesoporous Silica coated with different lipidic formulations as drug delivery system

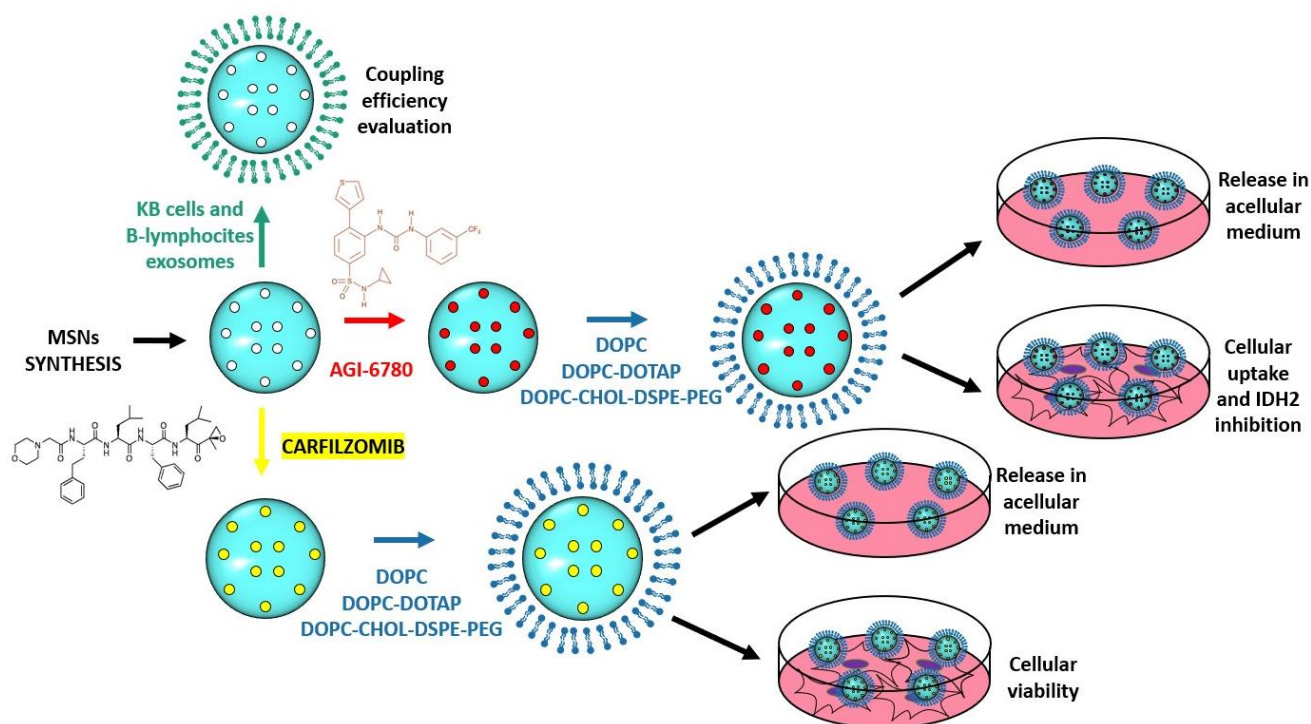


Figure 10. Graphical representation of the experimental section

The most important goal in chemotherapy is to achieve the tumour-specific delivery of the drugs [113], avoiding the many side-effects of these treatments and allowing to reach the same therapeutic effect with lower doses of drug. In fact, therapies that are nowadays based on chemotherapy and immunosuppression provoke the onset of several adverse effects: as the main purpose of anticancer drugs is the blocking of the uncontrolled proliferation characteristic of cancer cells, they also affect cells that naturally have high proliferation, such as blood cells, hair follicles, stomach cells or reproductive system's cells. Moreover, despite the multitude of anti-cancer drugs presented in the market and their ability to create potent and lethal interaction with cancer cells *in vitro*, their therapeutic efficacy remains affected by their low aqueous solubility and eventually not reaching a high enough concentration in the site of absorption [113]. With the aim overcome these obstacles, a growing number of novel drug delivery systems, particularly nanostructures, have been developed and their most important parameters were evaluated, in particular the loading capacity and drug release profiles [113]. Focusing on Mesoporous Silica, its excellent features, including huge surface area (up to 1200 m²/g) and ordered porous interior, let it to be used as a reservoir to store different anti-cancer drugs with high loading capacity and tuneable release mechanisms [113]. Concerning the porosity, it is very high (1 cm³/g), the pore size can be customized ranging from 2 up to 10 nm to selectively load either hydrophobic or hydrophilic anticancer agents, and the pores can be obtained with an hexagonal symmetry or in a worm-like structure making MSNs a very versatile platform [113].

One of the most important things is that the colloidal stability of MSNs in biological media has to be strictly preserved to avoid aggregation and degradation phenomena [114], as it can negatively impact on the endocytosis process and the further molecule delivery inside the tumour cells. A recent strategy was proposed yet enveloping the MSNs in double lipidic layers. This nanoconstruct, also called "protocell" by J. Brinker and co-workers [115], has several advantages: despite guaranteeing the colloidal stability of MSNs,

it increases the biocompatibility toward the cell surface, improves the uptake by endocytosis inside the tumour cell, and reduces off-target delivery of drugs. Actually, the lipidic bilayer offers an actionable gate-keeper [116] [117], avoiding the loss of drug loaded into the mesopores in the extracellular medium, while guaranteeing the drug delivery only intracellularly.

In this Master Thesis the efficiency of MSNs coated by three different types of lipidic bilayers (MSN@SLB) to encapsulate a specific drug and deliver it to cancer cells of Multiple Myeloma was analyzed. Exosome were also tested as biomimetic coating for MSNs, but only the synthetic lipidic formulations were used to camouflage the drug-loaded MSNs.

Multiple Myeloma (MM) is a disease ranging from monoclonal gammopathy of unknown significance (MGUS) to plasma cell leukemia. MM is characterized by a proliferation of malignant plasma cells and a subsequent overabundance of monoclonal paraprotein (M protein). It has been demonstrated that mutations in the IDH1/2 genes are a rare event in MM (0.5%) [118].

The first encapsulated drug was AGI-6780, a potent and selective inhibitor of mutant IDH2/R140Q a tumor-associated mutant of isocitrate dehydrogenase IDH2. IDH is a metabolic enzyme that catalyze the oxidative decarboxylation of isocitrate, producing alpha-ketoglutarate (α KG) and CO_2 . In humans, IDH exists in three forms: IDH1, IDH2 and IDH3. Concerning the focus of this Master Thesis, IDH2 plays a key role in cellular metabolism and acts in the tricarboxylic acid (TCA) cycle catalyzing the reversible oxidative decarboxylation of isocitrate to alpha-KG, NADPH, and CO_2 . In addition, by providing mitochondrial NADPH, IDH2 protects from ROS-mediated oxidative damage, avoiding lipid peroxidation and DNA damage [118]. Therefore, given the critical role of IDH2 in mitochondrial bioenergetics, cellular stress responses and macromolecular synthesis, its inhibition is expected to affect growth and survival of cancer cells to some extent [119]. Interestingly, aberrant expression of wild-type IDH2 was recognized in several cancers. Specifically, IDH2 was found downregulated in melanomas, kidney cancer, hepatocellular carcinoma, gastric cancer and gliomas [120]. On the contrary, IDH2 was described highly expressed in multiple malignancies, such as esophageal squamous cell, ovarian, and lung cancers, and high levels of IDH2 were correlated with poor survival [121] [122]. Bergaggio *et al* results suggested the hypothesis that inhibition of wild-type IDH2 may have therapeutic potentials regardless of IDH2 expression levels. Moreover, it has been reported that the inhibition of IDH2 expressions could increase the efficacy of conventional cancer therapies, such as chemotherapy, radiotherapy, photodynamic therapy, and small molecule inhibitors [120] [123]. This combinatorial effect occurs when IDH2 expression is both down or upregulated, and also when it is expressed at normal levels, increasing the applicability of IDH2 as potential targets for cancer therapy. However, inhibitors directed against native IDHs are not present on the market. AGI-6780 reduced (R)-2HG levels in cell lines overexpressing IDH2/R140Q with an EC50 of 20 nM, and induced differentiation of TF-1 erythroleukemia and primary human acute myelogenous leukemia cells *in vitro*. AGI-6780 binds allosterically at the dimer interface of IDH2. AGI-6780 shows good selectivity against other dehydrogenases, including the closely related IDH1-WT or R132H mutant enzymes [119]. The inhibition of IDH2 is per se non-cytotoxic in MM, except in very high doses, and also the IDH2 inhibitor AGI-6780 has failed the clinical translation as a free drug, owing to its very low bioavailability and high hydrophobicity *in vivo* [119]. Recently, the combination of IDH2 inhibitor (AGI-6780) together with FDA-approved proteasome inhibitor (PI) Carfilzomib (CFZ) was proposed as a powerful therapeutic strategy against MM [120], even in cases of developed drug resistance to Carfilzomib alone. Bergaggio *et al*. [123] demonstrated that IDH2 hyperactivity (but also normal activity) antagonizes the therapeutic efficacy of first and second generation PI and this is the reason why pharmacological IDH2 inhibition is a suitable strategy to enhance the therapeutic efficacy of PI in MM and other B-cell haematological malignancies.

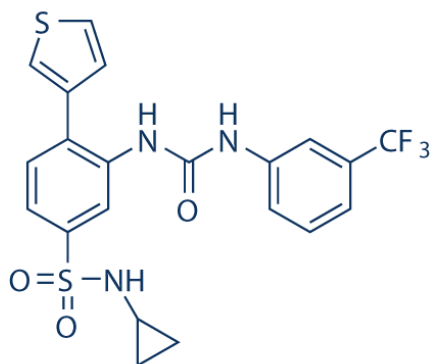


Figure 11. AGI-6780 chemical formula [119]

The second encapsulated drug was Carfilzomib, that is a drug belonging to the second generation of proteasome inhibitors, which revealed to be both tolerable and active against relapsed and/or refractory multiple myeloma, in addition to allow a long-duration inhibition. Proteasome inhibitors are a particular type of anticancer drug which are able to interfere with the ubiquitin proteasome pathway (UPP). UPP is a complex protein degradation pathway present in all eukaryotic cells, with essential functions in homeostasis. Cancer cells use this enzymatic pathway to produce proteins that promote both cell survival and proliferation, in addition to inhibit mechanism of cell death. Proteasome Inhibitors can shift this fine equilibrium to cell death. Subsequently, Carfilzomib received accelerated approval in 2012 by the FDA as a single agent for the treatment of multiple myeloma in patients who have received at least two prior lines of therapy, and with disease that was refractory to the most-recent line of treatment [120]. Recent studies, already published, reveal that combination of CFZ with AGI-6780, an inhibitor of mutant isocitrate dehydrogenase (IDH2/R140Q), could induce apoptosis in cultures cell lines, even those with developed drug resistance, which happens in the case where CFZ is used alone [121]. The NPs loaded with a combination of two drugs are called “Synthetically lethal nanoparticles” [120]. Previous studies already explored the possibility to encapsulate a proteasome inhibitor in MSNs: Shen J. *et al* [127] used hollow MSNs to encapsulate Bortezomib, the first clinically approved proteasome inhibitor for treating multiple human malignancies, whose poor water-solubility and low stability and the emergence of tumour resistance have restrained its therapeutic efficacy. The results of the encapsulation of this drug in MSNs were very promising: *in vivo* tumor-suppression assay further indicated that these loaded constructs showed approximately 1.5 folds stronger anti-tumor activity than free Bortezomib.

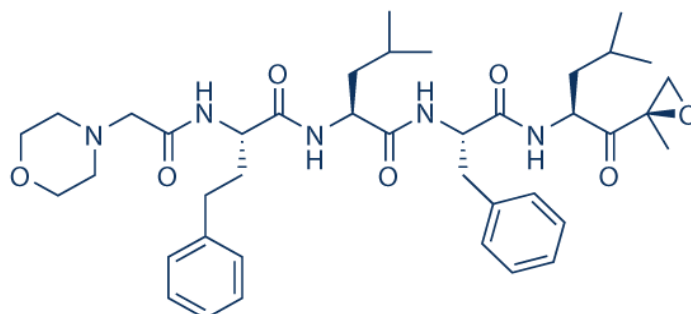


Figure 12. CARFILZOMIB chemical formula

1. Materials and Methods

1.1. MSNs Synthesis

Firstly to synthesise mesoporous silica nanoparticles a template-assisted sol-gel self-assembly (Stöber process) was performed. To do that, one solution of 14.3 g of triethanolamine (TEA, 99%, Sigma-Aldrich) and 1.92 g of tetraethyl orthosilicate (TEOS, 98%, Sigma-Aldrich) was prepared and heated at 90 °C during 20 minutes without stirring in a 100 mL polypropylene reactor. A second solution was also prepared with 2.41 mL of cetyltrimethylammonium chloride (CTAC, Sigma-Aldrich) and 21.7 g of bidistilled water from Milli-Q system and heated at 60 °C. Further, the two solutions were quickly combined and stirred at 500 rpm during 30 minutes, to homogenize the solution.

To functionalize the external surface of MSNs with amino-propyl groups (-NH₂) a solution 1:1 of 20.6 µL of TEOS and 16.1 µL of (3-aminopropyl)trimethoxysilane (APTES, 98%, Aldrich) was prepared, where the molar amount corresponds to the 1% of the starting TEOS in the first solution mixture. This solution was added to the mixture after exactly 30 min from the reaction start, and left stirring (VELP Scientifica, AREX DIGITAL) overnight at 500 rpm at room temperature, which in the end leads to a white colloidal suspension.

After that, 100 mL of ethanol (EtOH, 96%, Sigma-Aldrich) was added to the solution and then centrifuged (VWR, Mega Star 600R) at 3'000 RCF for 10 minutes. The supernatant was removed (where pH was measured to know where to discard solution – silica- a basic one) and a solution of 2g of ammonium nitrate (NH₄NO₃, 98%, Sigma-Aldrich) in 100 mL of EtOH was added to the pellet, in a way to extract the organic template from the MSNs. The solution was heated at 90 °C for 45 minutes under reflux.

A further centrifugation was performed at 10'000 RCF for 5 minutes, the supernatant was removed and the pellet was redispersed in a solution of 10 mL of concentrated hydrochloric acid and 90 mL of ethanol and heated at 90°C for 45 minutes under reflux. The MSNs were then separated by centrifugation at 10'000 RCF for 5 minutes, washed thoroughly with ethanol and centrifuged (10'000 RCF for 5 minutes) for at least three times. The pelleted MSNs were finally resuspended in 15 mL ethanol and an aliquot of 500 µL was dried at 60°C in oven and EtOH removed, to measure the final concentration, which was between 13.6 mg/mL (MM3 - second synthesis batch) and 18.7 mg/mL (MM2 - first synthesis batch).

1.2. Lipid Bilayer Formation

The lipid bilayer was formed after drug uptake on the mesoporous silica nanoparticles. MSNs encapsulating CFZ and AGI-6780 (see Paragraph 1.5.2.1.), both obtained from Selleckchem (Munich, Germany), were then coated with three different synthetic lipid formulations.

The first was composed by DOPC (1,2-dioleoyl-sn-glycero-3-phosphocholine, 2.5 mg Avanti Polar). The second one was formulated by mixing DOPC and DOTAP (N-[1-(2,3-Dioleoyloxy)propyl]-N,N,N-trimethylammonium methyl-sulfate, Avanti Polar) at a mass ratio of 70 : 30 as mentioned in [114] (resulting in 1.75 mg DOPC and 0.75 mg DOTAP, i.e. a molar ratio of 2 : 1). The third lipid composition DOPC-cholesterol-DSPE-PEG₂₀₀₀ was prepared mixing DOPC, DSPE-PEG₂₀₀₀ (1,2-distearoyl-sn-glycero-3-phosphoethanolamine-N-[polyethylene glycol-2000]-amine, Avanti Polar) and cholesterol (Sigma Aldrich) at a mass ratio of 65.3 : 8.6 : 26.1 (resulting in 2.5 mg DOPC, 1.0 mg cholesterol, 0.33 mg DSPE-PEG₂₀₀₀), i.e. a molar ratio of 55 : 44 : 2, as mentioned in [115]. The respective amounts of lipids were mixed in chloroform in glass vials and then dried overnight in dark conditions. Further the dried lipid mixtures were dissolved in 1 mL of a solution composed by 600 µL of MilliQ bi-distilled water and 400 µL of 99% EtOH (H₂O:EtOH as 60:40 in volume). This mixture guarantees that the lipids are still dispersed as single macromolecules, preventing their assembly in liposomes. 1 mg of MSNs loaded with drug (AGI-6780 or CFZ) or labeled ATTO-550 (2 µL)

were separated by the solvent (either DMSO (Dimethyl Sulfoxide, $\geq 99\%$, Sigma-Aldrich) after drug uptake or EtOH after labelling) by centrifugation at 10'000 RCF for 5 minutes. The coupling between the lipids and the MSN was carried out by a solvent exchange method, as in [114]. In particular, 100 μL of lipid solution, prepared as above, was added to each MSN sample, once pelleted after centrifugation. After slight pipetting, 900 μL of MilliQ bi-distilled water was added, obtaining the samples MSN@DOPC, MSN@DOPC-DOTAP or MSN@DOPC-cholesterol-DSPE-PEG. In case of fluorescent labelling, the lipophilic dye DiOC₁₈(3) (3,3'-dioctadecyloxycarbocyanine perchlorate) (DiO; $\lambda_{\text{Ex}} = 488\text{nm}$, Invitrogen, CA, USA) was added (0.5 μL from a stock dye solution of 10 μM in DMSO) to each sample.

1.3. Exosomes isolation and coupling with MSNs

The exosomes used in this work have been extracted by differential ultracentrifugation method using an OptiMax (Beckman Coulter) ultracentrifuge, set with MLA-50 rotor, at 4°C in vacuum. They were isolated from KB cell culture (ATCC® CCL17TM was purchased by the American Type Culture Collection) and from healthy human cell line from blood white cells (B lymphoblasts) supernatants.

Exosomes from FBS were isolated through an overnight centrifugation at 100'000 g at 4°C and then suspended in cold PBS and stored at -80°C. Exosome from KB cell culture supernatants have been extracted by several sterile centrifugation and ultracentrifugation steps.

At first, the cell medium has been centrifuged at 130 g for 10', at a temperature of 4 °C. The pellet obtained by this first centrifugation was constituted by living cells. The supernatant was separated and centrifuged a second time at 2'000 g for 20' (4°C). The obtained pellet was made by dead cells. The supernatant was then separated again and centrifuged at 10'000 g for 30' (4°C) into ultracentrifuge polyallomer tubes, in order to remove cells debris. The supernatant was recollected and centrifuged at 100'000 g for at least 70' (4°C). The pellet obtained was a mixture of exosomes and contaminating proteins, which has been resuspended in 1 mL of sterile filtrated PBS and then centrifuged for the last time at 100'000 g for 60' (4°C). After this last step, the pellet contained only exosomes and other population of extracellular vesicles. It has been resuspended in sterile PBS or sterile physiologic solution (0.9% NaCl in water) and then the 50 μL aliquots have been put in cryovials at -80°C for storage.

Five different samples were prepared:

1.3.1. SV1 and SV2

At first, 1 mg of MSNs were coloured with ATTO-633 NHS ester dye (Sigma-Aldrich). An aliquot of 53 μL of the mother solution of MSNs in EtOH was mixed with 2 μL of ATTO-633 and 945 μL of EtOH, in order to obtain a final solution of 1 mL. This solution was inserted in an Eppendorf and magnetically stirred with the help of a small magnet. The Eppendorf was covered by an aluminium sheet and then stirred at 200 rpm overnight. After that, the MSNs were washed twice with EtOH (centrifuge speed 10'000 RCF for 5 minutes) and then dissolved in 1 mL of H₂O, previously filtered by a microfilter with 0.2 μm pores diameter. Before doing the coupling, the labelled MSNs were centrifuged (10'000 RCF for 5 minutes) and the supernatant discarded.

An aliquot of exosomes from KB cells in physiologic solution was labelled with the lipophilic dye DiOC₁₈(3) (3,3'-dioctadecyloxycarbocyanine perchlorate) (DiO; $\lambda_{\text{Ex}} = 488\text{nm}$, Sigma-Aldrich) (1:100 from the mother solution) mixing 50 μL of exosomes solution with 0.5 μL of DiO in an Eppendorf covered by an aluminium foil and leaving the Eppendorf in an orbital shaker at 37°C and 200 rpm for 30'.

To couple the MSNs with the exosomes from KB cells in a ratio of 1:1 in number, it has been necessary to evaluate the number of nanoparticles per mL by NTA analysis (NanoSight NS300, Malvern Panalytical, placed in the IRCCS of Candiolo, Turin). The following calculations were used (Eq 1-3):

$$n^{\circ} \text{ exosomes} * 50\mu\text{L} = n^{\circ} \text{ exosomes in 1 vial (50}\mu\text{L)} \quad \text{Eq 1}$$

$$n^{\circ} \text{ of MSNs} \frac{\text{nanoparticles}}{\text{mL}} : 1\text{mL} = n^{\circ} \text{ exosomes in 1 vial} : \text{amount of MSNs } [\mu\text{L}] \quad \text{Eq 2}$$

$$\text{amount of MSNs} = \frac{n^{\circ} \text{ of exosomes in 1 vial} * 1 \text{ mL}}{n^{\circ} \text{ of MSNs} \frac{\text{nanoparticles}}{\text{mL}}} [\mu\text{L}] \quad \text{Eq 3}$$

The analysed exosomes had a concentration of $1.65 * 10^{10}$ particles/mL, thus there was $8.25 * 10^8$ particles in a vial of 50 μL , while the MSNs (MM2) concentration was $9.91 * 10^{10}$ particles/mL_{EtOH}, while once labelled they were at a concentration of $0.525 * 10^{10}$ particles/mL_{H₂O}. Thus, to obtain a solution with a ratio of 1:1 in number, 1 mg of labelled MSNs, resuspended in 78.5 μL of microfiltered H₂O, were mixed with 25 μL of exosomes and 53.5 μL of microfiltered physiologic solution.

This solution was then put in an ultrasound bath (Branson) at 40kHz for 20'' for SV1 and 10'' for SV2. At the end of the coupling, the solution was centrifuged (10000 RCF for 5'), the supernatant was removed and the pellet was dissolved in a 100 μL of a solution made by filtered H₂O and physiological solution, with a 1:1 concentration (50 μL H₂O + 50 μL physiological solution). SV1 and SV2 were vortexed to resuspend the covered MSNs and then put in the Orbital Shaker at 37°C and 200 rpm to analyse them at different time points at the fluorescence microscope.

1.3.2. SV3 and SV4

They were obtained in the same way of SV1 and SV2, but the exosomes were derived from B lymphoblasts and at a concentration of $2.46 * 10^{11}$ particles/mL. Thus, the new volumes used for the coupling were: 22.5 μL of labelled exosomes in physiological solution, 27.5 μL of physiological solution and 1 mg of labelled MSNs resuspended in 50 μL of microfiltered H₂O. The coupling was also slightly different: after a first ultrasound bath at 40kHz (10'' for SV3 and 20'' for SV4) the samples were centrifuged (10'000 RCF for 5'), the supernatant was discarded and the pellet resuspended in 50 μL of physiological solution and 50 μL of microfiltered H₂O and vortexed. At this point the samples were again put in the ultrasound bath (same frequency and time) and then centrifuged (10'000 RCF for 5'). The supernatant was discarded, and the pellet was resuspended in 50 μL of physiological solution and 50 μL of microfiltered H₂O and vortexed.

1.3.3. SV5

They were obtained in the same way of SV3 and SV4, but the MSNs were labelled with ATTO-647 dye (Sigma-Aldrich) and the new volumes used for the coupling were: 22.5 μL of labelled exosomes in physiological solution, 27.5 μL of physiological solution and 50 μL of a solution composed by 1 mg of labelled MSNs dissolved in 1 mL of microfiltered H₂O: instead of resuspending 1mg of MSNs in 50 μL of microfiltered H₂O as in the previous preparations, in this case the 1mg of MSNs were resuspended in 1 mL of microfiltered H₂O and then 50 μL of this suspension were prelevated. So, in SV5 there were 1/20 of MSNs with respect to SV3 and SV4. As for SV3, the two ultrasound baths were set to 10'' in time.

1.4. Characterization of the Nanoparticles

The MSNs were analysed and characterized using different techniques in a way to evaluate their physical and chemical characteristics.

1.4.1. Fourier-transform Infrared spectroscopy (FTIR)

To evaluate the functional groups present in the nanoparticles, Infrared Spectroscopy was performed.

This technique uses infrared light, allowing the vibration of the atomic bonds of the molecules producing a signal, resulting in the obtention of a spectrum. Each spectrum is the molecular "fingerprint" of each chemical structure and in this way, it is possible to identify each structure by its own characteristic signal. IR radiation passes through the sample and the spectrometer determines which of this radiation is absorbed at a specific energy. The spectrum will show many different peaks for different energies corresponding to different wavenumber's (vibration's frequency), which recognize each chemical group [116].

Using a sample of 500 μg of NPs, centrifuged at 10'000 RCF 5 minutes and separated the EtOH supernatant, MilliQ bi-distilled water is added, pipetting one single drop, and placed in a silica wafer and waited to dry. The transmission beam mode was chosen to verify the presence of the amine functional groups. Spectra were acquired 4 cm^{-1} resolution and 16 scans accumulation, with a Nicolet 5700 FTIR Spectrometer

(ThermoFisher, Waltham, MA, USA equipped with a room temperature working DLaTGS detector), and background subtracted.

1.4.2. TEM – Transmission Electron Microscope analysis

To verify the NPs morphology, surface roughness, porosity and NP diameter, the TEM was used. TEM or transmission electron microscopy, as the name suggests, consists in the creation of an accelerated electron beam by an electron gun, where the high speed of the beam is due to electromagnetic coils and high voltages. This beam is focused to a small beam through a condenser lens and then through the sample. Parts of the beam are transmitted and other emitted from the sample. The emitted are focused by the objective lens and transformed into an image. This micrograph is obtained due to a projection onto a screen that is phosphorescent, which emits photons when it is irradiated by the electron beam, the image is then obtained by a film camera that is under the screen. Also TEM should have a vacuum system to avoid the collision between electrons and gas atoms [117] [118].

TEM was performed by a Tecnai F20ST from FEI. The samples were prepared by diluting 6 μL of MSNs suspension in ultrapure absolute ethanol (99%, Sigma) with a final concentration of 100 $\mu\text{g}/\text{mL}$ and drying a drop of the resulting suspension on a holey carbon-coated copper grid for TEM.

1.4.3. DLS - Dynamic Light Scattering and Z-Potential

To analyse the MSNs size and their Zeta potential, before (in EtOH) and after lipid coating (in water), the nanoparticles were characterized by DLS and Z-potential analysis with a Zetasizer Nano ZS90 (laser source He-Ne of 633 nm). Each sample of 0.5 mg of NPs lipid coated or uncoated was used, centrifugated at 10'000 RCF for 5 minutes, discarded the supernatant, added 1.5 mL of MilliQ bi-distilled water and sonicated for 5' before sample analysis.

A single beam of scattered light (monocromatic) should pass through the suspension of particles, which already had their random motion (brownian movement) and an increase of fluctuations is made by this light beam. Furthermore, the diffusion coefficient D can be measured and through the Stokes-Einstein equation the hydrodynamic radius R can be obtained (Eq 4).

$$R = \frac{kT}{6\pi\eta D} \quad \text{Eq 4}$$

Where k is the Boltzmann constant, T the temperature in Kelvins, and η the viscosity of the suspending medium. In short, it is feasible to obtain a size distribution of the particles, polydispersity index and Z-Potential as well.

1.4.4. Fluorescence Microscopy Imaging

Each sample of MSNs coupled with lipids or exosomes was characterized through fluorescence microscopy with co-localization method. The aim of this method was to evaluate the percentage of coupling between lipids or exosomes and MSNs. Typically, 1 mg of MSNs was labelled with 2 μL of Atto-550-NHS ester (from a stock solution in dymethylformamide, DMF) or ATTO-633 dye (Sigma-Aldrich) or ATTO-647 NHS ester dye (Sigma-Aldrich) and 1mL of EtOH, followed by stirring overnight at 350 or 200 rpm at room temperature in dark conditions. Then, a centrifugation at 10'000 RCF 5 minutes was performed, discarding the supernatant and adding 1 mL of EtOH for washing. This process was repeated twice and the final dye-labelled particle were obtained in 1 mL EtOH at a final concentration of 1 mg/mL.

After the coupling with labelled lipids or exosomes as described in the previous paragraphs, samples were prepared withdrawing 10 μL of the lipid-coated MSN solution and depositing them on the microscope slide, then the drops were coated by a cover-glass slip and this was fixed with common nail polish. The images were acquired using the wide-field optical fluorescence microscope Nikon Eclipse Ti, equipped with a super-

bright wide spectrum Shutter Lambda XL source with a collection of four filter cubes. The images were acquired with 60x and 100x PLN-APO immersion oil objectives and the data analyzed by the NIS-element software.

Images were thus acquired by exciting the dyes at their different wavelength channels:

- For the labelled silica: 550 nm (red channel if the dye was ATTO-550), 630 nm (far-red channel if the dye was ATTO-633) or 647 nm (far-red channel if the dye was ATTO-647);
- For the lipids and exosomes, 488nm (green channel for DiO).

The colocalization tool of NIS-Element software (NIS-Elements AR 4.5, Nikon) was used to evaluate the coupling percentages: after setting a threshold of 10 μm to disregard larger aggregates, the spots in the two channels were counted and an overlay of the two images was performed, counting only the spots in which the two fluorescences were colocalized. Around 600 fluorescent points were analyzed by this automatic routine and applying dimensional threshold, on each procedure. The percentage of colocalization for MSNs and lipids was then calculated with respect to the MSN channel and lipid channel as it's given in the following equations (Eq 5-8):

$$\%MSNs\ colocalized = \frac{n^{\circ} MSNs\ colocalized}{n^{\circ} MSNs} \quad \text{Eq 5}$$

$$\%lipids\ colocalized = \frac{n^{\circ} lipids\ colocalized}{n^{\circ} lipids} \quad \text{Eq 6}$$

$$\%exosomes\ colocalized = \frac{n^{\circ} exosomes\ colocalized}{n^{\circ} exosomes} \quad \text{Eq 7}$$

$$\% colocalized\ particles = \frac{n^{\circ} particles\ colocalized}{n^{\circ} MSNs + n^{\circ} lipids\ or\ exosomes - n^{\circ} particles\ colocalized} \quad \text{Eq 8}$$

1.5. Analysis on AGI-6780 and Carfilzomib

1.5.1. UV-VIS Spectroscopy

UV-Vis (Ultraviolet–Visible) Spectroscopy is an analytical chemistry technique used to analyse, characterize, and quantify. It is used to obtain a spectrum of absorbance versus concentration, of a compound in solution or as solid. What we observe is the absorbance of light energy or electromagnetic radiation that excites the electrons of the compound from the ground state to the first single excited state. The UV-Vis goes more or less from 200 to 800 nm on the range of wavelengths and the equation behind this technique is the Lambert-Beer law (Eq 9), whereby measuring the absorbance (dimensionless) A , it is possible to calculate the concentration of the solute, C . Where ϵ is the molar absorptivity and l the is total length the light travels through the sample.

$$A = \epsilon * C * l \quad \text{Eq 9}$$

$$A = \log \frac{I_0}{I} \quad \text{Eq 10}$$

Absorbance is also given by (Eq 10) that relates the incident intensity of light (I_0) and the transmitted (I) one, where \log is the logarithm of base 10.

Molar absorptivity, ϵ , is expressed in $[\text{L}\cdot\text{mol}^{-1}\cdot\text{cm}^{-1}]$ and depends on the incident wavelength λ , which can be determined by the highest peak on the spectrum of absorbance versus wavelength, there is a corresponding value of ϵ for which the Lambert-Beer law can be applied and, knowing the absorbance, the calculation of concentration is possible.

To know how much drug was encapsulated in the silica nanoparticles, a UV-Vis analysis was performed on the AGI-6780 and CFZ uptake as well.

First performing calibrations curves in cell culture medium (RPMI-1640, Rosewell Park Memorial Institute) and DMSO for both drugs and in water for AGI-6780. A microplate reader (Multiskan™ FC Microplate Photometer, from ThermoFischer Scientific, interfaced to a pc with the software SkanIt RE) was used and by that a 96-well plate quartz-glass (Hellma™, Hellma Optiks, Jena, Germany) was used as well. All the UV spectra were background subtracted using the respective medium, except the curve for CFZ in DMSO, which were not normalized.

For the calibration curves 5 different concentrations (0.1 μM , 1 μM , 10 μM , 100 μM and 1 mM) were collected considering the absorption peak at 283 nm for AGI-6780. In case of CFZ, 5 different concentrations were used too but they were different (0 μM , 5 μM , 25 μM , 50 μM and 100 μM) and then using the peak at 242 nm for CFZ in DMSO. For CFZ in RPMI, were used three different solutions for the calibration curve (1 μM , 10 μM , 100 μM), then using the peak at 246 nm.

The calibration curves were built with Origin 8.5 software and fitted linearly for each. After that a several number of uptakes and releases were analyzed using this technique, sometimes using the specific wavelength already detected, other times to have a wider analysis, the all spectra was recorded.

The calibration curve is the type of $y=mx+q$, where y is absorbance and x the concentration, the slope m is $\epsilon \cdot l$. Furthermore, after each analysis, and using the calibration curve it is possible to calculate the concentration in each sample, uptake or release of drug, knowing the absorbance measured by the the spectrometer. This has been done for both drugs [122].

1.5.2. Drug uptake and release of AGI-6780 and CFZ

1.5.2.1. Drug uptake of AGI-6780 and CFZ

To uptake the drugs in 1 mg of MSNs, the corresponding volume for the used batch was pipetted (52 μL for MM4 and 73.5 μL for MM3) and centrifuged at 10'000 RCF for 5 minutes, the supernatant (EtOH) was removed and the drug was added to the pellet. In case of AGI-6780 40 μL from the stock solution (10mM, stored at -80°C) were diluted in 360 μL of DMSO, resulting in 400 μL of AGI-6780 1mM in DMSO. In the case of CFZ drug, 8 μL from the stock solution (5mM stored at -80°C) were diluted in 392 μL of DMSO, resulting in 400 μL of CFZ 100 μM in DMSO.

The solutions were magnetically stirred at 350 rpm for 1 h at room temperature for AGI drug, while for 4 h for the CFZ drug. In addition to each sample, also a control sample (CS) with 200 μL of drug at 1mM of AGI-6780 in DMSO or 100 μM CFZ in DMSO were prepared and stirred. After the uptake, the samples were centrifuged at 10'000 RCF for 5 minutes, the supernatant of each sample was placed into the 96-well plate quartz-glass (100 μL of each sample for each well in triplicate). Also a control well was filled with 100 μL of pure DMSO, which was subtracted after absorbance measurements in AGI-6780 case as baseline measurement.

From the collected absorbance values, the residual drug concentration (in terms of μM) in the supernatant was calculated with the calibration curve of AGI-6780 (Eq 11 and 12) or CFZ in DMSO (Eq 13- 16).

$$y = 0.00298x + 0.02576 \quad \text{Eq 11}$$

Where y is the absorbance ABS, and x is the concentration C:

$$ABS = 0.00298C + 0.02576 \leftrightarrow C = \frac{ABS - 0.02576}{0.00298} \quad \text{Eq 12}$$

For CFZ, the calibration curve in DMSO has two ranges where the equations differs, from 10 to 100 μM (Eq.13 and 14) and another one from 0.01 to 1 μM (Eq.15 and 16).

$$y = 2.01949 \times 10^{-4}x + 3.46733 \quad \text{Eq 13}$$

$$ABS = 2.01949 \times 10^{-4}C + 3.46733 \leftrightarrow C = \frac{ABS - 3.46733}{2.01949 \times 10^{-4}} \quad \text{Eq 14}$$

$$y = 0.03386x + 3.4646 \quad \text{Eq 15}$$

$$ABS = 0.03386C + 3.4646 \leftrightarrow C = \frac{ABS - 3.4646}{0.03386} \quad \text{Eq 16}$$

Then, the adsorbed amount in μM in the MSNs sample was evaluated as a difference between the concentration of the control sample (CS) and the residual concentration of the single sample under examination (R), see Eq 17.

$$\text{Adsorbed amount } [\mu\text{M}] = CS [\mu\text{M}] - R [\mu\text{M}] \quad \text{Eq 17}$$

At the end of the test, the pelleted MSNs were stored at $-20\text{ }^\circ\text{C}$ and the microplate reader washed with milli-Q bi-distilled water and ethanol or with a 2% solution of Hellmanex and dried with nitrogen gas. The number of uptakes were 9 for CFZ and 19 for AGI-6780. The amount of MSNs in which the drugs were uptaken could vary between 1mg or 0.5 mg, depending on the purpose (for 0.5 mg obviously the volume of NPs, drug, lipids and water were half of what presented above).

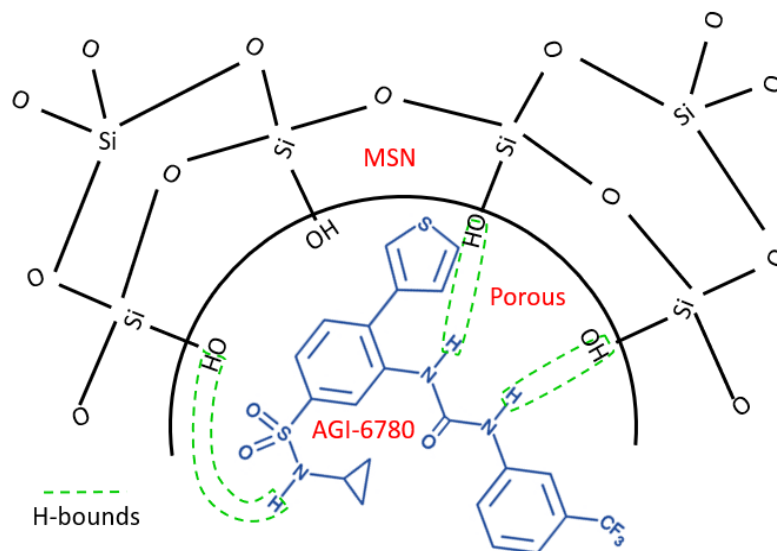


Figure 13. Illustration of the supposed encapsulation mechanism of the drug (here AGI-6780) in MSNs

1.5.2.2. Drug release of AGI-6780 in water

To analyse the effective residence time of the AGI-6780 drug in the MSN pores during the lipid bilayer formation, as well as the possible sealing effect of the different lipid bilayers over time, the nanostructure stability was tested in water medium, i.e. the starting water used for the self-assembly of the lipid bilayer. The drug-loaded MSNs (0.5 mg), both uncoated or coated by lipids (DOPC, DOPC-DOTAP and DOPC-chol-DSPE-PEG), were left in 450 μL water solution, as used during lipid self-assembly (or, in the case of pristine drug-loaded MSN, with freshly added water, 500 μL), further vortexed and then left in static conditions at either 4 $^{\circ}\text{C}$ or 37 $^{\circ}\text{C}$ (therefore, 500 μL of each were divided in 2, so 250 μL each sample). At selected time points, 30 min, 3h30 min, 24 h and 48 h, the drug-loaded particles were processed as in the drug-delivery experiments and the water supernatant analysed by microplate reader to collect the UV-Vis absorbance spectra of the drug at 283 nm (2 wells of 100 μL each for each coating and each temperature). After each time point the supernatant was added to each sample, vortexed and back again to respective temperatures. With the use of the calibration curve of AGI at 261 nm in water already performed and given by Eq 18, the amount of leaked AGI-6780 in water was then calculated. As in previous measurements a well with water was filled with 100 μL .

$$ABS = 0.00258C + 0.05956 \leftrightarrow C = \frac{ABS - 0.05956}{0.00258} \quad \text{Eq 18}$$

1.5.2.3. Drug release of AGI-6780 and CFZ in acellular environment

The release of AGI drug was first performed in acellular media, using the drug-loaded pristine MSNs (MM3) samples after 1 hour of drug uptake in DMSO and then stored as pellet at -20 $^{\circ}\text{C}$. As described above, the phospholipids DOPC-DOTAP and DOPC-chol-DSPE-PEG solution (50 μL) were added with the excess of water (450 μL) to 0.5 mg of drug-loaded MSN (36.7 μL), pipeting and vortexing. A control sample (0.5 mg) of drug-loaded MSNs without lipid shielding was also used, i.e. having the addition of 500 μL of water to replicate the lipid bilayer self-assembly procedure. Then, all the samples were split in aliquots of 100 μL each of MSN@SLB nanoparticles and then centrifuged at 10'000 RCF for 5 minutes. The water supernatant was removed and further analyzed by microplate reader, to calculate the drug leakage from the MSNs at this stage of lipid-bilayer formation (see previous Paragraph), always having a control sample of water (100 μL) in the microplate reader. Finally, the 100 μg sample aliquots were dispersed in 1 mL of RPMI 1640 (Pan Biotech), vortexing, thus having a final concentration of MSNs@SLB in RPMI of 100 $\mu\text{g}/\text{mL}$ (five replicates were used for each sample type), and then placed in the orbital shaker at 37 $^{\circ}\text{C}$ and speed 200 rpm. After selected time points of 2h, 4h, 6h, 24h, 48h, 72h, 96h (4d) and 168h (7d), the samples were centrifuged (10'000 RCF for 5 minutes), the supernatant was separated from NPs to stop the drug release and three aliquots of 100 μL from the supernatant were analysed by a microplate reader. Thus, the total amount of aliquots analysed per each sample type at each time point of the release was in total 15, allowing to calculate the standard deviation as error bar. For AGI-6780, the UV-Vis absorbance was acquired at 283 nm, according to the previous calibration curve of AGI-6780 in RPMI-1640 given by Eq 19 and 20 for the different concentration ranges, was possible to estimate the delivered concentration of drug in RPMI medium from the MSNs.

$$ABS = 0.0097C + 0.0144 \leftrightarrow C = \frac{ABS - 0.0144}{0.0097}, \text{from } 0 \text{ to } 10 \mu\text{M} \quad \text{Eq 19}$$

$$ABS = 0.0027C + 0.0564 \leftrightarrow C = \frac{ABS - 0.0564}{0.0027}, \text{from } 10 \text{ to } 1000 \mu\text{M} \quad \text{Eq 20}$$

After the reading, the aliquots were recovered and combined with their remaining supernatant and then recovered with each respective MSNs sample. Then the MSNs were dispersed by Vortex mixing and then placed back again into the orbital shaker (37 $^{\circ}\text{C}$, 200 rpm) to proceed further with the delivery, and the procedure was repeated for the further time points.

As control, three samples of RPMI only (1 mL for each one) were processed in the same way as the samples containing the drug-loaded MSNs and used for the background subtraction at each microplate reading (in particular 3 wells with 100 μ L each in the microplate reader were analyzed), allowing the normalization of each calibration curve as was done with DMSO.

The same procedure was repeated with CFZ, in this case The UV-Vis absorbance was acquired at 246 nm and the calibration curve of CFZ in RPMI was given by the Eq 21.

$$ABS = 0.0018C + 0.0107 \leftrightarrow C = \frac{ABS - 0.0107}{0.0018}, \text{ from } 0 \text{ to } 100 \mu M \quad \text{Eq 21}$$

1.6. Cell treatment

Cell treatment was performed at the Molecular Biotechnology Centre, University of Torino, Italy.

1.6.1. Cell culture conditions and reagents

Human multiple myeloma (MM) cell lines KMS-28 were kindly provided by Prof. Antonino Neri (University of Milan) and authenticated by DNA fingerprinting using GenePrint system (Promega, Madison, Wisconsin, USA). Cell lines were maintained in RPMI 1640 medium (EuroClone, Pero, Italy), supplemented with 2 mM of L-glutamine, 100 U/mL of penicillin, 100 μ g/mL of streptomycin (Gibco), 10% fetal bovine serum (FBS; Sigma-Aldrich, St. Louis, Missouri, USA), and grown at 37°C in humidified atmosphere with 5% CO₂.

1.6.2. Fluorescence microscopy imaging

1.6.2.1. Evaluation of the coupling between lipids and MSNs

Each sample of MSNs coupled with lipids ready after preparation was characterized through fluorescence microscopy with co-localization method. The aim of this method is evaluating the percentage of coupling between lipids and MSNs. Samples were prepared withdrawing 10 μ L of the lipid-coated MSN solution and depositing them on the microscope slide; then the drops were covered with a cover-glass slip and this was fixed with common nail polish. The images were acquired using a wide-field optical fluorescence microscope Nikon Eclipse Ti, equipped with a super-bright wide spectrum Shutter Lambda XL source with a collection of four filter cubes. The images were acquired with 60x and 100x PLN-APO immersion oil objectives and the data analyzed by the NIS-element software. MSNs, thanks to the presence of the amino-propyl functional groups, were labelled with Atto-647 NHS ester or with Atto-550 NHS ester (by reacting 1 mg of MSN particles overnight in dark with 2 μ g of dye in dimethylformamide, DMF). The lipids were labelled with DiO, as described above. Images were thus acquired by exciting the dyes at two different wavelength channels: 647 nm (far-red channel) and 488 nm (green channel). The colocalization tool of NIS-Element software (NIS-Elements AR 4.5, Nikon) was used to evaluate the coupling percentages, as previously reported [114]: after setting a threshold between 0.1 and 1 μ m to disregard larger aggregates, the spots in the far-red (identifying the MSNs) and green channels (corresponding to the lipid bilayer vesicles) were counted and an overlay of the two images was performed, counting only the spots in which the two fluorescences were colocalized. Around 600 fluorescent points were analyzed by this automatic routine by applying dimensional threshold. The percentage of colocalization was then calculated with respect to the MSN channel with the following formula, Eq 22:

$$\%MSN \text{ colocalized} = (n^{\circ} MSNs \text{ coocalized}) / (n^{\circ} MSNs) \quad \text{Eq 22}$$

1.6.2.2. Confocal and Time lapse fluorescent microscopy images of KMS-28

Cell imaging was performed either using a Leica SP8 confocal system (Leica Microsystems) equipped with an argon ion, a 561 nm DPSS and a HeNe 633 nm lasers. Images were collected using a HC PL APO 63x/1.4 oil immersion objective at a pixel resolution of 0.18x0.18x1.0 μ m. Furthermore, for time-lapse fluorescent

microscopic analysis, cells were imaged by wide-field fluorescence-inverted microscope (Eclipse Ti-E, Nikon, Tokyo, Japan), equipped with a super bright wide-spectrum source (Shutter Lambda XL), a high-resolution camera (Zyla 4.2 Plus, $4'098 \times 3'264$ pixels, Andor Technology, Belfast, UK), using a 40X or an immersion oil 60X objective, and controlled by the NIS-Element software (NIS-Elements AR 4.5, Nikon). $100'000$ cells/mL were seeded in polylysined 4-well chamber slides (Nunc™ Lab-Tek™ II CC2™ Chamber Slide System, Thermo Fisher Scientific™, MA, USA) and let adhere for 2h. $100 \mu\text{g/mL}$ of ATTO647-MSNs@DOPC solution was added. Pictures were acquired every 10 minutes for the first 3 hours, and then every hour for a total imaging time of 48 h. To ensure the health of the cells and to maintain them in their physiological condition during the acquisition time, an incubator gas chamber (Okolab) equipped with CO_2 sensors, temperature unit and an active humidity controller was used. Illumination conditions (neutral-density filters, lamp voltage, exposure time) were set to minimize phototoxicity.

1.6.3. Flow cytometry analysis

KMS-28 cells (1×10^5) were seeded into 24-well plates, filled up with 1 mL cell culturing medium and incubated under normal cell culture conditions. After 6 hours, increasing concentrations of ATTO647-MSNs@DOPC were added to the cell culturing medium. KMS-28 cells were collected at the indicated time points and flow cytometry measurements were performed with a FACSCanto II (BD, USA) counting at least $10'000$ cells. The cells were excited with a HeNe laser at 633 nm and the emitted light passed through a Band Pass 660/20 filter before reaching the detector. Data were processed with FACSDiva 8.0 software (BD Biosciences) and a histogram of fluorescence of single cells only was plotted.

1.6.4. IDH enzymatic activity

Isocitrate Dehydrogenase Activity was measured using the IDH assay kit (Sigma-Aldrich, St. Louis, Missouri, USA), according to the manufacturer's protocol. IDH activity was determined using isocitrate as a substrate of the reaction, which results in a colorimetric (450 nm) product proportional to the enzymatic activity present. One unit of IDH is the amount of enzyme that generates $1.0 \mu\text{mole}$ of NADH or NADP per minute at pH 8.0 at 37°C . IDH2 activity is reported as milliunit per milligram of protein extracted (mU/mg). To evaluate IDH2 and IDH1 activities, mitochondrial or cytoplasmic extracts were used, respectively.

1.6.5. Treatment with Nanoparticles

Cells were observed always before any treatment by microscope (Leica), to evaluate how crowded or not they are and if it is needed to pass them or not. Cells were counted using a hemocytometer and trypan blue exclusion assay. Briefly, cell suspension was mixed with an equal volume of 0.4% Trypan Blue solution (Thermo Fisher Scientific). Then, $10 \mu\text{L}$ of the mixture was loaded in Neubauer chamber to each side of it, tapping with the cover glass. In microscope it was possible to see four quadrants in the Neubauer chamber, so counting the number of cells in each and by that meaning the blue stain the death cells, so the rest were alive cells.

If each quadrant named by a, b, c, d as in Figure 14:

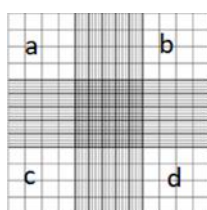


Figure 14. Neubauer chamber grid

Concentration of cells will be given by Eq 23

$$C = \frac{a + b + c + d}{4} * 2 * 10000 = \frac{n^{\circ} \text{ of cells}}{\text{mL}} \quad \text{Eq 23}$$

Where $\frac{a+b+c+d}{4} * 2$ is the dilution factor between Trypan blue and cells.

Followed by washing everything with ethanol and dry.

With the number of cells per mL and number of wells per plate, was feasible to calculate the volume of medium to add to the cells, which will be ready to be plated in a 24 well-plate plastic, 1mL (cells + RPMI) in each well.

About the MSNs that were used to treat cells, there were performed tests with generally 1mg of MSNs encapsulating Carfilzomib coated with DOPC-chol-DSPE-PEG. Tests with empty (no drug) NPs were also made to evaluate the cytotoxicity of them.

1.6.5.1. Treatment with MSNs (MM4 and MM3) encapsulating CFZ coated with lipids

In this experiment were used both MM3 and MM4 nanoparticles, after 48h from the lipid coating, stored in fridge. Encapsulating CFZ and covered by DOPC-chol-DSPE-PEG. Also, treatment with empty NPs and with the soluble drug (CFZ) were carried out. The nanoparticles carried from PoliTo were then centrifuged (Thermo Scientific, Heraeus Fresco 17) at MBC at 10'000 RCF during 5 minutes, the supernatant was removed, the pellet (1mg of NPs) resuspended in RPMI (100 μ L) to a specific concentration from where several dilutions were performed, so that the cells could be treated with different concentrations of NPs with drug. Thereafter, the plated cells were placed in incubator (Sanyo) at 37°C in humidified atmosphere with 5% CO₂, allowing the analysis of the cell viability at each time point, with FACS Fluorescence-Activated Cell Sorting (BD FACSCelesta, BD Bioscience).

1.6.6. Cell Viability

Cell viability was analyzed with Fluorescence-Activated Cell Sorting - FACS (BD FACSCelesta, (BD Bioscience), in every mentioned cell treatment experiment.

1.6.7. FACS - Fluorescence-Activated Cell Sorting

This technique consists in a cell counting and sorting mechanism, so it provides a method to sort a heterogeneous mixture of cells. Not only depends on light scattering but also on fluorescence. Firstly, FACS is a specialized type of flow cytometry, so it relies on flow cytometry principle where there is a cell counting mechanism, which also analyze the phenotype and health of the cells. In a physiological saline solution, the cells move through a focused liquid stream and go one by one through a tube due to the hydrodynamic forces applied by the sheath fluids. Further there will be a laser beam scattering light crossing the tube. Finally, two events happen, forward scattered (FS) light which will measure the size of the cell and side scattered light (SS) will measure the granularity and complexity of cells. These signals are then converted into digitalized data with the help of specific detectors connected to the PC. In fluorescence case, light is emitted by fluorescent molecules after excitation by a compatible wavelength laser. This can be obtained through fluorescing materials in the cell, from fluorescent dyes (e.g., TMRM) or fluorescence-tagged antibodies that have been used to label a specific structure on the cell. The sorting of the cells will be defined by the user in specific parameters, and based on that, FACS will use an electrode that will impose electrical charge on each cell and due to that they will be separated into different chambers by charge with help of electromagnets. Each event will have a signal intensity representation, which will give us the information required [123].

In our experiment, apoptosis was measured by flow cytometry after staining with tetramethyl rhodamine methyl ester (TMRM; Molecular Probes, Eugene, Oregon, USA) according to the manufacturer's instructions. Data were acquired using BD FACSCelesta cytofluorimeter (BD Biosciences). After the determined time point, cells viability was analyzed. At first, cells were observed in microscope. From each cell well was pipetted 200 μ L into each tube, which was used on FACS. Each sample was washed with PBS, centrifuged at 1'300 RCF for 4 minutes, the supernatant was removed. Leaving the pellet to which was added TMRM staining to evaluate cell viability. Finally, after approximately 15 min of incubation in darkness, percentage of TMRM+ cells was measured using FACS [124] [125].

1.7. Statistical Analysis

Statistical analyses were performed with GraphPad Prism 5.01 (GraphPad Software Inc.). Statistical significance of differences observed was determined by One-way ANOVA; differences were considered significant when P value was <.05 (*), <.01 (**), or <.001 (***)).

There were also performed deviation error associated with some of the performed graphs.

2. Results and Discussion

2.1. Lipid-coated MSNs design and characterization

To efficiently load and deliver the drug in a controlled and intracellular manner, without off-target release, MSNs with a size of around 50 nm and mesoporous pore size of about 3 nm were designed and then produced. As described in the Materials and Methods section, a template-assisted sol-gel chemical synthesis was applied to obtain MSNs displaying amine-functional groups at the external nanoparticle surface. Amine groups enable the labelling of the MSNs with fluorescent dye for cytofluorimetry and fluorescence microscopy studies and allow a positively charged surface, beneficial for the nanoparticles' stability in water.

Transmission Electron Microscopy (TEM) and Scanning TEM (STEM) show both the mesoporous silica nanoparticles (MSN) with high porosity, a diameter of around 50 nm and pores of around 3 nm (Figure 15a and b). Mesopores have a worm-like structure, asymmetrical but highly interconnected, ideal to store high amount of drug molecules. The nitrogen sorption isotherm in Figure 15d is of Type IV, typical of mesoporous materials. It further confirms that the obtained MSNs have both a specific surface area (912.7 m²/g), as evaluated by BET model, as well as a high pore volume (around 1.185 cm³/g) with uniform pore size of 3 nm, as evaluated by DFT model. Such properties may guarantee a high adsorption level of the drug. Fourier-Transform Infrared Spectroscopy (FTIR, in Figure 15c) shows the fingerprint of silica and confirms the chemical surface functionalization with amino-propyl groups.

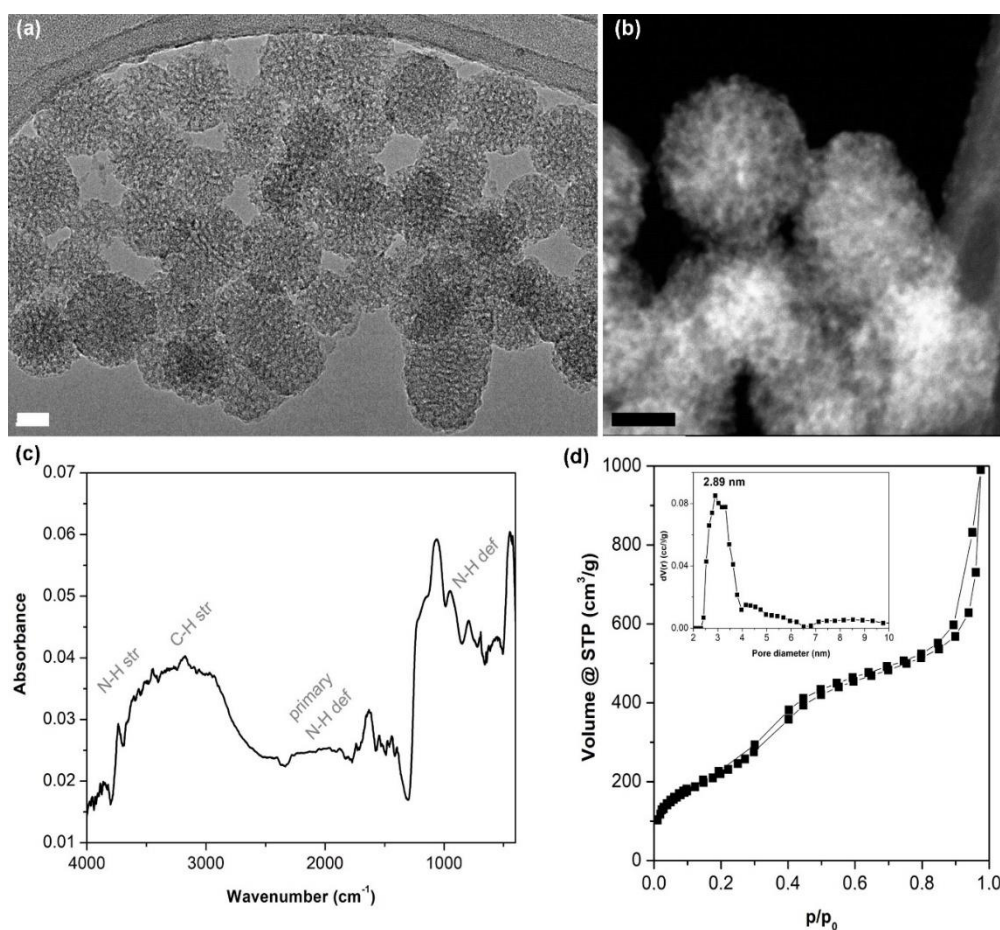


Figure 15. (a) Transmission Electron Microscopy (TEM) and (b) Scanning Transmission Electron Microscopy (STEM) of the mesoporous silica nanoparticles (MSN). Scale bar is 20 nm; (c) Fourier-Transform infrared Spectroscopy (FTIR); (d) Nitrogen sorption isotherms with DFT pore size distribution in the inset.

In particular, at $1'063\text{ cm}^{-1}$ and at $1'080\text{ cm}^{-1}$ there are the -OH bond bending vibration and the characteristic peak of the silicon oxide, respectively. The broad band from $3'000$ to $3'600\text{ cm}^{-1}$ is related to the stretching vibrations of -OH groups and from $3'000$ to $2'800\text{ cm}^{-1}$ are those of the alkyl groups (-CH_x) belonging to the propyl chain of the APTES functional moiety. Finally, at $3'700\text{ cm}^{-1}$ the stretching vibration related to the amine groups at the nanoparticles surface is observed.

Transmission Electron Microscopy (TEM) was also used to evaluate the coupling between MSNs coupled with DOPC, DOPC-chol-DSPE-PEG or exosomes in SV5, the sample that had the highest colocalization (see Paragraph 2.1.2.), as shown in Figure 16. In Figure 16a, b and c it is possible to identify fragments of exosomes, but not a perfect coating of MSNs which are not distinguishable in these images: it means that further optimization must be done in terms of coupling protocol. Figure 16d,e and f are not so clear, because during the water drying and because of the high-vacuum conditions in the TEM, the MSN@SLB tend to aggregate and lipid bilayer collapse, thus not remain dispersed as in colloidal solution. This aggregation makes the pictures of the particle and their lipidic coating very blurred. However, this effect is an artifact and the dimension and edges of each individual nanoparticle are still clearly visible.

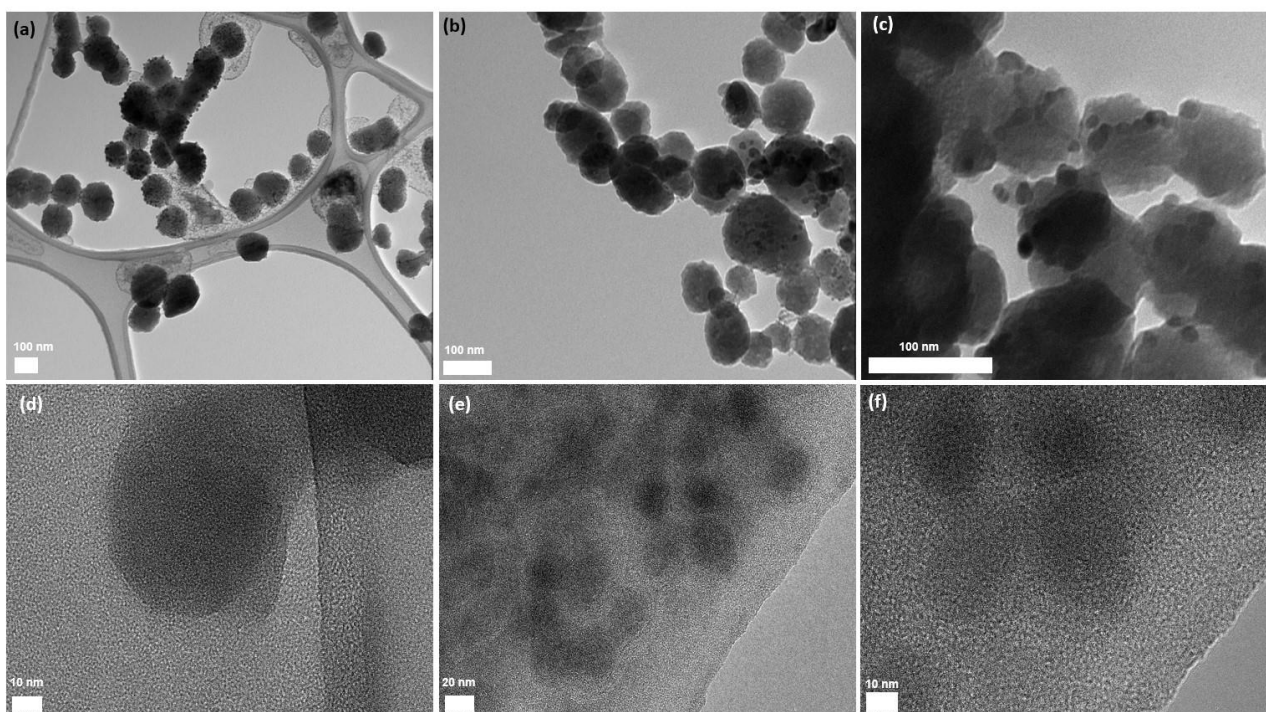


Figure 16. (a, b, c) Transmission Electron Microscopy (TEM) of MSNs coupled with exosomes, in particular sample SV5, at increasing magnifications. (d) Transmission Electron Microscopy (TEM) of MSNs coupled with DOPC. (e, f) Transmission Electron Microscopy (TEM) of MSNs coupled with DOPC-chol_DSPE-PEG

2.1.1. DLS - Dynamic Light Scattering and Z-Potential

2.1.1.1. Dynamic Light Scattering

The MSNs size distributions in both ethanol (EtOH) and dd water were also measured at dynamic light scattering (DLS). As reported in Figure 17a, these amine-functionalized nanoparticles show a moderate agglomeration, as compared with the TEM results, both in ethanol and water solutions, with a hydrodynamic diameter of 220 nm and 190 nm, respectively. They also have a polydispersed size distribution in both media, with PDI (PolyDispersive Index) of 0.83 in ethanol and 0.91 in water.

To induce high drug retention of the drug molecule uptaken in the silica pores and further improve the MSNs stability in water-based media, Supported phosphoLipidic Bilayer (SLB) made of various lipids were self-assembled on the outer MSN surface. In particular, three lipid mixtures were used as SLB, as described in details in the Material and Method section: (1) DOPC (1,2-dioleoyl-sn-glycero-3-phosphocholine) lipids; (2)

DOPC-DOTAP (where DOTAP is N-[1-(2,3-Dioleoyloxy)propyl]-N,N,N-trimethylammonium methyl-sulfate) at a mass percentage ratio of 70 : 30; (3) DOPC-Cholesterol-DSPE-PEG (1,2-distearoyl-sn-glycero-3-phosphoethanolamine-N-[polyethylene glycol-2000]-amine), at a mass percentage ratio of 65.3: 8.6 : 26.1. The process used to self-assemble the phospholipidic bilayers on the silica outer surface is based on the solvent exchange method, as previously reported [114] [30]. Briefly, the driving idea is to have lipid mixtures in a solution of 60 %vol. water and 40 %vol. EtOH, which guarantees that the lipids are still dispersed as single macromolecules, preventing their assembly in liposomes. Then, after being in contact with silica nanoparticles, the water content is dramatically increased, forcing the phospholipids to self-assemble as bilayers on the most energetically favoured conditions, i.e. the surface offered by the silica nanoparticles.

To prove the effective coating of phospholipidic bilayer on the MSN, dynamic light scattering (DLS), Z-potential measurement and co-localization fluorescence microscopy experiments were firstly run using the MSNs without drugs.

The DLS results are reported in Figure 17 and 18, showing a comparison of the size distributions among the pristine MSN in water (black curves) versus the MSN@SLB (in Figures from 17b to 17d). As it can be observed, both the size distributions and the related PDIs of each MSN@SLB are lower than the pristine MSN, pointing out a monodisperse distribution peaking at 142 nm for MSN@DOPC (red curve), 106 nm for MSN@DOPC-DOTAP (pink curve), 106 nm MSN@DOPC-chol-DSPE-PEG (orange curve). Such better stabilization is also supported by the variation of the Z-Potential values (Table 6, Paragraph 1.2.2), confirming the coating of the

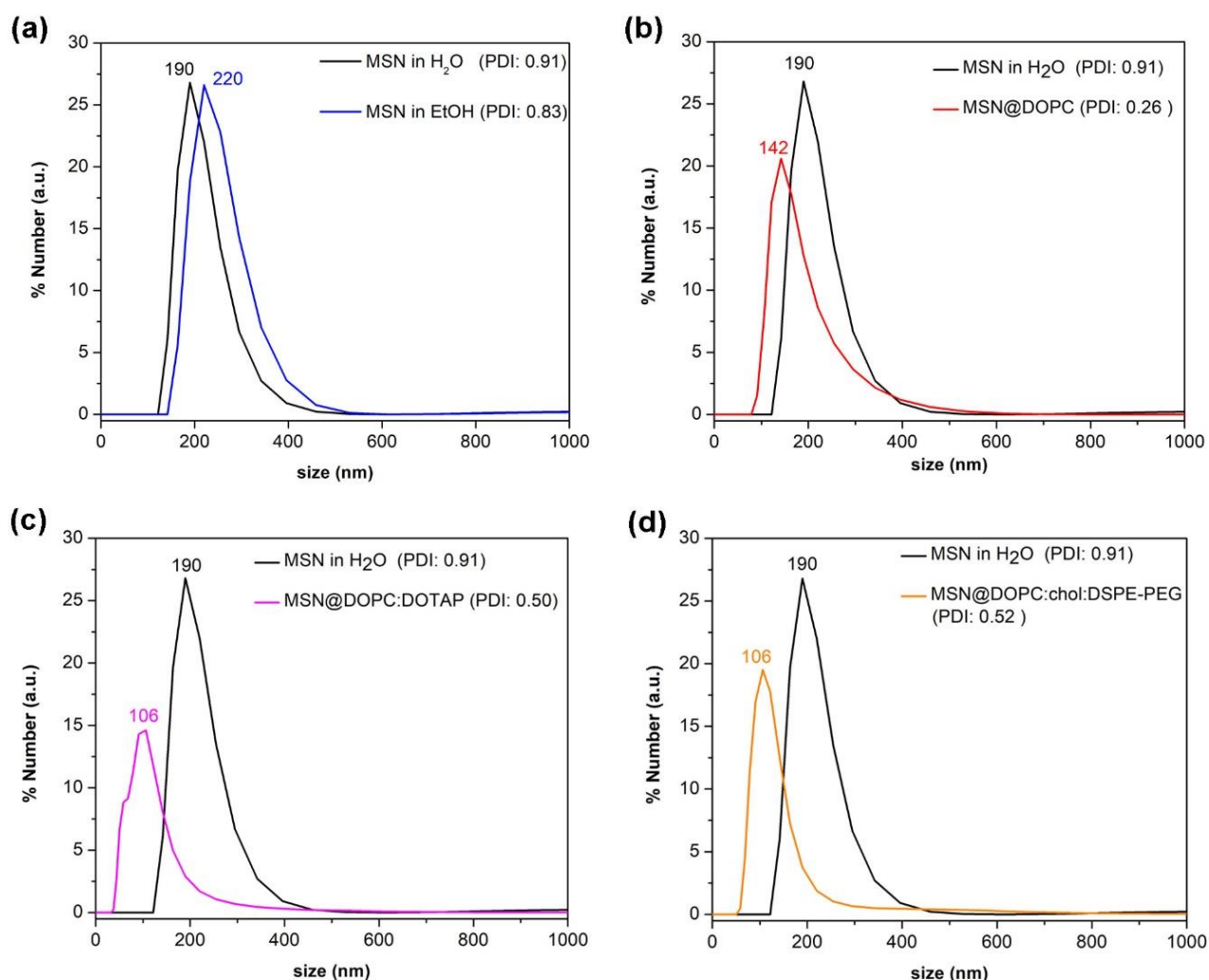


Figure 17. Particle size distribution measured by dynamic light scattering (DLS), comparing the pristine MSN with MSN coated by the various SLBs

nanoparticles by lipid bilayers and supporting their role as efficient steric stabilizer preventing the aggregation of MSN in water. Such data are also supported by the previous literature [114].

DLS results have been helpful to understand how the hydrodynamic radius of MSNs changes with different conditions and another important measurement was the hydrodynamic radius of MSNs both in EtOH and in water after 20" in ultrasound bath, as done for Z-Potential, to reproduce the coupling step of MSNs with exosomes. In Figure 18 the results of these measurements are reported. The large peak in correspondence to 400 to 800 nm in MSNs EtOH is probably due to the incomplete dispersion of the suspension. In fact, it disappears both in H₂O and in EtOH after 20" in the ultrasound bath.

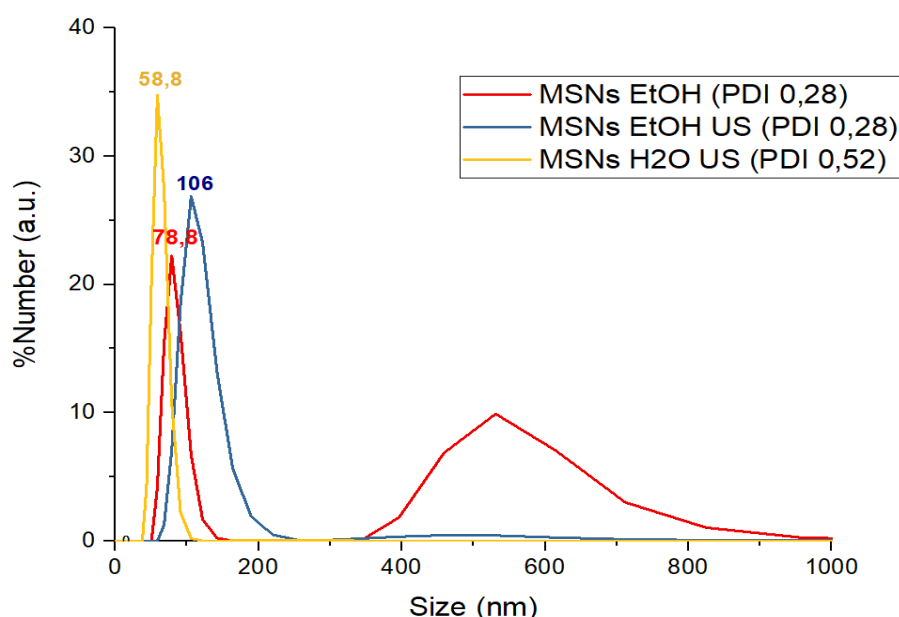


Figure 18. Dynamic Light Scattering of MSNs without lipids in the three different conditions

2.1.1.2. Z-Potential

Z-Potential was used to evaluate the stability of our MSNs and their tendency to aggregate, especially in an aqueous environment, and how this changes in different conditions. It is well-known that a colloidal suspension can be considered stable if the value of Z-Potential is greater than 25mV in absolute value. As it is reported in Table 6 pristine MSNs in H₂O present a Zeta Potential of 25.9 mV, so the suspension can be considered stable. Since the protocol to couple MSNs with exosomes provides sonicating for 10 or 20 seconds, the Z-Potential of MSNs after 20" of ultrasound bath was measured to see if this process could modify the stability of the suspension. In this case the Z-Potential was about 38 mV, so the suspension after being treated with ultrasound is more stable. Finally, the stability of MSNs with the various lipid shells were tested trough Z-Potential and while MSNs with DOPC-DOTAP and DOPC-chol-DSPE-PEG. Z-Potential was greater in absolute value that pristine MSNs, the ones coupled with DOPC were less stable.

Table 6. Z-Potential of MSNs in the different conditions

Sample in H ₂ O	Z-Potential (mV)
----------------------------	------------------

MSN	25.9
MSN 20'' US	38
MSN@DOPC	7.4
MSN@ DOPC:DOTAP	31.7
MSN@ DOPC-CHOL-DSPE-PEG	22.2

2.1.2. Fluorescence microscopy imaging: Evaluation of the coupling between lipids or exosomes and MSNs

Further wide-field fluorescence microscopy images in Figure 19 and Figure 20 show in the green channel (left panels) the DiO-labelled phospholipids (Figure 19) or exosomes (Figure 20), in the red channel (middle panels) the ATTO 550-labelled MSNs (Figure 19) or ATTO-647-labelled MSNs (Figure 20), and the merged channels in the right panels, showing a broad level of colocalization of the dyes in all the three MSN@SLB formulations. It has to be noted that the optical resolution of wide-field fluorescence microscopy is not high enough to allow for a resolution of single MSN@SLB nanoparticles. Here, the colocalization technique is just used to

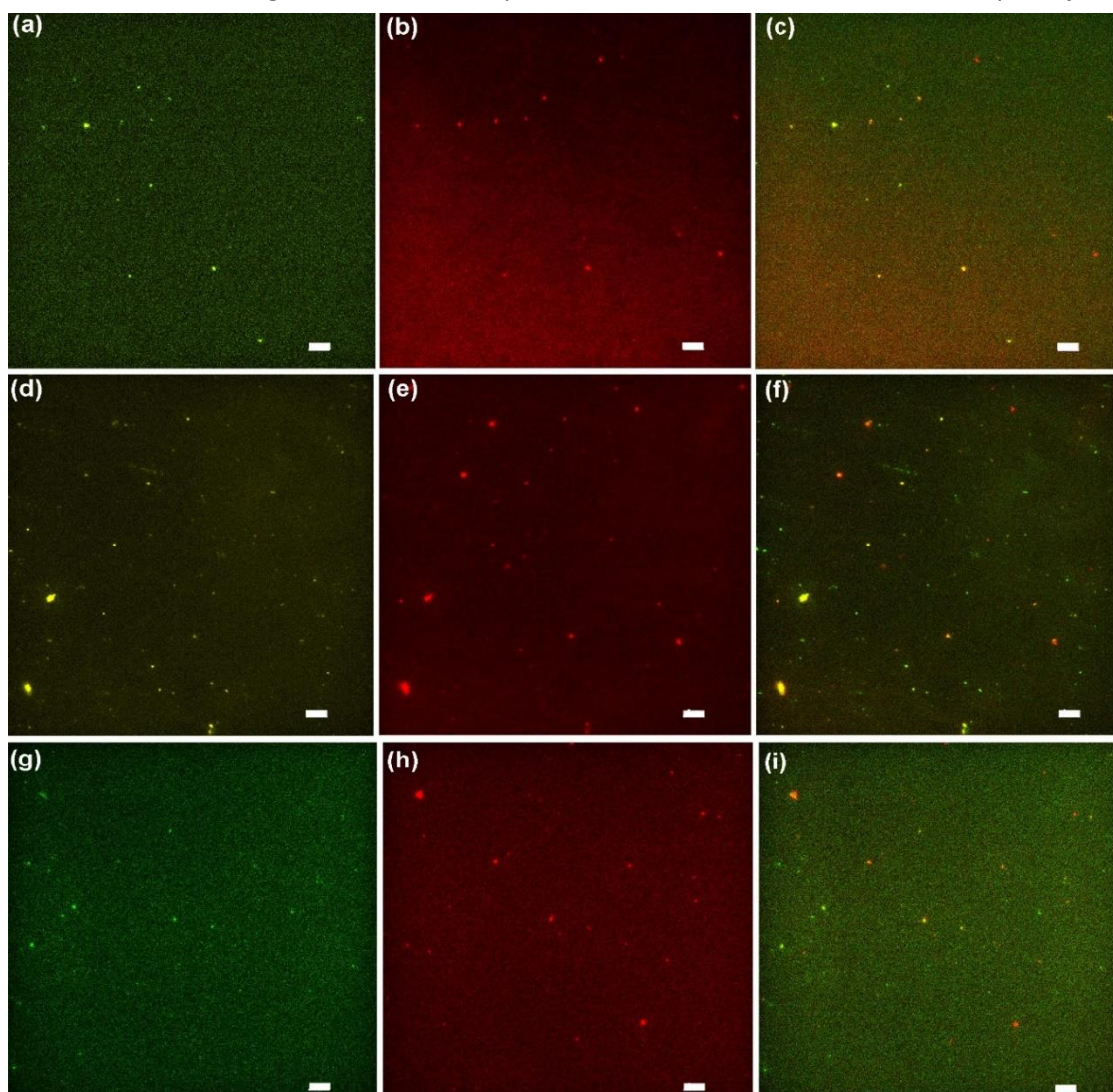


Figure 19. Fluorescence co-localization microscope images of the various lipid-coated MSN. (a-c) MSN@DOPC; (d-f) MSN@DOPC-DOTAP; (g-i) MSN@DOPC-chol-DSPE-PEG. Figures on the left column refer to the emission in the green channel ($\lambda_{\text{ex}} = 488 \text{ nm}$); those in the central column to the red channel ($\lambda_{\text{ex}} = 550 \text{ nm}$), and the right column refers to the merged channel for co-localization evaluation (yellow indicates colocalization of MSN with lipids). Scale bars are $10 \mu\text{m}$.

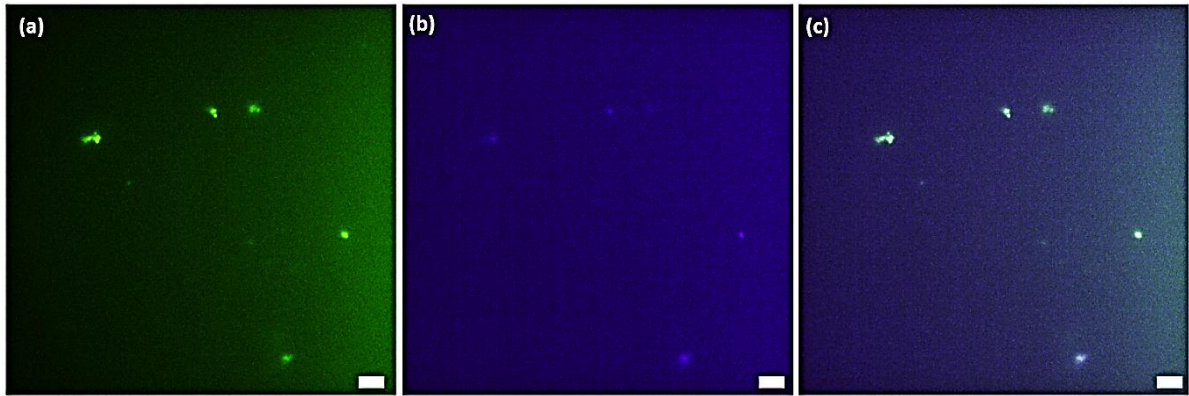


Figure 20. Fluorescence co-localization microscope images of the exosomes-coated MSN. (a) Refers to the emission in the green channel ($\lambda_{ex} = 488 \text{ nm}$); (b) refers to the red channel ($\lambda_{ex} = 647 \text{ nm}$), and (c) refers to the merged channel for co-localization evaluation (yellow indicates colocalization of MSN with lipids). Scale bars are $10 \mu\text{m}$.

support the previous characterizations and provide an estimation of the colocalization (%) of the two dyes. Such estimation leads to values of 24% for MSN@DOPC, 60% for MSN@DOPC-DOTAP, 41% MSN@DOPC-chol-DSPE-PEG and 37% for MSN@EXO (for SV5; SV1, SV2, SV3 and SV4 exhibited lower colocalization). For SV3 and SV4 the variation of colocalization at different time points was also evaluated: after 1h of incubation the colocalization was 0% for SV3 and 11% for SV4, while after 19h of incubation the colocalization was 20% for SV3 and 14% for SV4, suggesting that 19h of incubation was the best choice for the incubation time. These data, together with the other characterizations, in particular DLS and Z-Potential for the phospholipidic bilayers and TEM for the exosomes, confirm with good confidence that most of MSNs are encapsulated by the phospholipidic bilayers and that are well colocalized with the exosomes.

2.2. MSN@SLB internalization into multiple myeloma cells

To gain insights on the capability of the lipid bilayer to act as a biomimetic for the inorganic silica material, cellular internalization of the lipid-shielded MSNs, in particular of MSNs@DOPC without loaded drug, was measured in the multiple myeloma cell line KMS-28. The internalization efficiency and kinetics of increasing concentrations of ATTO647-labelled MSNs were monitored overtime by cytofluorimetry (Figure 21a and b)

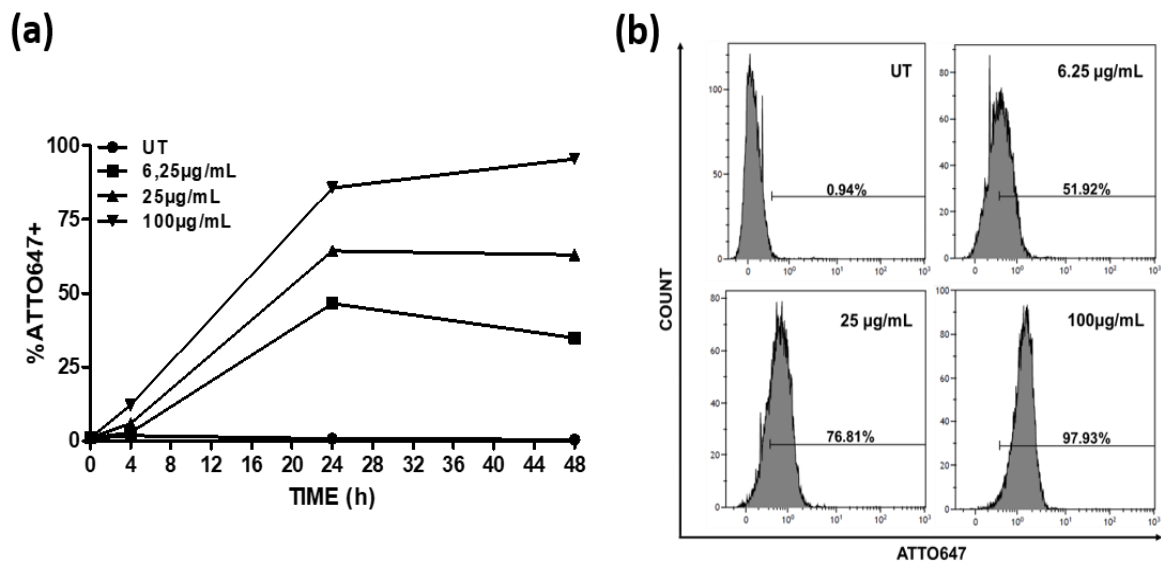


Figure 21. Cytofluorimetric analysis of MSNs@DOPC internalization in KMS-28 cancer cells. (a) KMS-28 cells were treated using different concentration of ATTO647-MSNs@DOPC ($6.25 \mu\text{g/mL}$, $25 \mu\text{g/mL}$, $100 \mu\text{g/mL}$ versus untreated, UT, cells) and at various time points. (b) Flow-cytometry analysis 48 hours post treatment of KMS-28 cells treated with increasing concentrations of ATTO647-MSNs@DOPC versus untreated cells.

and fluorescence microscopy (Figure 22). Flow-cytometry analysis clearly shows that MSNs internalization in KMS-28 cells is proportional to their concentration and reaches a maximum value at 24 hours post treatment, with only a slight increase at 48 hours for the highest nanoparticles concentration, i.e. 100 $\mu\text{g}/\text{mL}$.

Confocal microscopy images of KMS-28 cells were overlaid with the bright-field images, as presented in Figures 22a and 22b. After 48 hours untreated cells (Figure 22a) do not display any significant fluorescence,

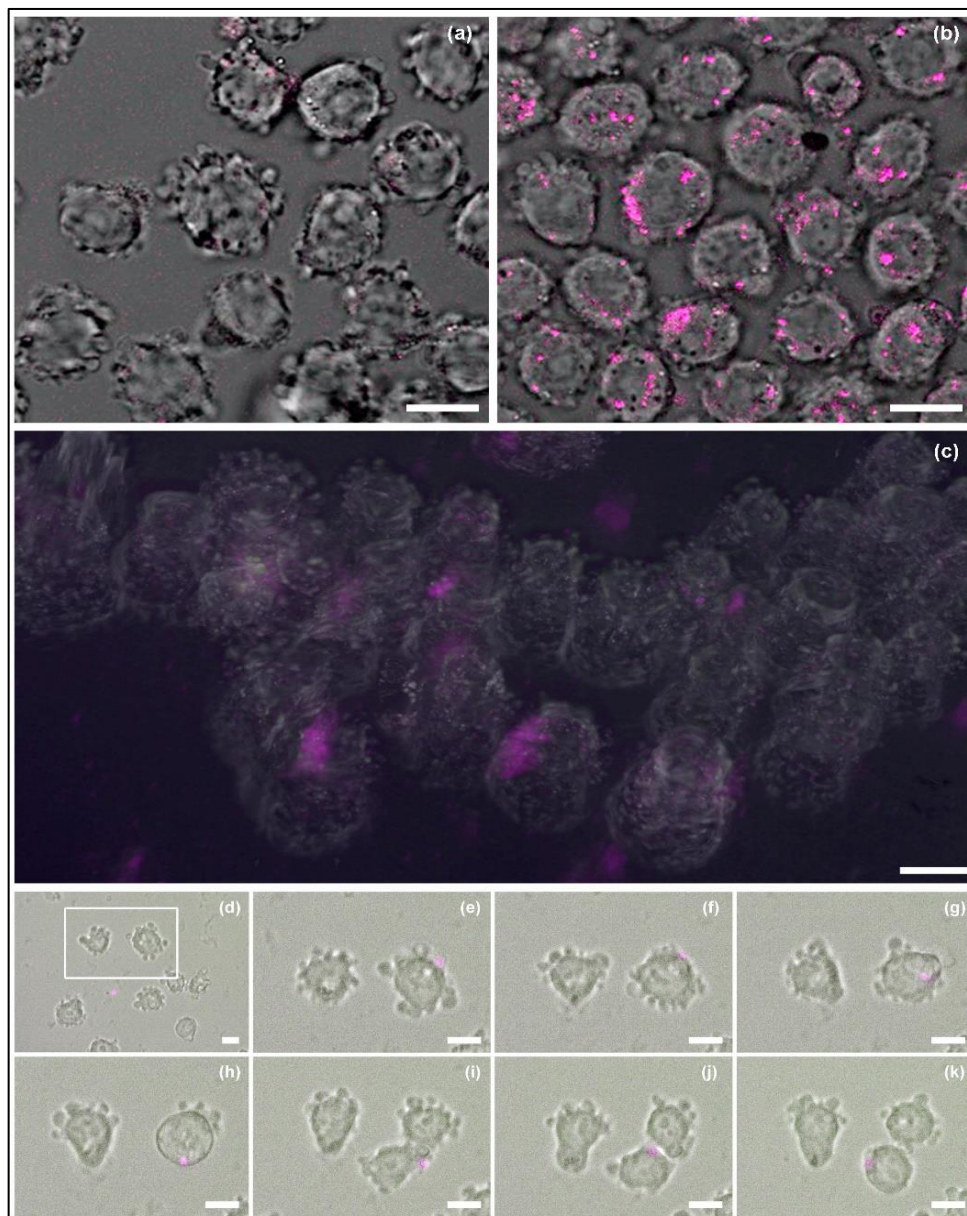


Figure 22. Fluorescent microscopy characterization of MSNs@DOPC nanoconstruct during internalization in KMS-28 cancer cells. Confocal microscopy images of KMS-28 cells after 48 hours (a) untreated or (b) treated with 100 $\mu\text{g}/\text{mL}$ of ATTO647-MSNs@DOPC. In (c), high magnification 3D software elaboration of cells treated with 100 $\mu\text{g}/\text{mL}$ of ATTO647-MSNs@DOPC after 48 hours of timelapse fluorescence microscopy acquisition. From (d) to (k) time lapse fluorescence microscope image sequences of the MSN@DOPC nanoconstruct internalization in multiple myeloma cells are reported. In (d) image of some myeloma cells after 13 hours of incubation are evidenced in the white box closer to a MSN@DOPC particle (violet spot). Panels (e), (f) and (g), report 15, 16, and 19 hours details, respectively, of the MSN@DOPC nanoconstruct internalized in the perimembranal region. In panel (h), after 20 hours of incubation, the cell is preparing itself to mitosis while, at 21 hours of incubation (i), the mother cell has divided in two daughter cells, and one of them has maintained the MSN@DOPC particle inside. In the last two panels and is evident as at 22 (j) and 24 (k) hours of incubation the MSN@DOPC particle is still maintained inside the daughter cell. All the scale bars are 10 μm .

while the micrographs of cells treated with 100 $\mu\text{g}/\text{mL}$ of MSNs@DOPC, show evident red spots resulting from the intracellular localization of ATTO647-labelled MSN@DOPC (Figure 22b). These results confirmed

that MSNs@DOPC were efficiently internalized into multiple myeloma cell lines KMS-28 or at least adherent to the cell surface. However, further in-depth studies by time-lapse fluorescence microscopy and z-stacking helped us to rule out the presence of outer-cell adherent nanoparticles and confirm the mechanism of cell internalization.

The whole acquisition of the timelapse fluorescence microscopy images lasted for 48h and confirmed what has already been observed in confocal microscopy (Figure 22a and b), namely that KMS-28 cancer cells after 48 hours of treatment are still viable and have successfully internalized ATTO647-MSNs@DOPC (Figure 22c). Eight representative images (Figures from 22d to 22k), among all those collected during our time lapse experiment, have been selected to better represent what happened during the 48 hours.

As shown in Figure 22d, a MSN@DOPC nanoconstruct is approaching to multiple myeloma cells and in the subsequent hours it is internalized by a cell and retained inside a perimembranal compartment (Figures from 22e to 22g).

After 20 hours of incubation (Figure 22h) the cell started the mitotic process, increasing also its dimension and during the next hour (Figure 22i) the mother cell divided in two daughter cells, and one of them maintained the MSN@DOPC particle intracellularly (Figures 22j and 22k). This fact evidences that cells were yet able to replicate themselves even at the end of 48 hours of treatment. It thus further confirms the high biocompatibility of MSN@DOPC nanoconstruct at the concentration and timing proposed in this preliminary study.

2.3. MSN@SLB for AGI-6780 uptake and stability over time

Drug uptake was performed on the pristine MSN, before self-assembling the lipidic bilayer. The optimal uptake conditions were obtained for 1 hour of AGI-6780 uptake (concentration of 1 mM in DMSO) with 46 ± 3 μM of uptaken drug per 1 mg of silica ($n=8$). It is thought that the drug physisorption relies on hydrogen bonding interactions with the silica pore surface, which is rich of hydroxyl groups. After drug adsorption, the AGI-loaded MSNs were covered by lipid bilayers, obtaining AGI-MSN@SLB. During this process, which requires to mix the drug-loaded MSNs with the lipids solution (made of 60% water and 40% EtOH) and water, for few seconds, a certain amount of drug is leaked out from the silica pores and dissolved in the water medium.

By analyzing the water solution after the lipid self-assembly, various amount of drug were found in solution, depending on the lipid bilayer type. Actually, the drug loss in water after immediate constitution of the lipidic bilayer was found to be quite high, i.e. up to 21 μM , from 0.5 mg MSN@DOPC (that is 42 μM per mg of silica), while less in MSN@DOPC-DOTAP samples, up to 10 μM of AGI-6780, from 0.5 mg of sample (or 20 μM per mg of silica) and almost zero in MSN@DOPC-cholesterol-DSPE-PEG. Such rough calculation of the residual amount of AGI-6780 in the silica pores after the lipid formation leads to the results reported in Table 7.

Table 7. Amount of AGI-6780 drug adsorbed in the MSN (calculated for 1 mg of silica) and remaining after the lipid self-assembly

Sample	Uptaken amount (μM per 1 mg of silica)
MSN	46 ± 3
Residual amount after lipid self-assembly (μM per 1 mg of silica)	
MSN@DOPC	3 ± 2
MSN@DOPC-DOTAP	25 ± 9
MSN@DOPC-cholesterol-DSPE-PEG	45.5 ± 0.1

This result motivated us to further investigate the various nanoconstructs stability over time, to optimize the amount of leaked drug in water media and the storage times and temperatures before getting the nanoconstructs in contact with cell cultures. We thus analyzed the AGI-6780 concentration leaked from the nanoconstructs in water solution up to 48 hours and at two different temperatures, i.e. 4 and 37 °C.

The results of the stability of various MSN@SLB (0.5 mg of samples) after 24h in water are shown in Figure 23a, where the results are reported as percentage of the drug inside the nanoparticles after the lipidic shielding formation (Table 7). We observed that only the sample of MSN@DOPC stored in water at 4 °C had a continuous leakage of drug in water media and we assumed that the low temperature could induce the formation of rigid lipidic island on the silica surface, with non-uniform coating of the silica surface. In contrast, the lipid formulation containing cholesterol, shows a better drug retention and after 24h the drug leakage was almost 0% and this can be ascribed to the fluidity impaired to the lipid membrane by cholesterol.

Preliminary drug release tests in cell culture medium in absence of cells were then conducted on the AGI-6780-loaded silica (i.e. MSN@DOPC-DOTAP and MSN@DOPC-choI-DSPE-PEG) at 37 °C in RPMI-1640 medium and, as a reference, on the uncoated AGI-6780-loaded silica nanoparticles. It has to be noted that the possible drug leaked in water medium after the lipid self-assembly was discarded by centrifugation and the pelleted nanoconstructs resuspended in fresh RPMI-1640 medium.

Figure 23b reports the progressive release of the hydrophobic drug AGI-6780 out from the pores of uncoated MSN. It is noticeable that the trend increases in the first 24 hours up to 26% of the total adsorbed drug in the silica (corresponding to $12 \pm 5 \mu\text{M}$), then it remains more or less constant until 72 hours of release. At last, after 5 days, the release increases sharply. At the end of the test, i.e. after 7 days, the release curve has not reached a plateau yet, corresponding to around 55% of the total uptaken drug, i.e. $26 \pm 4 \mu\text{M}$.

In contrast, when a double lipidic layer is self-assembled on the MSN surface after the uptake of AGI, almost no drug delivery is observed in cell culture medium. This absence of drug release is persistent up to 7 days of daily monitoring, reaching in the worst case around 2.2% of released drug with respect to the total adsorbed amount, which corresponds to $0.6 \mu\text{M}$ of AGI-6780. This result actually demonstrates that the lipid bilayer,

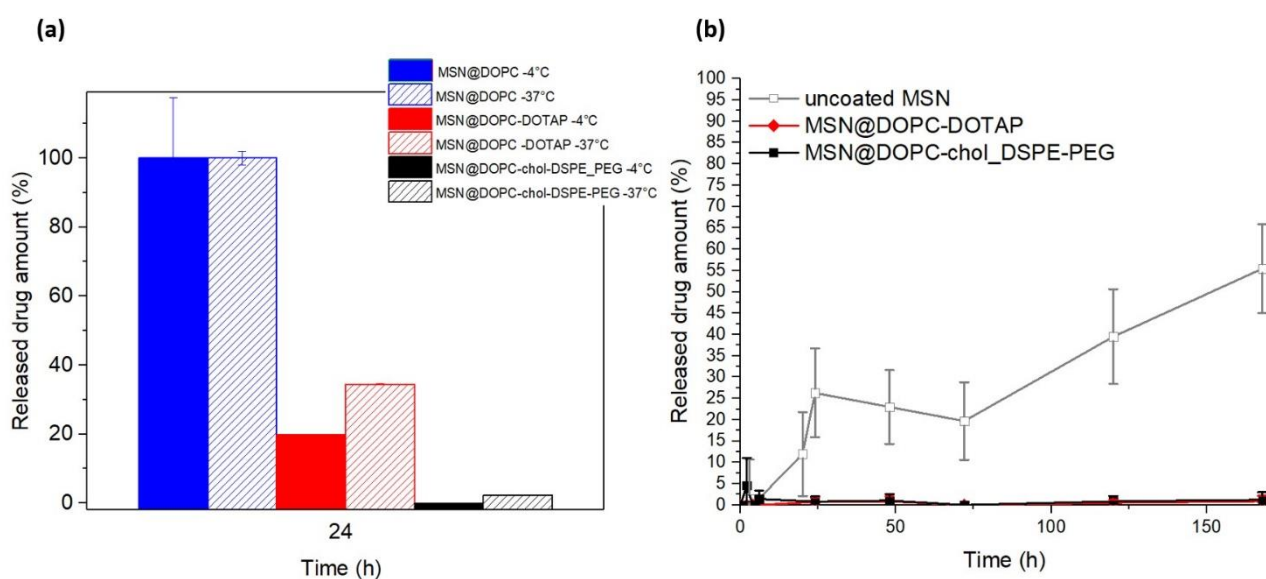


Figure 23. (a) Stability of the various nanoconstructs in water after 24h at two different storage temperatures, 4 °C and 37 °C. (b) Release of AGI drug from pristine MSN (in grey) and from two lipid-coated mesoporous silica, i.e. MSN@DOPC-DOTAP (in red), MSN@DOPC-choI-DSPE-PEG (in black)

irrespectively from its composition, is able to tightly seal the AGI-6780 inhibitor inside the silica mesopores, providing possibly a successful drug release only once internalized into cancer cells, as shown below.

After the above-reported drug delivery, an artificial breakage of the lipidic membrane is operated by adding Triton X-100, a surfactant well-known for its ability to disrupt the self-assembly of lipidic bilayers, as reported in [114]. Actually, a prompt delivery of the AGI drug is observed reaching the average concentration of 30 ± 9 μM of AGI-6780 in 48 hours for all the MSN@SLB lipid formulation, yet corresponding to the almost the 66% of the total AGI-6780 incorporated initially in the MSN pores, or almost completely when considering the residual amount after lipid self-assembly (Table 7). This triton-triggered delivery thus demonstrated, as previously reported in the literature [114], the effective sealing operated by the lipids and thus the ability of the whole MSN@SLB to reach intact and without drug loss the target cells.

2.4. IDH2 enzymatic inhibition tests with AGI-6780 loaded MSNs

To finally test the ability of the lipid-coated nanoparticles to efficiently release the IDH2 inhibitor drug to cancer cells, the AGI-6780-loaded MSN@SLB were prepared and incubated at the concentration of $100 \mu\text{g}/\text{mL}$ with the KMS-28 cancer cells. We decided to work with the MSN@SLB particles with lowest amount of loaded drug, to look at the possible most critical or even inefficient conditions. As actually mentioned above, a portion of drug is leaked in water medium after the lipid self-assembly. This portion is the highest in the MSN@DOPC sample type, while lower in the other two lipidic formulations. The leaked drug in water was first discarded by centrifugation and the nanoconstructs resuspended in fresh RPMI-1640 medium before getting in contact with the cells.

The results of drug-loaded MSN@DOPC are shown in Figure 24 and compared to the untreated cells (UT), the MSN@DOPC constructs without drug, and the cells treated with drug dissolved at a concentration of $5 \mu\text{M}$ in the cell medium.

While untreated and MSN@DOPC-treated cells do not display any enzymatic activity inhibition, the presence of the drug AGI-6780 actually inhibits the enzymatic activity of IDH2 in a time dependent manner. The positive control is observed using a $5 \mu\text{M}$ concentration of free drug dissolved in the cancer cell medium.

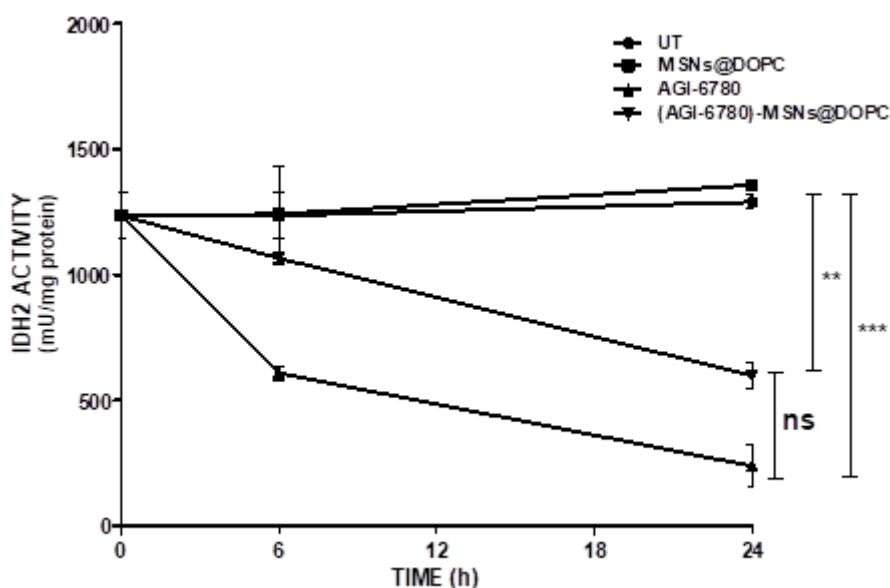


Figure 24. IDH2 enzymatic activity. KMS-28 cells were left untreated (UT) or treated with $100 \mu\text{g}/\text{mL}$ MSNs@DOPC, $5 \mu\text{M}$ AGI-6780 or $100 \mu\text{g}/\text{mL}$ (AGI-6780)-MSNs@DOPC were analyzed for IDH2 activity 0, 6 and 24 hours post-treatment. IDH2 activity is reported as millunit per milligram of protein extracted (mU/mg). Data are the mean \pm s.d. of two independent experiments (* $P < .05$; ** $P < .01$; *** $P < .001$)

It is worth to note that the drug-loaded MSN@DOPC slightly inhibit the enzymatic activity of the cell after 6 hours, while after 24 hours the enzymatic activity of IDH2 is highly inhibited by almost the half. It has to be noted that at this time point, i.e. 24 hours, the highest internalization rate of MSN@DOPC is also achieved (as reported in Figure 21a).

Despite the MSN@DOPC construct showed the lowest amount of adsorbed drug after the lipid self-assembly process (see Table 7, where the amount of $3 \pm 2 \mu\text{M}$ per mg of MSN@DOPC is calculated), this amount is still enough to reduce the enzymatic activity of IDH2. Actually, in the enzymatic inhibition experiment, $100 \mu\text{g}$ of MSN@DOPC were used, thus this amount of nanoparticles can in principle carry 1/10 of the drug concentration estimated in Table 7. Despite this low amount of nanocarried drug, it is anyway sufficient to induce a consistent enzymatic inhibition if compared to the free drug dispersed in the cell culture medium. Therefore, we attribute this result to the great ability of the MSN@SLB nanoconstructs to be internalized in cancer cells and deliver intracellularly the AGI-6780 drug. Owing to the fact that the inhibition of IDH2 is not per se cytotoxic, except in high doses, the therapeutic role of IDH2 inhibitor is useful in synergy with other drugs, like chemotherapeutics or proteasome inhibitors [11]. In the present Master Thesis only on the encapsulation of the drug AGI-6780 and its role as IDH2 inhibitor when transported by nanocarriers is reported. In this regards, Figure 7 reports that our aim has been achieved and MSN@DOPC uploaded with the drug:

- Does not negatively affect the ability of AGI-6780 to inhibit IDH2 activity;
- Allow to inhibit the IDH2 enzymatic activity with an impressively lower amount of drug, when nano-vehicled, than in the case of the free drug (used in higher amount).

2.5. MSN@SLB for Carfilzomib uptake and stability over time

Drug uptake was performed on the pristine MSN, before self-assembling the lipidic bilayer. The optimal uptake conditions were obtained for 4 hours of Carfilzomib uptake (concentration of $100 \mu\text{M}$ in DMSO) with about $101.2 \pm 0.2 \mu\text{M}$ of uptaken drug per 1 mg of silica ($n=3$). After drug adsorption, the CFZ-loaded MSNs were covered by lipid bilayers, obtaining CFZ-MSN@SLB. During this process, which requires to mix the drug-loaded MSNs with the lipid solution (made of 60% water and 40% EtOH) and water, for few seconds, a certain amount of drug is leaked out from the silica pores and dissolved in the water medium.

By analysing the water solution after the lipid self-assembly, a null amount of drug was found in solution, for every lipid bilayer type, as reported in Table 8.

Table 8: Amount of CFZ drug adsorbed in the MSN (calculated for 1 mg of silica) and remaining after the lipid self-assembly.

Sample	Uptaken amount (μM per 1 mg of silica)
MSN	101.2 ± 0.2
Residual amount after lipid self-assembly (μM per 1 mg of silica)	
MSN@DOPC	101.2 ± 0.2
MSN@DOPC-DOTAP	101.2 ± 0.2
MSN@DOPC-cholesterol-DSPE-PEG	101.2 ± 0.2

Preliminary drug release tests in cell culture medium in absence of cells were then conducted on the CFZ-loaded silica (i.e. MSN@DOPC-DOTAP and MSN@DOPC-cholesterol-DSPE-PEG) at 37 °C in RPMI-1640 medium and, as a reference, on the uncoated AGI-loaded silica nanoparticles. It has to be noted that the possible drug leaked in water medium after the lipid self-assembly was discarded by centrifugation and the pelleted nanoconstructs resuspended in fresh RPMI-1640 medium.

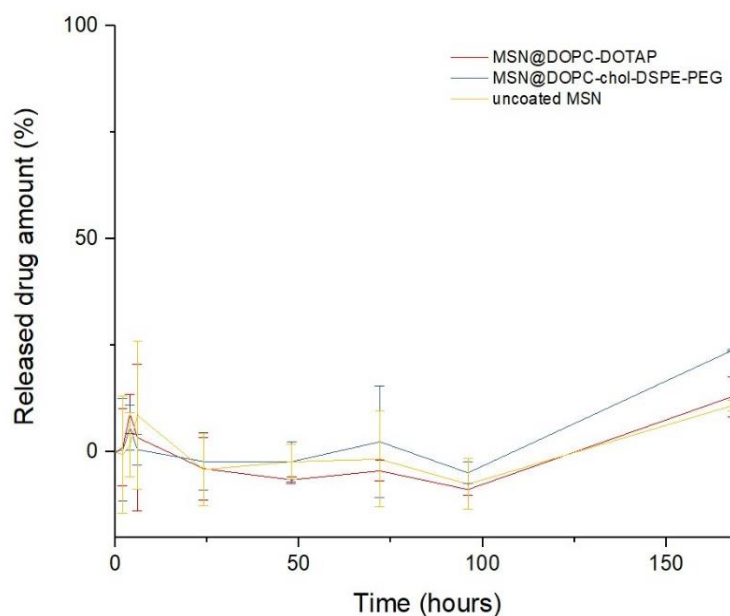


Figure 25. Release of CFZ drug from pristine MSN (in yellow) and from two lipid-coated mesoporous silica, i.e. MSN@DOPC-DOTAP (in red), MSN@DOPC-cholesterol-DSPE-PEG (in blue)

At the beginning of the release there a burst release for both pristine and lipid-coated MSNs, with some differences: for lipid coated MSN the burst release takes place at 4h, corresponding to $9.1 \pm 4.6 \mu\text{M}$ (about 9% of the loaded amount for MSN@DOPC-DOTAP) and for MSN@DOPC-cholesterol-DSPE-PEG corresponding to $5.8 \pm 5.4 \mu\text{M}$, about 5.7% of the loaded amount).

It is noticeable that the trend increases in the first 6 hours up to $8 \pm 17 \mu\text{M}$ (corresponding roughly to the 8.6% of the total adsorbed drug in the silica), then it remains more or less constant until 96 hours of release and then the release increases sharply. At the end of the test, i.e. after 7 days, the release curve has not reached a plateau yet, corresponding to around 3.6% of the total uptaken drug, i.e. $3.6 \pm 5.5 \mu\text{M}$.

Unfortunately when a double lipidic layer is self-assembled on the MSN surface after the uptake of CFZ, the drug release observed in cell culture medium after 7 days is higher than in the pristine MSNs: MSN@DOPC-DOTAP reaches $16.5 \pm 0.5 \mu\text{M}$ (about 16.3% of the loaded amount) and MSN@DOPC-cholesterol-DSPE-PEG reaches $14.6 \pm 0.5 \mu\text{M}$ (about 14.4% of the loaded amount).

These results are quite different from the ones obtained with AGI-6780: in every case MSNs@SLB have an initial release in the first hours and then the release goes to zero till a certain time point. The difference is that in MSNs loaded with CFZ we have this behavior also for pristine MSNs, in which the later release (after 96 hours) is even lower than in MSN@SLB. This is an unexpected behavior and more tests have to be performed to clarify this kinetics.

2.6. Cellular viability tests with Carfilzomib loaded MSN@SLB

Human multiple myeloma cell line was treated with different concentration of MSN@DOPC-cholesterol-DSPE-PEG loaded with Carfilzomib and then the viability of the cells was analysed at specific time points. The same treatment was done using MSN@DOPC-cholesterol-DSPE-PEG without any drug in two different concentration and using free drug (as shown in Figure 21b) in different concentrations. As it is shown in Figure 26a, the best

results in terms of cellular viability were achieved using the highest concentrations of MSNs, i.e. 100 µg/ml and 50µg/ml. From Table 8 it is known that 101.2 ± 0.2 µM of Carfilzomib was uptaken per 1 mg of MSN, but these results stand that MSNs@DOPC-choI-DSPE-PEG (at the concentration of 100 µg/ml and 50µg/ml) loaded with CFZ give results similar to the free drug at the concentration of 5nM. These results, merged with the ambiguity of the release in acellular medium (Figure 25) induce to think that the rilevation of the CFZ amount trough the UV-vis spectrometer is not so accurate and it will be necessary to use other instruments to conduce more reliable experiments.

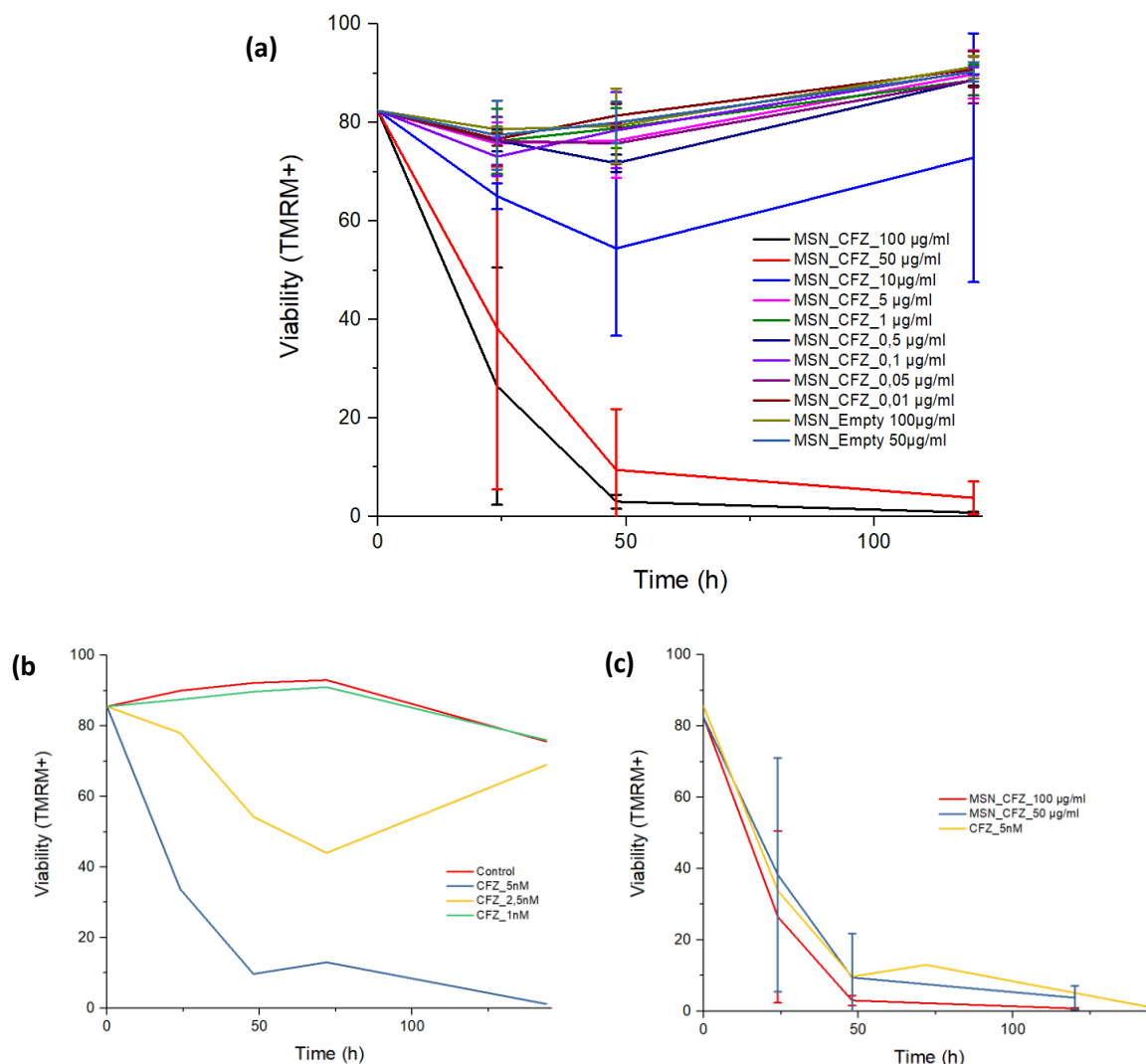


Figure 26. (a) Human multiple myeloma cells viability after treating them with different concentration of MSNs@DOPC-choI-DSPE-PEG loaded with CFZ, (b) same cell line viability with free CFZ at different concentration. In (c) a merge of the results obtained with the concentrations of loaded MSNs and pure CFZ that gave the best results in terms of cellular viability

Conclusions

EVs are nowadays considered one of the main actors in the nanomedicine scene, thanks to their incredible features in terms of biocompatibility, cargo loading, cellular uptake and immune system escaping. A step forward has been done when researchers started to customize these exceptional nanovectors, engineering their surface with specific biomolecules for different purpose, as *tracking in vivo* or targeting the desired cell type. Unfortunately, engineered EVs and the EVs that are naturally-derived by cells have to fight against the today lack of reliable purification protocols, the difficulty of producing EVs with a controllable composition and the inefficient cargo-loading capacity, that are the main obstacles to a scalable clinical application of EVs. For what concerns the engineered EVs, another obstacle is the removal of the uncoupled molecules or cargo (like drugs or nanoparticles) after the coupling process, to purify the obtained formulation. For these reasons some researches decided to change the route, starting to produce synthetic, chimeric EVs, to obtain nanovectors that contain only the components that have been proved to be useful for the formulation purpose, inserting them in synthetic lipid nanovesicles. The future prospective of this line of research is the formation of clean, purified, high controllable and pharmaceutically acceptable EVs-like nanovesicles that will allow researchers to abandon the difficult and little controllable protocols of EVs extraction and selection. The main obstacle to obtain this is the need to identify which are the components of the EVs that are fundamental to have the therapeutic and targeting effect, to understand how they behave if introduced in a synthetic lipid membrane and to develop protocols to isolate and purify them in a scalable and controllable way. Of course, this challenge has to be faced up by multidisciplinary collaborations, that include biologists, chemists, material scientists and engineers.

For what concerns the experimental section, the aim was to develop an innovative and multifunctional drug delivery platform to fight against Multiple Myeloma. In this Master Thesis the biomimetic properties, high cell internalization efficiency, excellent drug uptake and release capabilities of mesoporous silica nanoparticles shielded by various lipid bilayer coatings have been reported. In particular it has been shown the efficient drug retention, the internalization and proper enzymatic inhibition of an IDH2 inhibitor drug namely the compound AGI-6780, when vectorized in the porous nanocarrier, toward multiple myeloma cancer cells *in vitro*. Another important evidence has been that MSN@SLB loaded with the proteasome inhibitor Carfilzomib can be improved to become a device in the fight against Multiple Myeloma. The nanocarrier shows actually unprecedented efficiency in drug release, significantly greater than the one of the free drugs just dispersed in cell culture media. This research is thus an excellent and novel proof of concept which can rehabilitate the use of unapproved drugs, discarded because of their poor biodistribution properties, and propose their successful use in the fight of cancer in a new nanovehicle administration form.

References

1. Bunggulawa, E.J.; Wang, W.; Yin, T.; Wang, N.; Durkan, C.; Wang, Y.; Wang, G.; Recent advancements in the use of exosomes as drug delivery systems. *J. Nanobiotechnology*. 2018, 16, 81.
2. De la Torre Gomez, C.; Goreham, R. V.; Bech Serra, J.J.; Nann, T.; Kussmann, M.; “Exosomics”—A Review of Biophysics, Biology and Biochemistry of Exosomes With a Focus on Human Breast Milk. *Front. Genet*. 2018, 9, 92..
3. Zaborowski, M.P.; Balaj, L.; Breakefield, X.O.; Lai, C.P.; Extracellular Vesicles: Composition, Biological Relevance, and Methods of Study. *Bioscience* 2015, 65, 783-797..
4. Kalra, H.; Drummen, G.P.; Mathivanan, S.; Focus on Extracellular Vesicles: Introducing the Next Small Big Thing. *Int. J. Mol. Sci.* 2016, 17, 170.
5. Susa, F.; Limongi, T.; Dumontel, B.; Vighetto, V.; Cauda, V.; Engineered Extracellular Vesicles as a Reliable Tool in Cancer Nanomedicine. *Cancers (Basel)* 2019,11, 1979.
6. Sutaria, D.S.; Badawi, M.; Phelps, M.A.; Schmittgen, T.D.; Achieving the Promise of Therapeutic Extracellular Vesicles: The Devil is in Details of Therapeutic Loading. *Pharm. Res.* 2017, 34, 1053–1066.
7. Gao, J.; Exosomes as Novel Bio-Carriers for Gene and Drug Delivery. *Int. J. Pharm.* 2017, 521, 167-175.
8. Lötvall, J.; Hill, A.F.; Hochberg, F.; Buzás, E.I.; Di Vizio, D.; Gardiner, C.; Gho, Y.S.; Kurochkin, I.V.; Mathivanan, S.; Quesenberry, P.; Sahoo, S.; Tahara, H.; Wauben, M.H.; Witwer, K.W.; Théry, C.; Minimal experimental requirements for definition of extracellular vesicles and their functions: a position statement from the International Society for Extracellular Vesicles. *J. Extracell. Vesicles* 2014, 3, 26913.
9. Yoo, Y.K.; Lee, J.; Kim, H.; Hwang, K.S.; Yoon, D.S.; Lee, Y.H.; Toward Exosome-Based Neuronal Diagnostic Devices. *Micromachines (Basel)* 2018, 9, 634.
10. Gurunathan, S.; Kang, M.H.; Jeyaraj, M.; Qasim, M.; Kim, J.H.; Review of the Isolation, Characterization, Biological Function, and Multifarious Therapeutic Approaches of Exosomes. *Cells* 2019, 8, 307.
11. Ding, M.; Wang, C.; Lu, X.; Zhang, C.; Zhou, Z.; Chen, X.; Zhang, C.Y.; Zen, K.; Zhang, C.; Comparison of commercial exosome isolation kits for circulating exosomal microRNA profiling. *Anal Bioanal Chem* 2018, 410, 3805–3814..
12. Zeringer, E.; Barta, T.; Li, M.; Vlassov, A.V.; Strategies for isolation of exosomes. *Cold Spring Harb. Protoc.* 2015, 2015, 4.
13. Momen-Heravi, F.; Balaj, L.; Alian, S.; Trachtenberg, A.J.; Hochberg, F.H.; Skog, J.; Kuo, W.P.; Impact of biofluid viscosity on size and sedimentation efficiency of the isolated microvesicles. *Front Physiol.* 2012, 3,162.

14. Tauro, B.J.; Greening, D.W.; Mathias, R.A.; Ji, H.; Mathivanan, S.; Scott, A.M.; Simpson, R.J.; Comparison of ultracentrifugation, density gradient separation, and immunoaffinity capture methods for isolating human colon cancer cell line LIM1863-derived exosomes. *Methods* 2012, 56, 293-304.
15. Zarovni, N.; Corrado, A.; Guazzi, P.; Zocco, D.; Lari, E.; Radano, G.; Muhhina, J.; Fondelli, C.; Gavrilova, J.; Chiesi, A.; Integrated isolation and quantitative analysis of exosome shuttled proteins and nucleic acids using immunocapture approaches. *Methods* 2015, 87..
16. Davies, R.T.; Kim, J.; Jang, S.C.; Choi, E.J.; Gho, Y.S.; Park, J.; Microfluidic filtration system to isolate extracellular vesicles from blood. *Lab. Chip.* 2012, 12, 5202-5210.
17. Contreras-Naranjo, J.C.; Wu, H.J.; Ugaz, V.M.; Microfluidics for exosome isolation and analysis: enabling liquid biopsy for personalized medicine. *Lab. Chip.* 2017, 17, 3558-3577.
18. Batrakova, E.V.; Myung, S.K.; Using exosomes, naturally-equipped nanocarriers, for drug delivery. *J. Control Release* 2015, 219, 396-405
19. Antimisiaris, S.G.; Mourtas, S.; Marazioti, A.; Exosomes and Exosome-Inspired Vesicles for Targeted Drug Delivery. *Pharmaceutics* 2018, 10, 218.
20. Chen, C.C.; Liu, L.; Ma, F.; Wong, C.W.; Guo, X.E.; Chacko, J.V.; Farhoodi, H.P.; Zhang, S.X.; Zimak, J.; Ségaliny, A.; Riazifar, M.; Pham, V.; Digman, M.A.; Pone, E.J.; Zhao, W.; Elucidation of Exosome Migration across the Blood-Brain Barrier Model *In Vitro*. *Cell. Mol. Bioeng.* 2016, 9, 50.
21. Luan, X.; Sansanaphongpricha, K.; Myers, I.; Chen, H.; Yuan, H.; Sun, D.; Engineering exosomes as refined biological nanoplatfoms for drug delivery. *Acta Pharmacol. Sin.* 2017, 38, 754-763.
22. Haney, M.J.; Klyachko, N.L.; Zhao, Y.; Gupta, R.; Plotnikova, E.G.; He, Z.; Patel, T.; Piroyan, A.; Sokolsky, M.; Kabanov, A.V.; Batrakova, E.V.; Exosomes as drug delivery vehicles for Parkinson's disease therapy. *J Control Release* 2015, 207, 18-30.
23. Sun, D.; Zhuang, X.; Xiang, X.; Liu, Y.; Zhang, S.; Li, C.; Barnes, S.; Grizzle, W.; Miller, D.; Zhang, H.G.; A Novel Nanoparticle Drug Delivery System: The Anti-inflammatory Activity of Curcumin Is Enhanced When Encapsulated in Exosomes. *Mol. Ther.* 2010, 18, 1606–1614.
24. Fuhrmann, G.; Serio, A.; Mazo, M.; Nair, R.; Stevens, M.M.; Active loading into extracellular vesicles significantly improves the cellular uptake and photodynamic effect of porphyrins. *J. Control Release* 2015, 205, 35-44.
25. Kim, M.S.; Haney, M.J.; Zhao, Y.; Mahajan, V.; Deygen, I.; Klyachko, N.L.; Inskoe, E.; Piroyan, A.; Sokolsky, M.; Okolie, O.; Hingtgen, S.D.; Kabanov, A.V.; Batrakova, E.V.; Development of exosome-encapsulated paclitaxel to overcome MDR in cancer cells. *Nanomedicine* 2016, 12, 655-664.
26. Srivastava, A.; Amreddy, N.; Babu, A.; Panneerselvam, J.; Mehta, M.; Muralidharan, R.; Chen, A.; Zhao, Y.D.; Razaq, M.; Riedinger, N.; Kim, H.; Liu, S.; Wu, S.; Abdel-Mageed, A.B.; Munshi, A.; Ramesh, R.; Nanosomes carrying doxorubicin exhibit potent anticancer activity against human lung cancer cells. *Sci Rep* 2016, 6, 38541.
27. Betzer, O.; Perets, N.; Angel, A.; Motiei, M.; Sadan, T.; Yadid, G.; Offen, D.; Popovtzer, R.; *In Vivo* Neuroimaging of Exosomes Using Gold Nanoparticles. *ACS Nano* 2017, 11, 10883-10893.

28. Illes, B.; Hirschle, P.; Barnert, S.; Cauda, V.; Engelke Hanna. Exosome-Coated Metal–Organic Framework Nanoparticles: An Efficient Drug Delivery Platform. *Chemistry of Materials* 2017, 10, 24638-24647
29. htam, T.A.; Kovalev, R.A.; Varfolomeeva, E.Y.; Makarov, E.M.; Kil, Y.V.; Filatov, M.V.; Wahlgren, J.; De L Karlson, T.; Brisslert, M.; Vaziri Sani, F.; Telemo, E.; Sunnerhagen, P.; Valadi, H.; Plasma exosomes can deliver exogenous short interfering RNA to monocytes and lymphocytes. *Nucleic Acids Res.* 2012, 40, e130.
30. Dumontel, B.; Susa, F.; Limongi, T.; Canta, M.; Racca, L.; Chiodoni, A.; Garino, N.; Chiabotto, G.; Centomo, M.L.; Pignochino, Y.; Cauda, V.; ZnO nanocrystals shuttled by extracellular vesicles as effective Trojan nano-horses against cancer cells. *Nanomedicine* 2019, 14, 2815-2833.
31. Hood, J.L.; Scott, M.J.; Wickline, S.A.; Maximizing Exosome Colloidal Stability Following Electroporation. *Anal. Biochem.* 2013, 448, 41–49.
32. Shtam, T.A.; Kovalev, R.A.; Varfolomeeva, E.Y.; Makarov, E.M.; Kil, Y.V.; Filatov, M.V.; Exosomes are natural carriers of exogenous siRNA to human cells *in vitro*. *Cell Commun Signal.* 2013,, 11, 88.
33. Mentkowski, K.I.; Snitzer, J.D.; Rusnak, S.; Lang, J.K.; Therapeutic Potential of Engineered Extracellular Vesicles. *AAPS J.* 2018, 20, 50.
34. C Pascucci, L.; Coccè, V.; Bonomi, A.; Ami, D.; Ceccarelli, P.; Ciusani, E.; Viganò, L.; Locatelli, A.; Sisto, F.; Doglia, S.M.; Parati, E.; Bernardo, M.E.; Muraca, M.; Alessandri, G.; Bondiolotti, G.; Pessina, A.; Paclitaxel is incorporated by mesenchymal stromal cells and released in exosomes that inhibit *in vitro* tumor growth: A new approach for drug delivery. *J. Control Release* 2014, 192, 262-270.
35. Liu, C.; Gao, H.; Lv, P.; Liu, J.; Liu, G.; Extracellular vesicles as an efficient nanoplatform for the delivery of therapeutics. *Hum. Vaccin. Immunother.* 2017, 13, 2678-2687.
36. Tang, K.; Zhang, Y.; Zhang, H.; Xu, P.; Liu, J.; Ma, J.; Lv, M.; Li, D.; Katirai, F.; Shen, G.X.; Zhang, G.; Feng, Z.H.; Ye, D.; Huang, B.; Delivery of chemotherapeutic drugs in tumour cell-derived microparticles. *Nat. Commun.* 2012, 3, 1282.
37. Mulens-Arias, V.; Nicolás-Boluda, A.; Silva, A.K.A.; Gazeau, F.; Theranostic Iron Oxide Nanoparticle Cargo Defines Extracellular Vesicle-Dependent Modulation of Macrophage Activation and Migratory Behavior. *Adv. Biosys.* 2018, 2, 1800079.
38. Silva, A.K.A.; Kolosnjaj-Tabi, J.; Bonneau, S.; Marangon, I.; Boggetto, N.; Aubertin, K.; Clément, O.; Bureau, M.F.; Luciani, N.; Gazeau, F.; Wilhelm, C.; Magnetic and Photoresponsive Theranosomes: Translating Cell-Released Vesicles into Smart Nanovectors for Cancer Therapy. *ACS Nano* 2013, 7, 6.
39. Piffoux, M.; Silva, A.K.A.; Lugagne, J.B.; Hersen, P.; Wilhelm, C.; Gazeau, F.; Extracellular Vesicle Production Loaded with Nanoparticles and Drugs in a Trade-off between Loading, Yield and Purity: Towards a Personalized Drug Delivery System. *Adv. Biosys.* 2017, 1, 1700044.
40. Lou, G.; Song, X.; Yang, F.; Wu, S.; Wang, J.; Chen, Z.; Liu, Y.; Exosomes derived from miR-122-modified adipose tissue-derived MSCs increase chemosensitivity of hepatocellular carcinoma. *J. Hematol. Oncol.* 2015, 8, 122.

41. Munoz, J.L.; Bliss, S.A.; Greco, S.J.; Ramkissoon, S.H.; Ligon, K.L.; Rameshwar, P.; Delivery of Functional Anti-miR-9 by Mesenchymal Stem Cell–derived Exosomes to Glioblastoma Multiforme Cells Conferred Chemosensitivity. *Mol. Ther. Nucleic Acids*. 2013, 2, e126.
42. Shimbo, K.; Miyaki, S.; Ishitobi, H.; Kato, Y.; Kubo, T.; Shimose, S.; Och, M.; .Exosome-formed synthetic microRNA-143 is transferred to osteosarcoma cells and inhibits their migration. *Biochem. Biophys. Res. Commun*. 2014, 445, 381-387.
43. Katakowski, M.; Bullera, B.; Zheng, X.; Lu, Y.; Rogers, T.; Osobamiro, O.; Shu, W.; Jiang, F.; Chopp, M.; Exosomes from marrow stromal cells expressing miR-146b inhibit glioma growth. *Cancer Lett*. 2013, 335, 201–204.
44. Stickney, Z.; Losacco, J.; Mc Devitt, S.; Zhang, Z.; Lu, B.; Development of exosome surface display technology in living human cells. *Biochem Biophys Res Commun*. 2016, 472, 53-59.
45. Alvarez-Erviti, L.; Seow, Y.; Yin, H.; Betts, C.; Lakhali, S.; Wood, M.J.; Delivery of siRNA to the mouse brain by systemic injection of targeted exosomes. *Nat Biotechnol*. 2011, 29, 341-345.
46. Tian, Y.; Li, S.; Song, J.; Ji, T.; Zhu, M.; Anderson, G.J.; Wei, J.; Nie, G.; A doxorubicin delivery platform using engineered natural membrane vesicle exosomes for targeted tumor therapy. *Biomaterials*. 2014, 35, 2383-2390.
47. Kooijmans, S.A.; Aleza, C.G.; Roffler, S.R.; Van Solinge, W.W.; Vader, P.; Schiffelers, R.M.; Display of GPI-anchored anti-EGFR nanobodies on extracellular vesicles promotes tumour cell targeting. *J. Extracell. Vesicles*. 2016, 5, 31053.
48. Ohno, S.; Takanashi, M.; Sudo, K.; Ueda, S.; Ishikawa, A.; Matsuyama, N.; Fujita, K.; Mizutani, T.; Ohgi, T.; Ochiya, T.; Gotoh, N.; Kuroda, M.; Systemically injected exosomes targeted to EGFR deliver antitumor microRNA to breast cancer cells. *Mol Ther*. 2013, 21, 185-191.
49. Hartman, Z.C.; Wei, J.; Glass, O.K.; Guo, H.; Lei, G.; Yang, X.Y.; Osada, T.; Hobeika, A.; Delcayre, A.; Le Pecq, J.B.; Morse, M.A.; Clay, T.M.; Lyerly, H.K.; Increasing vaccine potency through exosome antigen targeting. *Vaccine* 2011, 29, 9361-9367.
50. Rountree, R.B.; Mandl, S.J.; Nachtwey, J.M.; Dalpozzo, K.; Do, L.; Lombardo, J.R.; Schoonmaker, P.L.; Brinkmann, K.; Dirmeier, U.; Laus, R.; Delcayre, A.; Exosome targeting of tumor antigens expressed by cancer vaccines can improve antigen immunogenicity and therapeutic efficacy. *Cancer Res*. 2011, 71, 5235-5244.
51. Delcayre, A.; Estelles, A.; Sperinde, J.; Roulon, T.; Paz, P.; Aguilar, B.; Villanueva, J.; Khine S.S.; Le Pecq, J.B.; Exosome Display technology: Applications to the development of new diagnostics and therapeutics. *Blood Cells Mol Dis*. 2005, 35, 158-168.
52. Wang, J.; Dong, Y.; Li, Y.; Li, W.; Cheng, K.; Qian, Y.; Xu, G.; Zhang, X.; Hu, L.; Chen, P.; Du, W.; Feng, X.; Zhao, W.D.; Zhang, Z.; Liu, B.F.; Designer Exosomes for Active Targeted Chemo-Photothermal Synergistic Tumor Therapy. *Adv. Funct. Mater*. 2018, 28, 1707360.
53. Zhang, W.; Yu, Z.L.; Wu, M.; Ren, J.G.; Xia, H.F.; Sa, G.L.; Zhu, J.Y.; Magnetic and Folate Functionalization Enables Rapid Isolation and Enhanced Tumor-Targeting of Cell-Derived Microvesicles. *ACS Nano* 2017, 11, 277-290.

54. Dong, Z.; Zhao, Y.; Zhang, P.; Folate-Engineered Microvesicles for Enhanced Target and Synergistic Therapy toward Breast Cancer. *ACS Appl Mater Interfaces*. 2017, 9, 5100-5108.
55. Chen, G.; Zhu, J.Y.; Zhang, Z.L.; Zhang, W.; Ren, J.G.; Wu, M.; Hong, Z.Y.; Lv, C.; Pang, D.W.; Zhao, Y.F.; Transformation of Cell-Derived Microparticles into Quantum-Dot-Labeled Nanovectors for Antitumor siRNA Delivery. *Angew Chem Int Ed Engl*. 2014, 54, 1036-40.
56. Wang, J.; Li, W.; Zhang, L.; Ban, L.; Chen, P.; Du, W.; Feng, X.; Liu, B.F.; Chemically edited exosomes with dual ligand purified by microfluidic device for active targeted drug delivery to tumor cells. *ACS Appl. Mater. Interfaces*. 2017, 9, 27441-27452.
57. Lai, C.P.; Mardini, O.; Ericsson, M.; Prabhakar, S.; Maguire, C.A.; Chen, J.W.; Tannous, B.A.; Breakefield, X.O.; Dynamic biodistribution of extracellular vesicles *in vivo* using a multimodal imaging reporter. *ACS Nano* 2014, 8, 483-494.
58. Morishita, M.; Takahashi, Y.; Nishikawa, M.; Ariizumi, R.; Takakura, Y.; Enhanced class I tumor antigen presentation via cytosolic delivery of exosomal cargos by tumor cell-derived exosomes displaying a pH-sensitive fusogenic peptide. *Mol Pharm*. 2017, 14, 4079-4086.
59. Ramasubramanian, L.; Kumar, P.; Wang, A.; Engineering Extracellular Vesicles as Nanotherapeutics for Regenerative Medicine. *Biomolecules* 2019, 10, 48.
60. Presolski, S.I.; Hong, V.P.; Finn, M.G. Copper-Catalyzed Azide–Alkyne Click Chemistry for Bioconjugation. *Curr Protoc Chem Biol*. 2011, 3, 153–162.
61. Jewett, J.C.; Bertozzi, C.R.; Cu-free click cycloaddition reactions in chemical biology. *Chem Soc Rev*. 2010, 39, 1272-1279.
62. Cataldi, M.; Vigliotti, C.; Mosca, T.; Cammarota, M.R.; Capone, D.; Emerging Role of the Spleen in the Pharmacokinetics of Monoclonal Antibodies, Nanoparticles and Exosomes. *Int J Mol Sci*. 2017, 18, 1249.
63. Smyth, T.; Petrova, K.; Payton, N.M.; Persaud, I.; Redzic, J.S.; Surface Functionalization of Exosomes Using Click Chemistry. *Bioconjug Chem*. 2014, 25, 1777-1784.
64. Kooijmans, S.A.A.; Fliervoet, L.A.L.; Van der Meel, R.; Fens, M.H.A.M.; Heijnen, H.F.G.; Van Bergen en Henegouwen P.M.P.; Vader, P.; Schiffelers, R.M.; PEGylated and targeted extracellular vesicles display enhanced cell specificity and circulation time. *J Control Release*. 2016, 224, 77-85.
65. Liang, Y.; Eng, W.S.; Colquhoun, D.R.; Dinglasan, R.R.; Graham, D.R.; Mahal, L.K.; Complex N-Linked Glycans Serve as a Determinant for Exosome/Microvesicle Cargo Recruitment. *J Biol Chem*. 2014, 289, 32526-32537.
66. Williams, C.; Pazos, R.; Royo, F.; González, E.; Roura-Ferrer, M.; Martinez, A.; Gamiz, J.; Reichardt, N.C.; Falcón-Pérez, J.M.; Assessing the role of surface glycans of extracellular vesicles on cellular uptake. *Sci Rep* 2019, 9, 11920.
67. Cai, L.; Gu, Z.; Zhong, J.; Wen, D.; Chen, G.; He, L.; Wu, J.; Gu, Z.; Advances in glycosylation-mediated cancer-targeted drug delivery. *Drug Discov Today* 2018, 23, 1126-1138.

68. Mereiter, S.; Balmaña, M.; Campos, D.; Gomes, J.; Reis, C.A.; Glycosylation in the Era of Cancer-Targeted Therapy: Where Are We Heading? *Cancer Cell*. 2019, 36, 6-16.
69. Tian, T.; Wang, Y.; Wang, H.; Zhu, Z.; Xiao, Z.; Visualizing of the cellular uptake and intracellular trafficking of exosomes by live-cell microscopy. *J Cell Biochem*. 2010, 111, 488-496.
70. Choi, E.S.; Song, J.; Kang, Y.Y.; Mok, H.; Mannose-Modified Serum Exosomes for the Elevated Uptake to Murine Dendritic Cells and Lymphatic Accumulation. *Macromol Biosci*. 2019, 19, e1900042.
71. Kim, M.S.; Haney, M.J.; Zhao, Y.; Yuana, D.; Deygen, I.; Batrakova, E.V.; Engineering macrophage-derived exosomes for targeted paclitaxel delivery to pulmonary metastases: *in vitro* and *in vivo* evaluations. *Nanomedicine*. 2018, 14, 195-204.
72. Pi, F.; Binzel, D.W.; Lee, T.J.; Li, Z.; Sun, M.; Rychahou, P.; Li, H.; Haque, F.; Wang, S.; Croce, C.M.; Guo, B.; Evers, B.M.; Guo, P.; Nanoparticle orientation to control RNA loading and ligand display on extracellular vesicles for cancer regression. *Nat Nanotechnol*. 2017, 13, 82–89.
73. Jia, G.; Han, Y.; An, Y.; Ding, Y.; He, C.; Wang, X.; Tang, Q.; NRP-1 targeted and cargo-loaded exosomes facilitate simultaneous imaging and therapy of glioma *in vitro* and *in vivo*. *Biomaterials*. 2018, 178, 302-316.
74. Nakase, I.; Futaki, S.; Combined treatment with a pH-sensitive fusogenic peptide and cationic lipids achieves enhanced cytosolic delivery of exosomes. *Sci Rep* 2015, 5, 10112.
75. Qi, H.; Liu, C.; Long, L.; Ren, Y.; Zhang, S.; Chang, X.; Qian, X.; Jia, H.; Zhao, J.; Sun, J.; Hou, X.; Yuan, X.B.; Kang, C.; Blood Exosomes Endowed with Magnetic and Targeting Properties for Cancer Therapy. *ACS Nano*. 2016, 10,3323-3333.
76. Gao, X.; Ran, N.; Dong, X.; Zuo, B; Yang, R.; Zhou, Q.; Moulton, H.M.; Seow Y.; Yin H.; Anchor peptide captures, targets, and loads exosomes of diverse origins for diagnostics and therapy. *Sci Transl Med*. 2018, 10, 444.
77. Smyth, T.; Kullberg, M.; Malik, N.; Smith-Jones, P.; Graner, M. W.; Anchordoquy, T. J.; Biodistribution and delivery efficiency of unmodified tumor-derived exosomes. *J Control Release*. 2015, 199, 145-155.
78. Royo, F.; Cossío, U.; de Angulo, A.R.; Llop, J.; Falcon-Perez J.M;. Modification of the glycosylation of extracellular vesicles alters their biodistribution in mice. *Nanoscale*. 2019, 11, 1531-1537.
79. Dusoswa, S.A.; Horrevorts, S.K.; Ambrosini, M.; Kalay, H.; Paauw, N.J.; Nieuwland, R.; Pegtel, M.D.; Würdinger, T.; Van Kooyk, Y.; Garcia-Vallejo, J.J.; Glycan modification of glioblastoma-derived extracellular vesicles enhances receptor-mediated targeting of dendritic cells. *J Extracell Vesicles*. 2019, 8, 1648995.
80. Hung, M.E.; Leonard, J.N.; Stabilization of Exosome-targeting Peptides via Engineered Glycosylation. *J Biol Chem*. 2015, 290, 8166-8172.
81. Lin, Y.; Wu, J.; Gu, W.; Huang, Y.; Tong, Z.; Huang, L.; Tan, J.; Exosome–Liposome Hybrid Nanoparticles Deliver CRISPR/Cas9 System in MSCs. *Adv. Sci*. 2018, 5, 1700611.

82. Sato, Y.T.; Umezaki, K.; Sawada, S.; Mukai, S.; Sasaki, Y.; Harada, N.; Shiku, H.; Akiyoshi, K.; Engineering hybrid exosomes by membrane fusion with liposomes. *Sci Rep* 2016, 6, 21933.
83. Piffoux, M.; Silva, A.K.A.; Wilhelm, C.; Gazeau, F.; Taresté, D.; Modification of Extracellular Vesicles by Fusion with Liposomes for the Design of Personalized Biogenic Drug Delivery Systems. *ACS Nano* 2018, 12, 6830-6842.
84. Piffoux, M.; Silva, A.K.A.; Wilhelm, C.; Gazeau, F.; Taresté, D.; Modification of Extracellular Vesicles by Fusion with Liposomes for the Design of Personalized Biogenic Drug Delivery Systems. *ACS Nano* 2018, 12, 6830-6842.
85. Lu, M.; Huang, Y.; Bioinspired exosome-like therapeutics and delivery nanoplatfoms. *Biomaterials*. 2020, 242, 119925.
86. Jang, S.C.; Kim, O.Y.; Yoon, C.M.; Choi, D.S.; Roh, T.Y.; Park, J.; Nilsson, J.; Lötvall, J.; Kim, Y.K.; Gho, Y.S.; Bioinspired exosome-mimetic nanovesicles for targeted delivery of chemotherapeutics to malignant tumors. *ACS Nano*. 2013, 7, 7698-7710.
87. García-Manrique, P.; Gutiérrez, G.; Blanco-López, M.C.; Fully Artificial Exosomes: Towards New Theranostic Biomaterials. *Trends Biotechnol.* 2018, 36, 10-14.
88. Zhu, L.; Gangadaran, P.; Kalimuthu, S.; Oh, J.M.; Baek, S.H.; Jeong, S.Y.; Lee, S.W.; Lee, J.; Ahn, B.C.; Novel alternatives to extracellular vesicle-based immunotherapy-exosome mimetics derived from natural killer cells. *Artif Cells Nanomed Biotechnol.* 2018, 46, S166-S179.
89. Wu, J.Y.; Ji, A.L.; Wang, Z.X.; Qiang, G.H.; Qu, Z.; Wu, J.H.; Jiang, C.P.; Exosome-mimetic nanovesicles from hepatocytes promote hepatocyte proliferation *in vitro* and liver regeneration *in vivo*. *Sci Rep* 2018, 8, 2471.
90. Hwang, D.W.; Choi, H.; Jang, S.C.; Yoo, M.Y.; Park, J.Y.; Choi, N.E.; Oh, H.J.; Ha, S.; Lee, Y.S.; Jeong, J.M.; Gho, Y.S.; Lee, D.S.; Noninvasive imaging of radiolabeled exosome-mimetic nanovesicle using ^{99m}Tc-HMPAO. *Sci Rep*. 2015, 5, 15636.
91. Jo, W.; Kim, J.; Yoon, J.; Jeong, D.; Cho, S.; Jeong, H.; Yoon, Y.J.; Kim, S.C.; Ghod, Y.S.; Park, J.; Large-scale generation of cell-derived nanovesicles. *Nanoscale*. 2014, 6, 12056-64.
92. Jeong, D.; Jo, W.; Yoon, J.; Kim, J.; Gianchandani, S.; Gho, Y.S.; Park, J.; Nanovesicles engineered from ES cells for enhanced cell proliferation. *Biomaterials*. 2014, 35, 9302-9310.
93. Yang, Z.; Xie, J.; Zhu, J.; Kang, C.; Chiang, C.; Wang, X.; Wang, X.; Kuang, T.; Chen, F.; Chen, Z.; Zhang, A.; Yu, B.; Lee, R.J.; Teng, L.; Lee, L.J.; Functional exosome-mimic for delivery of siRNA to cancer: *in vitro* and *in vivo* evaluation. *J Control Release*. 2016, 243, 160-171.
94. Senthilkumar, K.; Prakash, G.; Lakshmi, R.R.; Liya, Z.; Min, O.J.; Won, L.H.; Arunnehr, G.; Hwan, B.S.; Young, J.S.; Sang-Woo, L.; Jaetae, L.; Byeong-Cheol, A.; A New Approach for Loading Anticancer Drugs Into Mesenchymal Stem Cell-Derived Exosome Mimetics for Cancer Therapy. *Front Pharmacol.* 2018, 9, 1116.
95. Tao, S.C.; Rui, B.Y.; Wang, Q.Y.; Zhou, D.; Zhang, Y.; Guo, S.C.; Extracellular vesicle-mimetic nanovesicles transport LncRNA-H19 as competing endogenous RNA for the treatment of diabetic wounds. *Drug Deliv.* 2018, 25, 241-255.

96. Oh, K.; Kim, S.R.; Kim, D.K.; Seo, M.W.; Lee, C.; Lee, H.M.; Oh, J.E.; Choi, E.Y.; Lee, D.S.; Gho, Y.S.; Park, K.S.; *In Vivo* Differentiation of Therapeutic Insulin-Producing Cells from Bone Marrow Cells via Extracellular Vesicle-Mimetic Nanovesicles. *ACS Nano*. 2015, 9, 11718-11727.
97. Wu, J.Y.; Ji, A.L.; Wang, Z.X.; Qiang, G.H.; Qu, Z.; Wu, J.H.; Jiang, C.P.; Exosome-Mimetic Nanovesicles from Hepatocytes promote hepatocyte proliferation *in vitro* and liver regeneration *in vivo*. *Sci Rep* 2018, 8, 2471.
98. Kim, Y.S.; Kim, J.Y.; Cho, R.; Shin, D.M.; Lee, S.W.; Oh, Y.M.; Adipose stem cell-derived nanovesicles inhibit emphysema primarily via an FGF2-dependent pathway. *Exp Mol Med*. 2017, 49, e284.
99. Park, K.S.; Svennerholm, K.; Shelke, G.V.; Bandeira, E.; Lässer, C.; Jang, S.C.; Chandode, R.; Gribonika, I.; Lötvall, J.; Mesenchymal stromal cell-derived nanovesicles ameliorate bacterial outer membrane vesicle-induced sepsis via IL-10. *Stem Cell Res Ther*. 2019, 10, 231.
100. Choo, Y.W.; Kang, M.; Kim, H.Y.; Han, J.; Kang, S.; Lee, J.R.; Jeong, G.J.; Kwon, S.P.; Song, S.Y.; Go, S. Jung, M.; Hong, J.; Kim, B.S.; M1 Macrophage-Derived Nanovesicles Potentiate the Anticancer Efficacy of Immune Checkpoint Inhibitors. *ACS Nano* 2018, 12, 8977-8993.
101. Yoona, J.; Joa, W.; Jeongb, D.; Kimb, J.; Jeonga, H.; Parkab, J.; Generation of nanovesicles with sliced cellular membrane fragments for exogenous material delivery. *Biomaterials* 2015, 59, 12-20.
102. Jo, W.; Jeong, D.; Kim, J.; Cho, S.; Jang, S.C.; Han, C.; Kang, J.Y.; Gho, Y.S.; Park, J.; Microfluidic fabrication of cell-derived nanovesicles as endogenous RNA carriers. *Lab Chip* 2014, 14, 1261-1269.
103. De La Peña, H.; Madrigal, J.A.; Rusakiewicz, S.; Bencsik, M.; Cave, G.W.; Selman, A.; Rees, R.C.; Travers, P.J.; Dodi, I.A.; Artificial exosomes as tools for basic and clinical immunology. *J Immunol Methods*. 2009, 344, 121-132.
104. Lu, M.; Zhao, X.; Xing, H.; Xun, Z.; Zhu, S.; Lang, L.; Yang, T.; Cai, C.; Wang, D.; Ding, P.; Comparison of exosome-mimicking liposomes with conventional liposomes for intracellular delivery of siRNA. *Int J Pharm*. 2018, 550, 100-113.
105. Lu, M.; Zhao, X.; Xing, H.; Liu, H.; Lang, L.; Yang, T.; Xun, Z.; Wang, D.; Ding, P.; Cell-free synthesis of connexin 43-integrated exosome-mimetic nanoparticles for siRNA delivery. *Acta Biomater*. 2019, 96, 517-536.
106. Vázquez-Ríos, A.J.; Molina-Crespo, Á.; Bouzo, B.L.; López-López, R.; Moreno-Bueno, G.; de la Fuente, M.; Exosome-mimetic nanoplatfoms for targeted cancer drug delivery. *J Nanobiotechnol* 2019, 17, 85.
107. Martínez-Lostao, L.; García-Alvarez, F.; Basáñez, G.; Alegre-Aguarón, E.; Desportes, P.; Larrad, L.; Naval, J.; Martínez-Lorenzo, M.J.; Anel, A.; Liposome-bound APO2L/TRAIL is an effective treatment in a rabbit model of rheumatoid arthritis. *Arthritis Rheum*. 2010, 62, 2272-2282.
108. De Miguel, D.; Basáñez, G.; Sánchez, D.; Malo, P.G.; Marzo, I.; Larrad, L.; Naval, J.; Pardo, J.; Anel, A.; Martínez-Lostao, L.; Liposomes Decorated with Apo2L/TRAIL Overcome Chemoresistance of Human Hematologic Tumor Cells. *Mol Pharm*. 2013, 10, 893-904.

109. Li, K.; Chang, S.; Wang, Z.; Zhao, X.; Chen, D.; A novel micro-emulsion and micelle assembling method to prepare DEC205 monoclonal antibody coupled cationic nanoliposomes for simulating exosomes to target dendritic cells. *Int J Pharm.* 2015, 491, 105-112.
110. Zhang, K.L.; Wang, Y.J.; Sun, J.; Zhou, J.; Xing, C.; Huang, G.; Li, J.; Yang, H.; Artificial chimeric exosomes for anti-phagocytosis and targeted cancer therapy. *Chem Sci.* 2019, 10, 1555-1561.
111. Molinaro, R.; Corbo, C.; Martinez, J.O.; Taraballi, F.; Evangelopoulos, M.; Minardi, S.; Yazdi, I.K.; Zhao, P.; De Rosa, E.; Sherman, M.; De Vita, A.; Toledano Furman, N.E.; Wang, X.; Parodi, A.; Tasciotti, E.; Biomimetic proteolipid vesicles for targeting inflamed tissues. *Nat Mater.* 2016, 15, 1037-1046.
112. Molinaro, R.; Evangelopoulos, M.; Hoffman, J.R.; Corbo, C.; Taraballi, F.; Martinez, J.O.; Hartman, K.A.; Cosco, D.; Costa, G.; Romeo, I.; Sherman, M.; Paolino, D.; Alcaro, S.; Tasciotti, E.; Design and Development of Biomimetic Nanovesicles Using a Microfluidic Approach. *Adv Mater.* 2018, 30, e1702749.
113. Barui, S.; Cauda, V.; Multimodal Decorations of Mesoporous Silica Nanoparticles for Improved Cancer Therapy. *Pharmaceutics.* 2020, 12, 527.
114. Cauda, V.; Schlossbauer, A.; Bein, T.; Bio-degradation study of colloidal mesoporous silica nanoparticles: Effect of surface functionalization with organo-silanes and poly(ethylene glycol). *Microporous and Mesoporous Materials.* 2010, 132, 60-71.
115. Durfee, P.N.; Lin, Y.; Dunphy, D.R.; Muñiz, A.Y.; Butler, K.S.; Humphrey, K.R.; Lokke, A.J.; Agola, J.O.; Chou, S.S.; Chen, I.; Wharton, W.; Townson, J.L.; Willman, C.L.; Brinker, C.J.; Mesoporous Silica Nanoparticle-Supported Lipid Bilayers (Protocells) for Active Targeting and Delivery to Individual Leukemia Cells. *ACS Nano.* 2016, 10, 8325–8345.
116. Schlossbauer, A.; Sauer, A.; Cauda, V.; Schmidt, A.; Engelke, H.; Rädler, J.; Rothbauer, U.; Zolghadr, K.; Bräuchle, C.; Bein, T.; Cascaded photoinduced drug delivery to cells from multifunctional core-shell mesoporous silica. *Advanced Healthcare Materials.* 2012, 1, 316-320.
117. Zhang, J.; Yuan, Z.; Wang, Y.; Chen, W.; Luo, G.; Cheng, S.; Zhuo, R.; Zhang, X.; Multifunctional envelope-type mesoporous silica nanoparticles for tumor-triggered targeting drug delivery. *J. Am. Chem. Soc.* 2013, 135, 5068-5073.
118. Langer, C.; Ibañez, M.; Liebisch, P.; Zenz, T.; Knop, S.; Einsele, H.; Paschka, P.; Doehner, H.; Doehner, K.; IDH1 and IDH2 mutations are Not Frequent In Multiple Myeloma. *Blood.* 2010, 116, 4992.
119. Tommasini-Ghelfi, S.; Murnan, K.; Kouri, F.; Mahajan, A.; May, J.; Stegh, A.; Cancer-associated mutation and beyond: The emerging biology of isocitrate dehydrogenases in human disease. *Science Advances.* 2019, 5, eaaw4543.
120. Molenaar, R.; Maciejewski, J.; Wilmink, J.; van Noorden, C.; Wild-type and mutated IDH1/2 enzymes and therapy responses. *Oncogene.* 2018, 37, 1949-1960.

121. Bergaggio, E.; Piva, R.; Wild-type idh enzymes as actionable targets for cancer therapy. *Cancers*. 2019, 11, 563.
122. Chen, X.; Xu, W.; Wang, C.; Liu, F.; Guan, S.; Sun, Y.; Wang, X.; An, D.; Wen, Z.; Chen, P.; The clinical significance of isocitrate dehydrogenase 2 in esophageal squamous cell carcinoma. *Am J Cancer Res*. 2017, 7, 700-714.
123. Li, J.; He, Y.; Tan, Z.; Lu, J.; Li, L.; Song, X.; Shi, F.; Xie, L.; You, S.; Luo, X.; Wild-type idh2 promotes the warburg effect and tumor growth through hif1 α in lung cancer. *Theranostics*. 2018, 8, 4050-4061.
124. Bergaggio, E.; Riganti, C.; Garaffo, G.; Vitale, N.; Mereu, E.; Bandini, C.; Pellegrino, E.; Pullano, V.; Omedè, P.; Todoerti, K.; Cascione, L.; Audrito, V.; Riccio, A.; Rossi, A.; Bertoni, F.; Deaglio, S.; Neri, A.; Palumbo, A.; Piva, R.; IDH2 inhibition enhances proteasome inhibitor responsiveness in hematological malignancies. *Blood*, 2019, 133, 156-167.
125. Selleckem product's description.
126. Urban, D.; Martinez, N.; Davis, M.; Brimacombe, K.; Cheff, D.; Lee, T.; Henderson, M.; Titus, S.; Pragani, R.; Rohde, J.; Assessing inhibitors of mutant isocitrate dehydrogenase using a suite of pre-clinical discovery assays. *Sci Rep*. 2017, 7, 12758.
127. Ebeid, K.; Meng, X.; Thiel, K.W.; Do, A.; Geary, S.M.; Morris, A.S.; Pham, E.L.; Wongrakpanich, A.; Chhonker, Y.S.; Murry, D.J.; Leslie, K.K.; Salem, A.K.; Synthetically lethal nanoparticles for treatment of endometrial cancer. *Nat Nanotechnol*. 2018, 13, 72-81.
128. Shen, J.; Song, G.; An, M.; Li, X.; Wu, N.; Ruan, K.; Hu, J.; Hu, R.; The use of hollow mesoporous silica nanospheres to encapsulate bortezomib and improve efficacy for non-small cell lung cancer therapy. *Biomaterials*. 2014, 35, 316-326.
129. Cauda, V.; Engelke, H.; Sauer, A.; Arcizet, D.; Bräuchle, C.; Rädler, C.; Bein, T.; Colchicine-loaded lipid bilayer-coated 50 nm mesoporous nanoparticles efficiently induce microtubule depolymerization upon cell uptake. *Nano Lett*. 2010, 10, 2484–2492.
130. Durfee, P.N.; Lin, Y.; Dunphy, D.R.; Muñiz, A.J.; Butler, K.S.; Humphrey, K.R.; Lokke, A.J.; Agola, J.O.; Chou, S.S.; Chen, I.; Wharton, W.; Townson, J.L.; Willman, C.L.; Brinker, C.J.; Mesoporous Silica Nanoparticle-Supported Lipid Bilayers (Protocells) for Active Targeting and Delivery to Individual Leukemia Cells. *ACS Nano*. 2016, 10, 8325-8345.
131. FTIR Spectroscopy Basics, Thermo Fisher Scientific.
132. Rukari, T.; Babita, A.; Review Article TRANSMISSION ELECTRON MICROSCOPY-AN OVERVIEW. *irjips*. 2013, 1, 1-7.
133. Tang, C.Y.; Yang, Z.; Chapter 8 - Transmission Electron Microscopy (TEM). *Membrane Characterization*. 2017, 2017, 145-159.

134. Atkins, P.; de Paula, J.; *Physical Chemistry for Life Sciences*. Oxford University Press. 2008, 5,2.
135. Howard, H.M.; Shapiro, M.; *Practical Flow Cytometry*, 4th ed., Wiley-Liss, 2003.
136. MitoPT, TMRE & TMRM Assay Kits 500 tests, 2013.
137. Wallberg, F.; Tenev, T.; Meier, P.; *Analysis of Apoptosis and Necroptosis by Fluorescence-Activated Cell Sorting*. Cold Spring Harb Protoc. 2016, 2016, pdb.prot087387.